UNIVERSITÀ DEGLI STUDI DI PADOVA

DIPARTIMENTO DI FISICA E ASTRONOMIA "GALILEO GALILEI"

CORSO DI LAUREA MAGISTRALE IN FISICA

DEVELOPMENT OF BIOPHYSICAL TECHNIQUES FOR THE STUDY OF THE PERIPHERAL NERVOUS SYSTEM BY STEM CELLS

Laureanda: MARTINA NICOLETTI

Relatore: Prof. MARIO BORTOLOZZI

ANNO ACCADEMICO 2016/2017

Alla mia famiglia

ABSTRACT

Understanding the molecular mechanisms underlying human diseases requires a combination of biophysical techniques and cellular models. Stem cells are a very promising tool available to reproduce in vitro the pathology starting from patient's biopsies (e.g. skin samples). In particular, their differentiation into neurons and Schwann cells open unprecedented opportunities to generate a myelinating co-culture to study peripheral neuropathies, such as Charcot-Marie-Tooth disease, which is one of the long-term goals of our lab. In this thesis work, we contributed to the electrophysiological characterization of motor neurons and Schwann cells derived both from induced pluripotent stem cells (iPSCs) and mesenchymal stem cells (MSCs) obtained from healthy subjects, in collaboration with the local Hospital and the Stem Cell Centre of Sheffield. The electrophysiology experiments were performed at different time points and with different culture conditions in the whole-cell patch clamp configuration with standard current and voltage clamp protocols. Motor neurons and Schwann cells derived from iPSCs showed electrophysiological characteristics consistent with the expected cellular phenotype. The mean resting potential, V_m = (−73.5 ± 1.8) mV for neurons and V_m = (−36.4 ± 1.6) mV for Schwann cells, was correctly matching the values expected for these cells. Furthermore, neurons formed complex networks and were able to fire trains of action potentials generated by voltage-activated sodium and potassium channels. Neurons derived from MSCs did not show the typical properties of mature neurons. While voltage-activated potassium currents were correctly developed, only small voltage-activated sodium currents were detected, as well as the mean resting potential was lower (V_m = (−47.3 ± 2.4) mV) than the expected value (around −70 mV), suggesting incomplete neuronal maturation. The next step of this work is to co-culture matured iPSC-derived neurons and Schwann cells in a commercial microfluidic device to stimulate the myelination process, both by increasing the exchange of growth factors between neurons and Schwann cells (due to the limited space available) and by administering specific pro-myelinating drugs. If the co-culture model is successful, we aim to generate a model for the study of the connexin 32 (Cx32) mutations that are causing the X-linked form of Charcot-Marie-Tooth disease (CMT1X). This model could also be a very useful tool for "personalized medicine" and drugs screening.

SOMMARIO

Lo studio dei meccanismi molecolari alla base delle malattie umane richiede una opportuna combinazione di tecniche biofisiche e modelli cellulari. Attualmente, le cellule staminali derivate da biopsie di pazienti adulti costituiscono lo strumento più promettente per la riproduzione in vitro delle patologie. In particolare, il loro differenziamento in neuroni e cellule di Schwann ha aperto la possibilità di generare in vitro una co-coltura mielinizzata per lo studio di neuropatie periferiche come la malattia di Charcot-Marie-Tooth. La generazione di questo tipo di modello è l'obiettivo finale di un progetto di ricerca portato avanti nel laboratorio del prof. Bortolozzi, presso l'Istituto Veneto di Medicina Molecolare (VIMM, Padova). In questo lavoro di tesi, abbiamo contribuito alla caratterizzazione elettrofisiologica di moto-neuroni e cellule di Schwann derivate da cellule staminali pluripotenti indotte (iPSCs) e cellule staminali mesenchimali (MSCs) ottenute da biopsie di pelle di soggetti sani, in collaborazione con l'ospedale locale e con lo Stem Cell Center di Sheffield (UK). Gli esprimenti di elettrofisiologia sono stati eseguiti, utilizzando la tecnica del patch-clamp in configurazione whole-cell, a diversi stadi di differenziamento su cellule sottoposte a diversi protocolli di differenziamento. I moto-neuroni e cellule di Schwann derivati da iPSCs hanno mostrato caratteristiche elettrofisiologiche consistenti con quelle attese per lo specifico fenotipo cellulare. Il potenziale di riposo medio, $V_m = (-73.5 \pm 1.8)$ mV per i neuroni e $V_m = (-36.4 \pm 1.6)$ mV per le cellule di Schwann, risulta corrispondere correttamente ai valori attesi per queste cellule. Inoltre, i moto-neuroni in coltura hanno formato complesse reti neurali e si sono rivelati in grado di generare potenziali di azione multipli originati da canali sodio e potassio voltaggio-attivati. I neuroni differenziati a partire dalle MSCs non hanno mostrato le tipiche caratteristiche elettrofisiologiche dei moto-neuroni maturi, come è invece accaduto per quelli derivati da iPSCs. Le cellule hanno sviluppato correttamente i canali potassio; tuttavia solamente in una cellula è stata riscontrata la presenza di piccole correnti sodio-voltaggio attivate, così come il potenziale di riposo ($V_m = (-47.3 \pm 2.4)$ mV) è risultato più basso del valore atteso (attorno a -70 mV), indicando, dunque, una incompleta maturazione neuronale. Il prossimo passo è quello di generare una co-coltura con neuroni e cellule di Schwann impiegando un dispositivo microfluidico disponibile in commercio per stimolare il processo di mielinizzazione attraverso un aumento dello scambio di fattori di crescita specifici per neuroni e cellule di Schwann (grazie al ristretto spazio disponibile) e, la somministrazione di specifici agenti che favoriscono la mielinizzazione. Nel caso in cui la co-coltura risulti soddisfacente, vorremo generare un modello analogo per lo studio delle mutazioni della connessina 32 (Cx32) che sono associate alla forma X-linked della malattia di Charcot-Marie-Tooth (CMT1X). Un modello come questo può, inoltre, essere utilizzato come strumento per la medicina personalizzata e per testare possibili terapie farmacologiche.

TABLE OF CONTENTS

1.INTRODUCTION.

The main purpose of this thesis work is to study the electrophysiological properties of motor neurons and Schwann cells derived from two different sources of skin-derived stem cells: induced pluripotent stem cells (iPSCs) and mesenchymal stem cells (MSCs). The correct interpretation of the results requires to understand the general membrane properties of a cell. Therefore, the first part of this chapter is related to the biophysical properties of the cell membrane and its ion channels, with a particular focus on connexin 32-based channels whose dysfunction is related to the pathophysiology of Charcot-Marie-Tooth disease (CMT1X). A detailed description of neuron and Schwann cell membrane properties, as well as a brief introduction to the field of stem cells, will be also given in the second part of the chapter.

1.1 CELL MEMBRANES AND ION CHANNELS.

All living cells are enveloped by a plasma membrane that acts as a barrier between the cytoplasm and the extracellular space. The main constituents are phospholipids, which contain both lipophilic (fatty) and hydrophilic (polarized) residues. In a watery environment, phospholipids will arrange themselves spontaneously into structures where the lipophilic residues face each other (Figure 1)[1] .

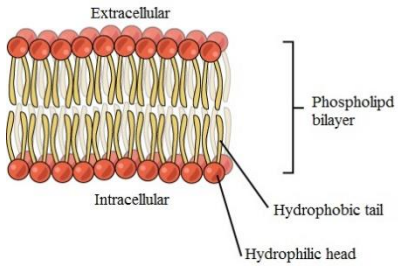

Figure 1. Bilayer arrangement of phospholipids in the cell membrane.

The phospholipids are a dynamic if not fluid substrate in which other membrane constituents are embedded. These are mostly proteins with a variety of functions: communication (receptors and ion channels), structure (cytoskeletal anchors) and cellular homeostasis (ionic pumps, enzymes). The barrier function of the membrane is critical in maintaining the concentration differences of solutes between the intracellular and extracellular medium. However, cells have had to evolve mechanisms for the transfer of water-soluble molecules across their membranes in order to assume essential nutrients and to excrete metabolic waste products. The flow of ions and molecules across the plasma membrane is achieved by specialized transmembrane proteins, each of which is responsible for the transfer of a specific ion or molecule. These transmembrane proteins can be divided in two main classes: ion channels, which facilitate the diffusion across the membrane by forming an aqueous pore, and carrier proteins (or transporters), which aid movement of molecules across the membrane against the concentration gradients. The transport performed by carrier proteins is usually named “active transport” because it requires energy provided by the cellular metabolic activity (for example the breakdown of ATP to ADP).

Channels possess specific properties that make them very effective in controlling membrane permeability to small water-soluble molecules. First, they show selective permeability, permitting some ions to flow but not others. Second, they are not continuously opened, like the aqueous pores, thanks to the presence of a “gating mechanism” that can close the pore. The gating mechanism consists in a change in protein conformation induced by a gating factor. According to the gating factor ion channels can be classified into three main categories.

- Voltage-gated channels (VGCs), which open or close depending on the membrane potential. These channels have voltage sensors: charged residues that shift their position within the protein in response to membrane potential changes.

- Ligand-gated channels (LGCs), which open or close depending on the binding of an extracellular factor, such as a hormone or neurotransmitter, or an intracellular factor, such as calcium ions or activated G protein subunits.

- Mechanically-gated channels (MGCs), which are regulated by mechanical stretch of the membrane.

In addition, modulatory mechanisms can influence gating independent of the primary gating factor. Very common is phosphorylation of the protein on the cytosolic side, which provides a mechanism for fine tuning of the channel activity.

1.2 ELECTRICAL PROPERTIES OF THE CELL.

A cell derives its electrical properties mostly from the electrical properties of its membrane, which, in turn, acquires the properties from its lipids and proteins, such as ion channels and transporters. An electrical potential difference exists between the interior and exterior of the cell, usually denoted as V or ΔV and termed *membrane potential*. The potential difference across the cell relates the potential of the cell interior to that of the external solution, which is conventionally taken as zero. It arises when there is a difference in the electrical charge on the two sides of the cell membrane. Such difference can result both from active electrogenic pumping and from passive ion diffusion [2].

Inorganic ions form the vast majority of particles in the intracellular and extracellular media. As a result, the media possess a gross distribution of ions that is fairly constant over a broad range of cell types. Table 1 reports an overview of concentrations of the principal ions in the extracellular and intracellular medium [1].

The membrane potential of an unstimulated cell is called *resting potential*, and derives from the equilibrium potential of all ions present in the medium.

Ion	Intracellular range (mM)	Extracellular range (mM)
Na^+	5-20	130-160
K^+	130-160	4-8
Ca^{2+}	50-1000nM	1.2-4
Mg^{2+}	10-20	1-5
Cl^-	1-60	100-140
HCO_3^-	1-3	20-30

Table 1. Intracellular and extracellular distribution of the main ions found in animal fluids.

The *equilibrium potential* for a ionic species A is the membrane potential at which there is no net movement of ions from one side of the other. The equilibrium potential for a specific ion can be calculated using the *Nernst equation*:

$$\Delta \mathbf{V} = \frac{\mathbf{RT}}{\mathbf{zF}} \mathbf{ln} \frac{[\mathbf{A}]_\mathbf{o}}{[\mathbf{A}]_\mathbf{i}}. \tag{1.1}$$

with $[A]_o$ and $[A]_i$ the concentration outside and inside the cell, $\mathrm{R} = 8.314\ \mathrm{VC\ K^{-1}mol^{-1}}$, T the absolute temperature, *z* the charge of the ion, and $\mathrm{F} = 9.648\ \mathrm{C\ mol^{-1}}$ the Faraday's constant.

The Nernst equation gives the equilibrium potential of only one of the ionic species in the extracellular and intracellular media. However, to calculate the resting potential V_r is necessary to take in account the equilibrium potentials of all the ionic species. Furthermore, when V_r is determined by two or more ionic species, the contribution of each species is determined not only, by the concentrations of the ion inside and outside the cell, but also by the ease with which the ion crosses the membrane. One convenient measure of how easily the ion crosses the membrane is the permeability P of the membrane to that ion, which has units of velocity ($\mathrm{cm/s}$). The dependence of membrane potential on ionic permeabilities and concentrations is given by the Goldman equation:

$$V_r = \frac{RT}{F} \ln \left[\frac{P_K[K^+]_o + P_{Na}[Na^+]_o + P_{Cl}[Cl^-]_i}{P_K[K^+]_i + P_{Na}[Na^+]_i + P_{Cl}[Cl^-]_o} \right] \tag{1.2}$$

The (1.2) gives the resting potential for a cell membrane in which the main ion species that flow across the membrane are potassium, sodium, and chloride ions, e.g. a neuron.

The general equation to calculate the resting potential V_r accounting all ion species that can flow across the membrane can be written as:

$$0 = \sum_{k=1}^{N} z_{A_k}^2 P_k \frac{[A_k]_o - [A_k]_i e^{z_{A_k}^2 \frac{FV_r}{RT}}}{1 - e^{z_{A_k}^2 \frac{FV_r}{RT}}}, \tag{1.3}$$

with N the total number of ionic species, z_{A_k} the charge of the k-th species, and P_k the membrane permeability of the k-th species [3].

The usefulness of equations 1.2 and 1.3 is limited because they cannot be used to determine how rapidly the membrane potential changes in response to a change in permeability, and it is also inconvenient for determining the magnitude of the individual Na^+, K^+, and Cl^- currents. This information can be obtained using a simple mathematical model derived from electrical circuits. The model, called *equivalent circuit*, represents all the important electrical properties of the cell by a circuit consisting of conductors, resistors, batteries, and capacitors [4].

1.2.1 EQUIVALENT CIRCUIT FOR THE CELL MEMBRANE.

The first step in developing an equivalent circuit is to relate the membrane's discrete properties to its electrical properties. The phospholipid bilayer is an effective barrier for the movement of charged particles. Thus, it endows the membrane with an electrical capacitance, indeed the bilayer of phospholipids separates the cell cytoplasm and the extracellular fluid, both of which are highly conductive environments. The presence of a thin layer of opposing charges on the inside and the outside surfaces of the cell membrane, acting as a capacitor, give rise to an electrical potential across the membrane:

$$V = {}^{Q}/_{C} \tag{1.4}$$

where Q is the net excess positive or negative charge on each side of the capacitor C and C is the capacitance. typical

The electrical insulation is not perfect because in the membrane are present ion channels and transporters. This implies that the resistance of the membrane to the movement of ions across it is finite. The

conductance γ (units: siemens (S)) of a ion channel is defined as the inverse of the resistance R, and is a measure of the ease of flow of current between two points [5].

Ion channels can be represented as conductors in series with two additional circuits elements (Figure 2.A): a switch that represents the gate of the channel, which would be in its conducting position when the gate is open, and a battery that represents the *reversal potential* of the ionic current for that channel. The reversal potential is defined as the voltage at which the current changes its direction. For a perfectly selective channel the reversal potential equals the Nernst potential for the permeant ion.

Following these considerations, a possible representation that includes all the channel of the membrane is shown in Figure 2.B, where the switch is omitted because it works differently for different kinds of channels, the reversal potential is substituted by the resting potential, and R_m is the parallel of all ion channels resistance.

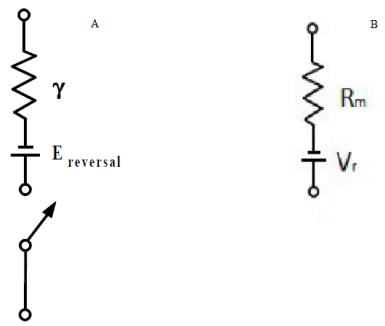

Figure 2. A: Equivalent circuit for a single membrane channel.

Biological membranes are typically less than 10nm thick, and the phospholipid bilayer acts as a barrier for the movement of charged particles. In contrast, the extracellular end the intracellular media are watery salt solutions, and very conductive to ions. Consequently, a transmembrane resting potential produces an electrical field across the membrane. For this reason, the membrane can be seen as an insulator between two conductors, thus it forms, with the intracellular and extracellular media, a capacitor C_m. The physical dimensions of the membrane are important in determining the capacitance: the capacitance is proportional to membrane surface area (the more membrane, the more charge can accumulate), and inversely proportional to membrane thickness [1].

Given that an intact cell has a membrane potential, resistance, and a capacitance, the electronic representation of a cell looks like Figure 3.

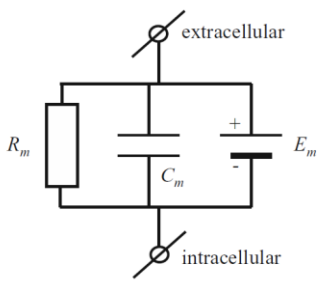

Figure 3. An electronic model of the plasma membrane of an intact cell.

1.3 CONNEXIN HEMICHANNELS AND GAP JUNCTIONS.

A special class of ion channels are *connexin-based channels*. This kind of channels constitutes the main cell-to-cell communication system in mammalians forming gap junction channels for the exchange of metabolites (e.g., ADP, glucose, and glutamate), second messengers and ions. Connexins are expressed in almost every cell type in the human body. Figure 5 summarizes the roles of connexin hemichannels and gap junctions in various organs and tissues[6].

Connexins (Cx) are proteins encoded by a multigene family of 21 members that typically form cell-cell channels. The most widely used nomenclature for connexins is based on predicted molecular mass (e.g. Cx32 for a predicted mass of ~32 kDa) [7].

Each connexin (Figure 4) has four α-helical transmembrane domains M1-M4 and two extracellular loops E1 and E2. NT and CT are N-terminal and C-terminal, respectively, and CL is the hydrophilic cytoplasmic loop. Within the connexin protein family, the most conserved parts are the N-terminal and the two extracellular loops. Differences in Cx molecular weights are mainly reflected in the length of the C-terminal end.

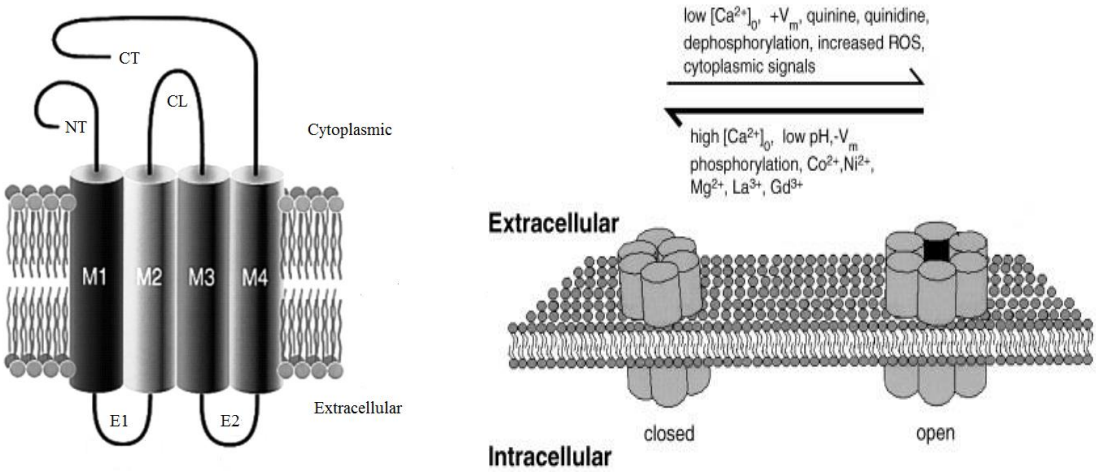

Figure 4.Membrane topology of a connexin monomer (left) and a cartoon showing some of the factors that influence the HCs gating (right) *(Modified from* [8]*).*

Connexins first oligomerize into hexameric structures, usually named *connexons*, in the Golgi apparatus, from where they are transported to the cell surface in vesicles. Here they fuse to the plasma membrane in an exocytotic process. Connexons transported to the plasma membrane are called *hemichannels* (HCs). Hemichannels can be formed by six identical (*homomeric*) or by different connexins (*heteromeric*) (Figure 6). HCs can be electrically and chemically activated, and mediate the rapid flow of ions across the membrane to regulate ionic homeostasis, and to facilitate the release ATP, NAD^{+}, glutamate and prostaglandins involved in autocrine and paracrine signaling, contributing to indirect intercellular communication.

Most hemichannels are activated by depolarization of the membrane potential, and channel opening is critically dependent on the concentration of extracellular Ca^{2+} ions and other divalent cations (**Errore. L'origine riferimento non è stata trovata.**). Also, HCs are regulated by intracellular Ca^{2+} concentration, but in opposite direction, increasing $[Ca^{2+}]_i$ from its resting value induces a significant opening of HCs. HCs formed by different Cx isoforms can differ significantly in their voltage regulation and external calcium. [9]

Connexin

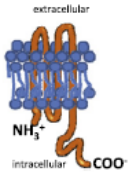

Role	Organ
Cell death	Brain, Inner ear, Kidney, Liver
Differentiation	Bone, Brain, Inner ear, Heart, Ovary, Lung, Liver
Proliferation/ survival	Brain, Bone, Heart, Lens, Ovary, Testis, Liver

Gap junction Channels

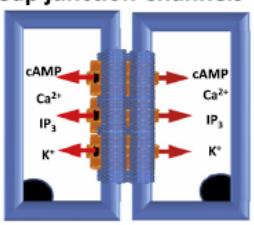

Role	Organ
Ionic conduction	Brain, Inner ear, Heart, Kidney, Lens, Lung, Liver
Metabolic coupling	Brain, Lens, Liver
2nd Messenger diffusion	Inner ear, Ovary, Lung, Liver

Hemichannels

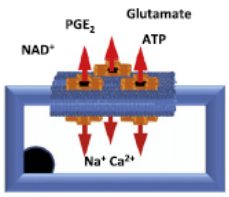

Role	Organ
Injury protection	Heart
preconditioning	Brain, Heart
Extracellular cell signaling	Bone, Brain, Kidney, Ovary, Lung, Liver
Mechanical stimulation response	Bone, Ovary

Figure 5. Gap junction channels and hemichannels formed by connexins play diverse roles in various organs and tissues.

Depending on the cell type and the connexin expressed, connexons can function as HCs providing a pathway for transmembrane signaling, or they can diffuse to dock with connexons of the neighbouring cells to form *gap junction channels* (GJCs), providing a pathway for the direct communication of two adjacent cells (Figure 5) [7]. The end-to-end docking process of two HCs is mediated by the extracellular loops, and this union is stabilized by hydrophobic interactions involving conserved cysteine residues. The functional gating of GJCs is primarily mediated by the cytoplasmic loop and the C-terminal segment. Two cells can form functional GJCs with an HC of different connexin composition, but not all connexins are compatible to form an intercellular channel. A GJC formed by from two different homomeric or heteromeric HCs is called *heterotypic*, while is called *homotypic* if the homomeric or heteromeric HCs are identical (Figure 6).

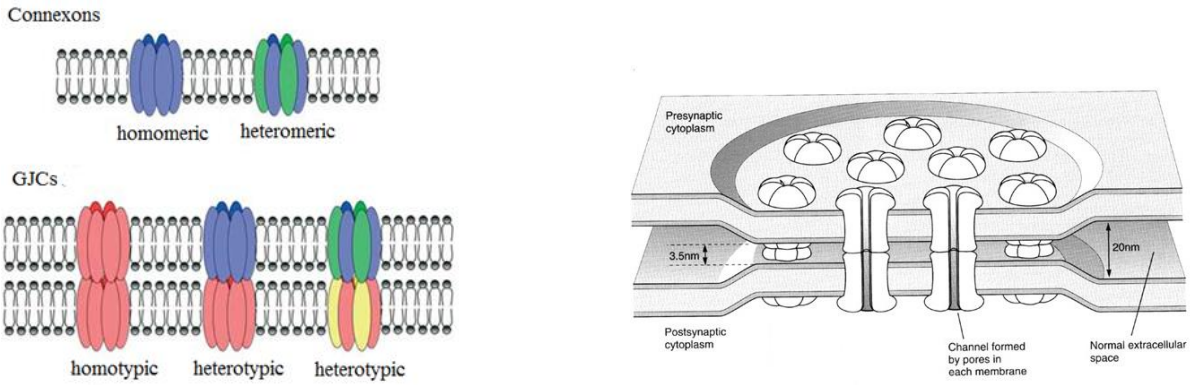

Figure 6. Different types of connexin hemichannels (left) and gap junction channels (right).

Gap junction plaques are clusters of GJCs that allow direct diffusion of ion and small molecules between adjacent cells (Figure 6). At the structural level GJs appear as specialized areas where two opposing membranes of adjacent cells come very close together so that the intercellular cleft is reduced to a width of about 2-3 nm. Each GJ is made up of many hundreds of intercellular channels [10].

The GJCs span through the membranes of adjacent cells and form an aqueous channel with a pore diameter between 6.5 and 15 Å that is permeable to hydrophilic molecules with molecular weight < 1kDa. This is a fundamental feature, because it provides a way for intercellular diffusion of ion for effective electrical coupling, as well as many cytoplasmic second messengers (e.g. $InsP_3$), nucleotides (ATP, ADP), metabolites and even vitamins. GJs may connect similar cells, forming a *homocellular gap junction*, or different cells, forming a *heterocellular gap junction* [7].

1.3.1 HEMICHANNELS DYSFUNCTIONS AND CONNEXINOPATHIES.

Since connexins are expressed in almost every cell type in the mammalians and have a fundamental role in cell and tissue homeostasis, it is expected that mutations in the connexin genes should be associated with a wide variety of diseases. These mutations have been linked to several human hereditary diseases, known as *connexinopathies*. Many mutations interfere with HC regulation by voltage and calcium. For example, mutations in Cx32 and Cx47 expressed in Schwann cells and oligodendrocytes provoke disorders, respectively, in peripheral and central myelin. This thesis work will focus on Cx32 mutations, which are known to give rise to a common peripheral neuropathy: the X-linked form of Charcot-Marie-Tooth disease (CMT1X) (See 1.3.2) [11].

For connexins, as for almost all membrane proteins, mutations result in defects in trafficking, folding or assembly. In addition, it is possible that mutant connexins could disrupt the function of other proteins with which they interact directly. When mutants form functional channels, the pathology could be caused by altered permeability properties or by altered channel regulation [7]. Table 2 summarizes the principal hereditary diseases associated with mutations in connexin genes.

Diseases	Inheritance pattern	Connexin protein	Gene
Oculodendrodigital Dysplasia	AD (AR)	Cx43	GJA1
Cardiavascular diseases			
Atrial fibrillation	AD/ND	Cx40	GJA5
Visceroatrial heterotaxia	ND	Cx43	GJA1
Cataract	AD	Cx46 Cx50	GJA3 GJA8
Myelin-related diseases			
X-linked Charcot-Marie-Tooth	XR	Cx32	GBJ1
Pelizaeus-Merzbacher-like disease	AR	Cx46.6/ Cx47	GJA12/ GJC2

Hearing loss (non-syndromic or non-associated with skin disorders)	AR/AD	Cx26 Cx30 Cx31	GJB2 GJB6 GJB3
Skin diseases			
Keratitis ichthyosis deafness syndrome	AD	Cx26 Cx30	GJB2 GJB6
Vohwinkel syndrome	AD	Cx26	GJB2
Clouston syndrome	AD	Cx30	GJB6
Erythrokeratodermia Variabilis	AD	Cx30.3 Cx31	GJB4 GJB4

Table 2. Connexinopathies and corresponding connexins and genes. *AD, autosomal dominant; AR, autosomal recessive; XR, X-linked recessive;ND, not determined.*

1.3.2 CHARCOT-MARIE-TOOTH DISEASE.

Charcot-Marie-Tooth disease is a group of inherited chronic progressive conditions affecting peripheral nerves, described for the first time in 1886 by Jean Martin Charcot, Pierre Marie and Howard Henry Tooth. As a group, these diseases are fairly common with a population frequency of 1 in 3000. Some forms are characterized by demyelination of peripheral nerves with a consequent axonal loss (CMT1); while other forms (CMT2) show only axonal loss. Individuals carrying mutations in the genes encoding Cx32 develop the X-linked form of Charcot-Marie-Tooth disease (CMTX) [12], [13].

Since the first mutation was reported in 1993, over 400 different mutations associated with CMT1X have been identified in the gene GJB1, on the X chromosome, that encodes for Cx32. Cx32 is most abundant in liver, but is also expressed by many other tissues, including kidney, intestine, lung, spleen, stomach, pancreas, uterus, brain, and peripheral nerve. Cx32 is expressed in particular in Schwann cells and oligodendrocytes and plays an important role in the homeostasis of the myelinated axons [14].

Many Cx32 mutants fail to form functional GJs or form GJs with abnormal biophysical properties, for example a gain-of-function that affects the channels permeation or their regulation by voltage and calcium [15].

The clinical phenotype of CMT1X is characterized by progressive distal muscle atrophy and weakness, areflexia, and variable sensory abnormalities. Symptoms arise in a length dependent distribution meaning that the longest nerves are involved earliest. Nerve conduction velocities are reduced. In addition, the reductions in conduction velocities are variable from one nerve segment to another.

CMT1X, as the other forms of the CMT disease, remains still now without cure, but different way have to be proved, like stem cell therapy. In this context, the possibility to generate Schwann cells and their precursors from adult non-neural tissue such as skin is of significant clinical interest. Schwann cells derived from stem cells can provide beneficial therapeutic effects in the peripheral nervous system by re-myelination, provision of trophic support, and a role in promoting axon regeneration.

1.4 PERIPHERAL NERVOUS SYSTEM.

The nervous system is a complex network of nerves and cells that carry messages to and from the brain and the spinal cord to various parts of the body. The nervous system is divided in two fundamental components: the *central nervous system* (CNS), which is made up of the brain and the spinal cord, and the *peripheral nervous system* (PNS). The peripheral nervous system consists of the nerves and ganglia outside the brain and the spinal cord. The function of the PNS is to connect the central nervous system to the body (muscles, glands, sensory receptors) and its organs (e.g. skin, heart, lungs), by the cranial and spinal nerves, which contain both sensory and motor fibers. The PNS is made up of the somatic (voluntary) and autonomic (involuntary, with sympathetic and parasympathetic divisions) nervous system.

In the nervous system two main types of cell can be identified: *neurons* and glial cells, usually named *glia*. They share many characteristics with cells in general, and develop from common neuroepithelial cells of the embryonic nervous system, and thus share many structural and molecular characteristics.

In the next sections are described the biophysical properties of neurons and glial cells of the peripheral nervous system, which are interested by the X-linked form of the Charcot-Marie-Tooth disease.

1.4.1 NEURONS.

Neurons are the core component of the nervous system. Compared to other cells they are endowed with the ability to communicate precisely and rapidly with other cells in the body. Two features give neurons this ability. First, they have a high degree of morphological and functional asymmetry: they have receptive dendrites at one end and a transmitting axon at the other. Second, neurons are both electrically and chemically excitable. Their cell membrane contains specialized proteins, ion channels and receptors, that facilitate the flow of specific inorganic ions. There are three main categories of neurons: *sensory neurons,* which respond to stimuli affecting cells of the sensory organs sending signals to the spinal cord and brain, *motor neurons* that receive signals from the CNS to cause muscle contraction and affect glandular outputs, and *interneurons*, which connect neurons within the same region of the CNS in neural networks. Given this general distinction, neurons are highly specialized for the processing and transmission of cellular signals from the various parts of the body, so they are expected to perform many different functions in different sites. This diversity of functions is expressed in a wide variety in their shape, size, and electrochemical properties. There are about 100 distinct types of neurons. This cytological diversity is apparent at the molecular level: although neurons all inherit the same complement of genes, each express a restricted set and thus produce only certain molecules (enzymes, structural proteins, membrane constituents) and not others. In large part, this expression depends on the cell developmental history.

Despite morphological differences between different types of neurons, in each neuron three different regions can be recognized: the *soma* or cell body, the *dendrites*, and the *axon*. The dimensions of these components vary widely between different types of neurons (e.g. the soma can range from 4 to 100 µm, and the axon has a variable length that can reach 1.5 meters in adults).

The soma is the body of the neuron, and is the site where most of the protein synthesis occurs, since it contains the nucleus of the cell. Axon and dendrites are filaments that extrude from it. The soma may give rise to numerous dendrites, but never to more than one axon. Dendrites typically branch profusely, getting thinner with each branching, and extending their longest branches for a few micrometers from the soma. The axon is thin, cable-like projection that can extend tens, hundreds, or even tens of thousand times the diameter of the soma in length, and emerge from the part of the soma called axon hillock. The axon hillock is also the part of the neuron that has the greatest density of voltage-dependent sodium channels: this

makes it the most easily excitable part of the neuron. Neurons have only one axon, but this axon undergoes extensive branching, enabling communication with many target cells. The axon terminal forms synapses, which are specialized structures where neurotransmitters are released to communicate with target neurons.

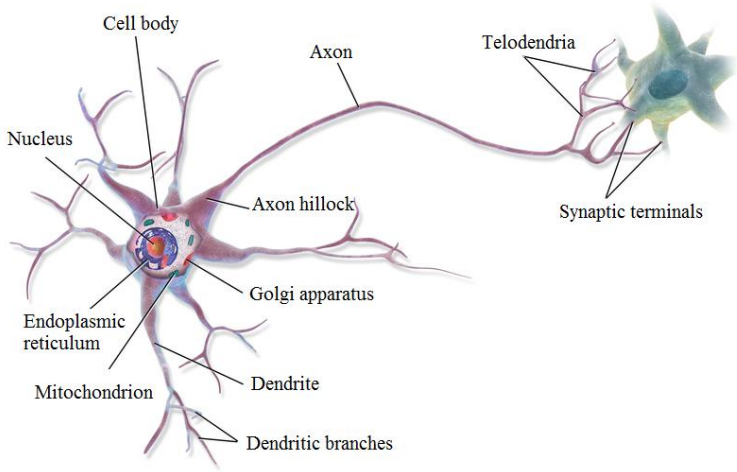

Figure 7. Structure of a typical PNS neuron.

The ability of carrying information by chemical and electrical signals is determined by the specific membrane properties of the neurons, the type channels expressed and their kinetics, because these signals are all produced by temporary changes in the electric current into and out of the cell.

Two types of channels, resting and gated, have distinctive roles in neuronal signalling. Resting channels are primarily important in maintaining the resting membrane potential, thus most of them are open in absence of signalling. In contrast, most voltage-gated channels are closed when the membrane is at rest and require depolarization[1] to open [4].

The resting potential of a neuron is determined, at first instance, by three main types of ion channels: K^+, Cl^-, and Na^+ channels. As discussed in 1.1.2 the resting potential is determined by the concentration of the ionic species present inside and outside the cell membrane, and by the ease with which the specific ion crosses the membrane. The resting potential can be derived from the Goldman equation, which gives for a neuron:

$$\mathrm{V_r} = \frac{\mathrm{RT}}{\mathrm{F}} \ln \left[\frac{\mathrm{P_K}[\mathrm{K^+Na^+}]_\mathrm{o} + \mathrm{P_{Na}}[\mathrm{Na^+}]_\mathrm{o} + \mathrm{P_{Cl}}[\mathrm{Cl^-}]_\mathrm{i}}{\mathrm{P_K}[\mathrm{K^+}]_\mathrm{i} + \mathrm{P_{Na}}[\mathrm{Na^+}]_\mathrm{i} + \mathrm{P_{Cl}}[\mathrm{Cl^-}]_\mathrm{o}} \right] = -70 \text{ mV} \tag{1.3}$$

The membrane of neurons rest at a negative voltage a bit above $\mathrm{E_k}$, because the permeability to K^+ ions is much higher that to other ions.

The usefulness of the Goldman equation is limited because it cannot be used to determine how rapidly the membrane potential changes in response to a change in the permeability. According to the equivalent

[1] Depolarization consists in a reduction or reversal of charge separation between the interior and the exterior of the cell, leading to a less negative membrane potential.

electrical representation for ionic channels (Figure 2) it is possible to describe the functional properties of the neuron as an equivalent electrical circuit.

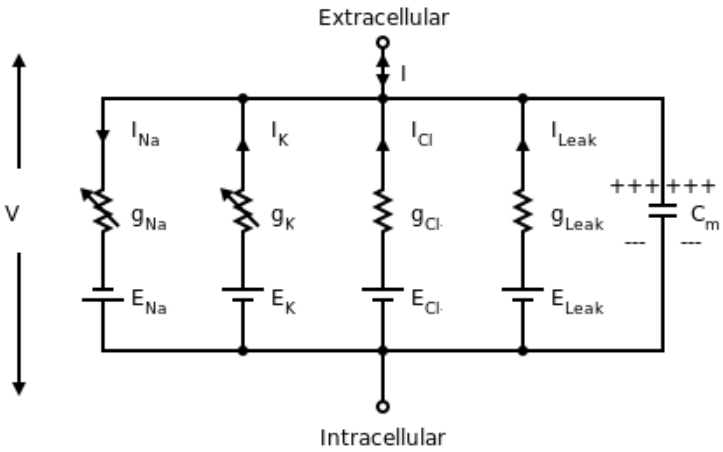

Figure 8. Equivalent circuit of a neuron.

Voltage-gated ion channels are characteristics of many non-excitable cells. In these cells, whose functions are other than to produce action potentials, ion channels may fulfil many roles, for example, maintenance of the resting potential, synthesis of ion channels for nearby excitable cells, buffering K^+ ions released by active nerves, and controlling proliferation.

An excitable cell generates a response which is very different from the passive behaviour: once the stimulus current exceeds certain value, the threshold, the voltage shoots up to a value which is close to the Nernst potential for Na^+ ions, then undershooting the initial voltage before returning back to the resting potential. This phenomenon is called *action potential*. Action potentials cannot be explained with static membrane properties; however, these properties influence the speed at which the action potential is propagated.

Action potential have four important properties, that influence the characteristics of neuronal signaling. First, they have a threshold for initiation, around -50mV. Second, the action potential is an all-or-none event. The size and the shape of two action potentials generated by two different depolarizing current pulses above the threshold are identical. Third, the action potential is conducted without decrement over Finally, action potential is followed by a refractory period during which the cell is not able to fire further action potentials.

Voltage-gated currents related to $Na^+$and K^+ ion channels. can be easily studied in patch-clamp experiments. The form of an action potential results from the combination of the characteristics of these channels.

The mechanisms of action potential generation can be summarized with following six steps:

1. The activation point (around -55 mV) for sodium channels is reached, thus sodium channels open causing a sodium influx. An inward sodium current, $I_{Na} = g_{Na} * (V_m - E_{Na})$, where $g_{Na}$is the conductance of all sodium channels, is generated.
2. The membrane potential becomes more and more positive, due to the sodium influx, and moves towards E_{Na} (55 mV). Now the potassium channels open and potassium leaves the cell.

This movement of Na^+ ions accounts for the rising phase of the action potential. If nothing else happened, the action potential would be one-way event. Fortunately, there are other two voltage-activated processes that follow Na^+ channels activation and limit the time spent near E_{Na}.

3. At the peak, the sodium channels inactivate since the membrane is made positive to E_{Na}. The force pushing Na^+ out is now greater than the chemical driving force pulling Na^+ in, and hence I_{Na} becomes outward.
4. During the downfall phase of the action potential, sodium channels are still inactive, thus only potassium ions are passing through the membrane. As potassium is leaving the cell the membrane potential starts to approach to the resting value.
5. At this point, potassium channels close and sodium channels begin to leave the refractory phase and reset to its resting phase.
6. The diffusion of potassium away from the cell causes a very slight increase in membrane voltage. It finally returns to its resting value where it stays until a new action potential is generated.

The period between 5 and 6 is called refractory period and it prevents the action potential from travelling backward.

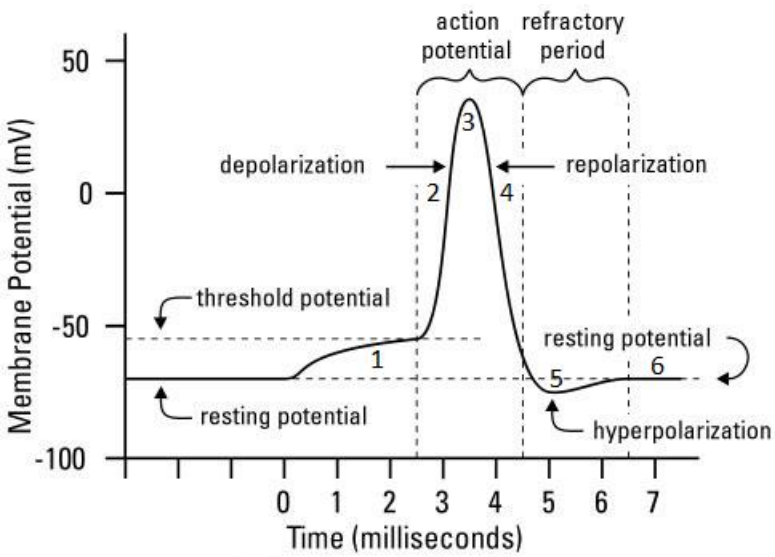

Figure 9. Action potential.

For almost 100 years, since the first action potential was observed in the mid-1800s, biologists were studying this phenomenon, when Alan Hodgkin, Andrew Huxley, and Bernard Katz provided the first quantitative insight into the mechanisms underlying the action potential. In particular, Hodgkin and Huxley developed a mathematical model, based on the experimental observations, which explains and predicts the form of the action potential on the basis of the characteristics of the voltage-gated Na^+ and K^+ ion channels. Voltage-gated $K^+$and Na^+ channels similar to those described by Hodgkin and Huxley have been found in almost every type of neuron examined. In addition, most neurons contain voltage-gated Ca^{2+} channels that open in response to membrane depolarization.

The nervous system of almost all mammalian is a very complex architecture with the ability to process many different kinds of complex information. Thus, many different types of neurons are required to carry out all the functions required to the nervous system. The distinction between the various types of neurons is determined by their morphology and electrical properties. In particular, the electrical properties can be

fine-tuned through the expression of a distinct complement of ion channels to match the dynamic demand of the information processed by the cell. Therefore, each type of ion channel is expressed in many variants that differ in their kinetics, voltage-activation range, and sensitivity to various ligands. There are several types of K^+ channels. Four of these variants are particularly important for the nervous system. The slowly activating K^+ channels described by Hodgkin and Huxley are called *delayed rectifier channels*. The *calcium-activated channels*, are activated by an increase in the intracellular $Ca^{2+}$when nearby voltage-gated Ca^{2+} channels open in response to depolarization. The *a-type K^+channels,* activated rapidly by depolarization, almost as rapidly as the Na^+ channels, and also inactivated rapidly when the depolarization is prolonged. The *M-type K^+ channels* require only a small depolarization to open; however, they activate very slowly, requiring ten milliseconds to open. Similarly, at least five major types of voltage-activated Ca^{2+} and eight types of voltage-gated Na^+ channels are expressed in the nervous system. This great heterogeneity in the channels gives to neurons the ability to process very complex information. In a typical neuron, the opening and the closing of these channels can be modulated by various cytoplasmic factors, like the calcium concentration, and by the action of neurotransmitters [4].

The distribution and the type of voltage-gated channels is different in different regions of the neuron. Each type of channels is specialized for supporting the specific function of the interested region of the cell. For example, the axon is specialized in carrying signals over long distances; thus, a as a simple relay line. The conduction down the axon is mediated primarily by voltage-gated sodium and potassium channels similar to that of the squid giant axon. In contrast the input integrative, and output regions typically perform more complex processing of the information they receive, before passing it along. Dendrites in many types of neurons have voltage-gated ion channels, such as Ca^{2+}, K^+, HCN, and Na^+channels. In some neurons, the action potential forms in a trigger zone at the initial segment of the axon. This region has the lowest threshold for action potential generation because of the high density of Na^+ channels.

Detailed molecular studies have revealed that all voltage-gated channels have a similar architecture. These channels are composed of pore-forming α-subunits. Each of these subunits contains six transmembrane segments (S1-S6). A seventh hydrophobic region, called *P-region*, connects the S5 and S6 segments. It forma a loop that deeps into and out of the extracellular side of the membrane and forms the selectivity filter of the channel. All voltage-gated K^+ are made up of four pore-forming subunits, each of which contributes one P-region to the pore fully assembled channel. Voltage-gated Ca^{2+} ad Na^+channels conisist in one large pore-forming subunits containing four internal repeats of this basic motif [4].

1.4.2 THE HODGKIN-HUXLEY MODEL.

The Hodgkin-Huxley model provides a quantitative description of $K^+$and Na^+channels that are responsible for the generation of the action potential. The model is based on the idea to predict the electrophysiological properties of a neuron from its equivalent electrical circuit [16].

The first step of the description of the circuit is to write the total current flowing across the cell membrane:

$$C_m \frac{dV_m}{dt} + I_{ion} = I_{ext}, \tag{1.4}$$

where C_m is the membrane capacitance, V_m is the membrane potential, and I_{ion} is the net ionic current flowing across the membrane. The most significant advantage is that the capacity and the ionic currents are completely separated.

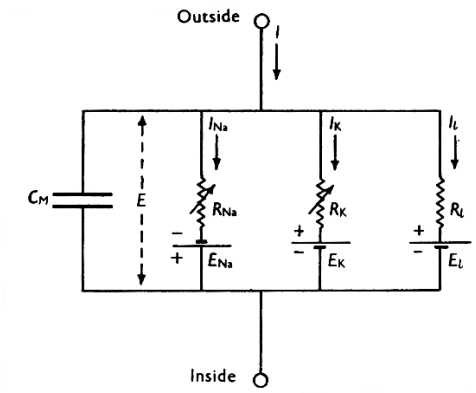

Figure 10. Equivalent electrical circuit for a neuron used in the Hodgkin-Huxley original model [16]**.**

Hodgkin and Huxley focused their studies on the ionic currents, developing a model based on electrophysiological recording on the giant squid axon. The ionic currents of the axon can be divided into three main categories: potassium, sodium, and leakage currents. The movement of each of these currents is proportional to the conductance times driving force:

$$I_{Na} = g_{Na}(V_m - E_{Na}), \quad (1.5.A)$$
$$I_K = g_k(V_m - E_K), \quad (1.5.B)$$
$$I_L = g_L(V_m - E_K). \quad (1.5.C)$$

The solution of this system of equations to obtain the ionic conductances is less simple than expected, since the conductances of the channels are functions of the time. Furthermore, it is important to note that every channel could contain many gates. Each gate can be in a *permissive* (i.e it allows ions to pass through) or in a closed state. The probability to be in the permissive state depends, in turns, on the value of the membrane voltage.

Now, if p_i is the probability of a gate to be open, it can also be thought as the fraction of the gates in the permissive state. Consequently (1-p_i) will be the fraction of gates in the closed state. The transition between the open and the closed state of a gate is a two-state kinetic process with the rate constants α_i and β_i:

$$C \underset{\beta_i}{\overset{\alpha_i}{\rightleftarrows}} O; \quad (1.6)$$

To obey the first-order kinetics of such a process, the differential equation that describes the evolution of p_i during time must be [17]:

$$\frac{dp_i}{dt} = \alpha_i(V)(1 - p_i) - \beta_i(V)p_i \quad .(1.7)$$

All gates must be in the permissive state for a channel to be considered open. When this occurs, the channel will contribute to the total conductance of the specific type of channels, which can be written as:

$$g_i = \bar{g}_i \prod_i p_i, \quad (1.8)$$

where $\bar{g}_i$ is the normalized constant that determines the maximum conductance when all the channels are open.

Hodgkin and Huxley labelled the probability of the gate to be in the permissive state as the name of the specific gate. They named the three gates as -*m, n,* and *h*, obtaining the following differential equations:

$$\begin{cases} \dfrac{dn}{dt} = \alpha_n(V)(1-n) - \beta_n(V)n, & \text{(1.9. A)} \\ \dfrac{dm}{dt} = \alpha_m(V)(1-m) - \beta_m(V)m, & \text{(1.9.B)} \\ \dfrac{dh}{dt} = \alpha_h(V)(1-h) - \beta_h(V)h. & \text{(1.9.C)} \end{cases}$$

In the resting state, defined by V=0, *n* has a resting value given by:

$$n_0 = \frac{\alpha_{n_0}}{\alpha_{n_0} + \beta_{n_0}}. \tag{1.10}$$

When the voltage is changed to V_c, the steady state becomes:

$$n_\infty = \frac{\alpha_n\,(V_c)}{\alpha_n\,(V_c) + \beta_n\,(V_c)}. \tag{1.11}$$

The solution of the equation 1.9.A which satisfies the boundary condition that $n = n_0$ at *t=0* is

$$n = n_\infty(V_c) - (n_\infty(V_c) - n_0)e^{-t/\tau_n} \tag{1.12}$$

In the same way, the equation for *m* and *h* can be solved, obtaining the following expressions:

$$m = m_\infty(V_c) - (m_\infty(V_c) - m_0)e^{-t/\tau_m}, \tag{1.13.A}$$

$$h = h_\infty(V_c) - (h_\infty(V_c) - h_0)e^{-t/\tau_h}. \tag{1.13.B}$$

Also, the exponential time constants can be expressed as functions of the rate constants:

$$\tau_m = \frac{1}{\alpha_m + \beta_m}, \tau_h = \frac{1}{\alpha_h + \beta_h}, \tau_h = \frac{1}{\alpha_h + \beta_h}. \tag{1.14}$$

Each class of channels has a specific amount of these three gates. Observing the sodium currents recorded during a voltage clamp experiment, it is evident that the inactivation process can be described with an exponential trend. In contrast, the activation phase shows a sigmoidal behavior. The rising phase of the sodium currents looks like an exponential raised at the third power. This suggests that there are three independent subunits within the Na^+channel protein. All of the subunits must be in the permissive state to open the channel. This gives an m^3 in the expression of the total sodium current, which accounts for the channels with all three voltage-sensing units activated. To obtain the fraction of channels that have undergone activation, but have not yet inactivated, is sufficient to multiply m^3 by *h*. Thus, the sodium channels conductance will be:

$$g_{Na} = \bar{g}_{Na} h m^3 \tag{1.15}$$

Doing similar considerations on recorded potassium currents, Hodgkin and Huxley obtained the following expressions for the potassium channels conductance:

$$g_K = \bar{g}_K n^4 \tag{1.16}$$

Thus, inserting the new expressions for potassium and sodium conductances in 1.5.A and 1.5.B they obtained the following expression for the total ionic current:

$$\begin{aligned} I_{ion} &= \bar{g}_{Na} m^3 h (V - E_{Na}) - \bar{g}_K n^4 (V - E_K) - \bar{g}_l (V - E_l) = \\ &= \bar{g}_{Na} (m_\infty(V) - (m_\infty(V) - m_0) e^{-t/\tau_m})^3 (h_\infty(V) - (h_\infty(V) - h_0) e^{-t/\tau_h})(V - E_{Na}) + \\ &- \bar{g}_K (n_\infty(V) - (n_\infty(V) - n_0) e^{-t/\tau_n})^4 (V - E_K) + \\ &- \bar{g}_l (V - E_l). \end{aligned} \tag{1.17}$$

The last step is to derive the expressions of the rate constants as functions of the voltage by taking for nay voltage the values of τ_n and n_∞, and solving the equation 1.11 for α_n and β_n. The same can be done for *h* and *m*, obtaining the following expressions:

$$\alpha_m(V) = \frac{0.1(25 - V)}{e^{\frac{(25-V)}{10}} - 1}, \qquad \alpha_n(V) = \frac{0.01(10 - V)}{e^{\frac{(10-V)}{10}} - 1}, \qquad \alpha_h(V) = 0.07 e^{\frac{-V}{20}}, \tag{1.18.A}$$

$$\beta_m(V) = 4.0 e^{-\frac{V}{18}}, \qquad \beta_n(V) = 0.125 e^{\frac{V}{80}} \qquad \beta_h(V) = \frac{1}{e^{\frac{(30-V)}{10}} - 1} \tag{1.18.B}$$

Finally, the expression for the total ionic current has to be inserted in the equation (1.4), giving the following equation that describes the circuit behaviour during time:

$$C\frac{dV}{dt} = \bar{g}_K n^4 (V - E_K) + \bar{g}_l (V - E_l) - \bar{g}_{Na} m^3 h (V - E_{Na}) + I_{ext} \tag{1.19}$$

Combining the equations 1.19 and 1.9.A, B, C, using the rate constants expressions 1.18.A, B, Hodgkin and Huxley obtained a complete system of equations that, once solved, generates the classic action potential shape observed in the current clamp experiment.

The great advantage of this mathematical model is that it can be adapted and extended to predict the behaviour of different classes of neurons of different species. In this work, we will use this model as a tool to help the interpretation of the experimental data recorded during patch clamp experiments on motor neuron derived from MSCs.

1.4.2 GLIAL CELLS IN THE PNS: SCHWANN CELLS.

Glial cells greatly outnumber neurons, there are 2 to 10 times more glia than neurons in the vertebrate CNS. The name of these cells derives from the Greek γλία which means glue, but glia do not commonly hold nerve cells together. Rather they surround cell bodies, axon and dendrites of neurons. Glia differ from neurons morphologically, they do not form axons and dendrites, and also functionally. Although they develop from the same embryonic precursor cells, their membrane properties are different from those of the neurons: they are not electrically excitable and not directly involved in electrical signalling. There are many kinds of glial cells. Nonetheless, glia in vertebrate nervous system can be divided in two major classes: *microglia* and *macroglia.* Microglia are immune system cells, while macroglia are part of the nervous system. Macroglia are divided into three classes: oligodendrocytes, Schwann cells, and astrocytes. Astrocytes are star-shaped glia cells found in the central nervous system. Their functions include: separation of the cells, thereby insulating neural groups, regulation of K^+concentration in the space between neurons, helping nourish surrounding neurons by releasing growth factors. Oligodendrocytes and Schwann cells are small cells with relatively few processes. Both cells form myelin sheath that insulate axons by tightly winding they membranous processes around the axon in a spiral. Oligodendrocytes are found in CNS, while Schwann cells are typical of the PNS [4] .

Schwann cell are one of the four major types of glial cell of the PNS. The others are: satellite glial cells, found in sensory parasympathetic and sympathetic ganglia, enteric glial cells, localized in the ENS, and olfactory ensheathing cells, which resides in the PNS and CNS portions of the primary olfactory system [18].

Three key physiological features appear to be common to most PNS glia, like the CNS counterparts:

- K^+ channels are the most abundant in glial cells, thus the K^+ conductances dominate over all other ion conductances.
- They are interconnected by gap junctions, with prominent role of Cx32 in Schwann cells and Cx43 in other PNS glia.
- They exhibit Ca^{2+} excitability, via ATP and P2 receptors.

In addition, PNS glial cells provide trophic support for neurons and are central to the injury response and the capacity for regeneration in the PNS[18].

Schwann cells play a fundamental role in the PNS, because of their myelinating function and their role in nerve pathology and repair.

There are two, equally numerous, types of Schwann cells: *myelinating* and *non-myelinating* Schwann cells. The divergence of myelinating and non-myelinating Schwann cells is determined by the diameter of the axons they associate with: axons above a critical diameter of 1µm become myelinated, while smaller axons remain unmyelinated. Myelinating Schwann cells can be identified by their expression of myelin proteins, which are not expressed in other PNS glia.

Non-myelinating Schwann cells surround small-diameter unmyelinated axons. They serve multiple functions, physically supporting and separating axons with fine processes as well as providing trophic support and ion homeostasis. A series of sequentially apposed Schwann cells surrounding the same group of axons, usually named as *Remark fibre* or bundle. A small space exists between the axonal and Schwann cell membranes (about 15 nm) that is continuous with the extracellular space via the a mesaxon, formed when a Schwann cell engulfs ad folds over an axon. These axons, commonly named *unmyelinated axons*.

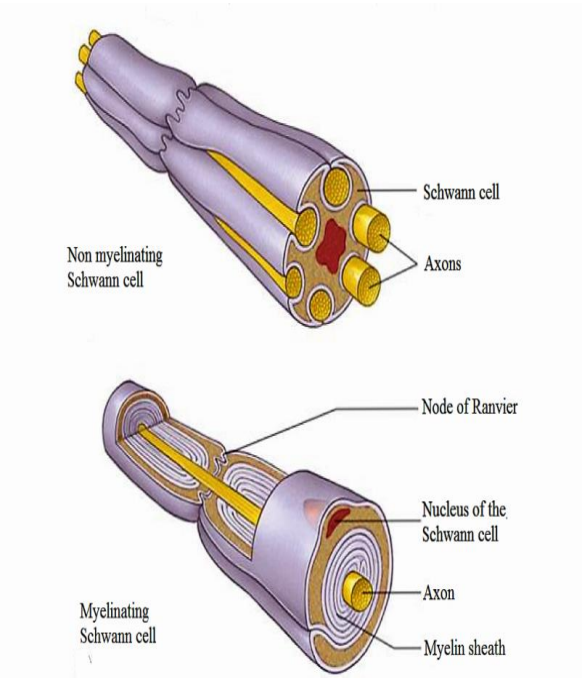

Figure 11. Schwann cells subtypes. *Non-myelinating Schwann cells (top) and myelinating Schwann cells (bottom).*

Myelinating Schwann cells have a relation 1:1 with axons. They surround axons with diameter above 1µm, forming a multilamellar structure that ensheathes axons. Each myelin-generating cell provides myelin for only one segment of a given axon. The periodic interruptions where short portions of the axon (1mm) are left uncovered by myelin are called *nodes of Ranvier*, whereas segments of myelinated axon between two nodes of Ranvier are called *internodes.* A high density of Na^+ channels is found at the nodes, amounting to 1500-200 μm^{-2}, more than sufficient to discharge the small electrical capacities of the node and adjacent myelin sheath.

The myelin sheath in the PNS is composed of two distinct domains, compact myelin and non-compact myelin, each containing distinct proteins. Compact myelin contains protein zero, peripheral myelin protein of 22 kD, and myelin basic proteins

The non-compact myelin is localized in proximity of the Ranvier nodes. The loop-shaped termination of the sheath at the node are called *paranodes*. Paranodes are cytoplasmic pockets of the respective Schwann cell. They form helix-shaped cytoplasmic bands, called *transverse bands,* that seal the myelin to the axolemma. The paranodes are laterally connected by *reflexive gap junctions* formed by Cx32. Reflexive GJs are also present in Schmidt-Lantermann incisures, which are structures where the cytoplasmic surface of the myelin sheath is not compact and therefore contains Schwann cell cytoplasm. These inclusions of cytoplasm are present in each layer of myelin. Reflexive gap junctions in non-compact myelin promote intracellular communication, since they provide a radial pathway across the myelin sheath. This pathway speeds up the communication trough the myelin layers that separate the adaxonal and abaxonal cytoplasm allowing the passage of important signalling molecules like Ca^{2+}, cAMP, cGMP, IP_3, and ATP. Furthermore this pathway could facilitate the spatial buffering of extracellular K^+, which permits the renewal of action potential propagation along the axon [19]. It is found that Cx32 HCs release ATP suggesting that they are also involved in the myelination and survival of the Schwann cell [9].

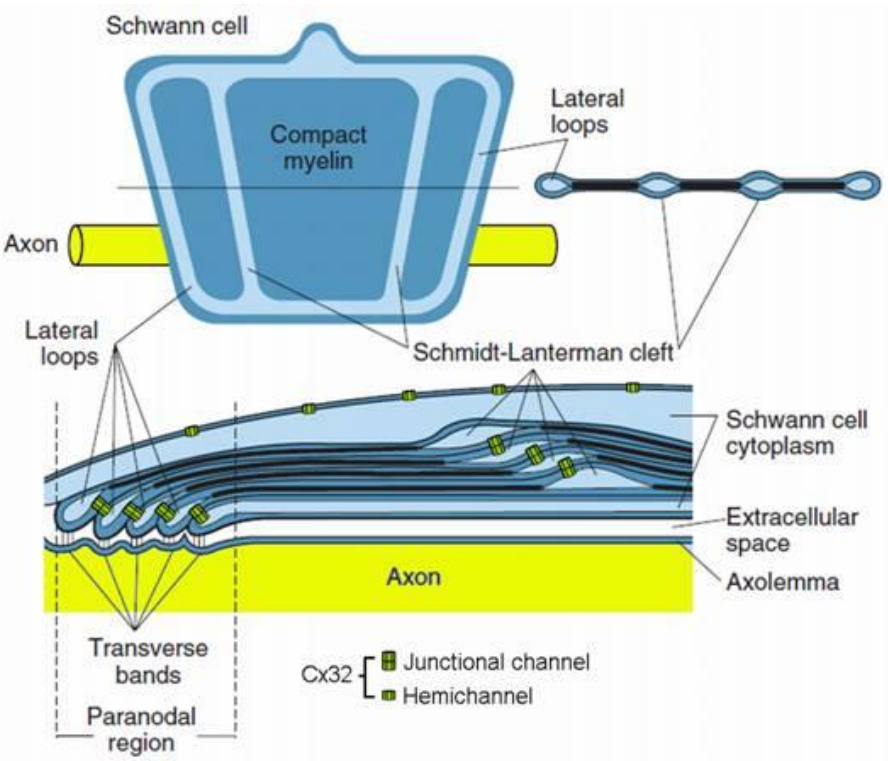

Figure 12. Myelin sheath in PNS. *The sheath is surrounded by a tube of cytoplasm and has additional tubes of cytoplasm, which make up Schmidt- Lantermann incisures, running through the internodal region. The horizontal section (top right) shows that these additional tubes of cytoplasm arise from regions where the cytoplasmic membrane have not fused. The diagram at the bottom is an enlarged view of a portion of the top left diagram, with the Schwann cell and its membrane wrapped around the axon. Cx32 forms junctional channels through the layers of non-compact myelin in paranodes and Schmidt-Lantermann incisures.*

Myelin is an electrical insulator and its function is to increase axonal conduction velocity by restricting the depolarizing ionic fluxes that generate the action potential to nodes of Ranvier. When the membrane at the node is excited, the local circuit generated cannot flow through the high resistance sheath and therefore flows out through and depolarize the membrane at the next node, which might be 1mm or farther away. Active excitation of the axonal membrane jumps from node to node; for this reason, this form of impulse propagation is called *saltatory conduction* (Figure 13) [20]

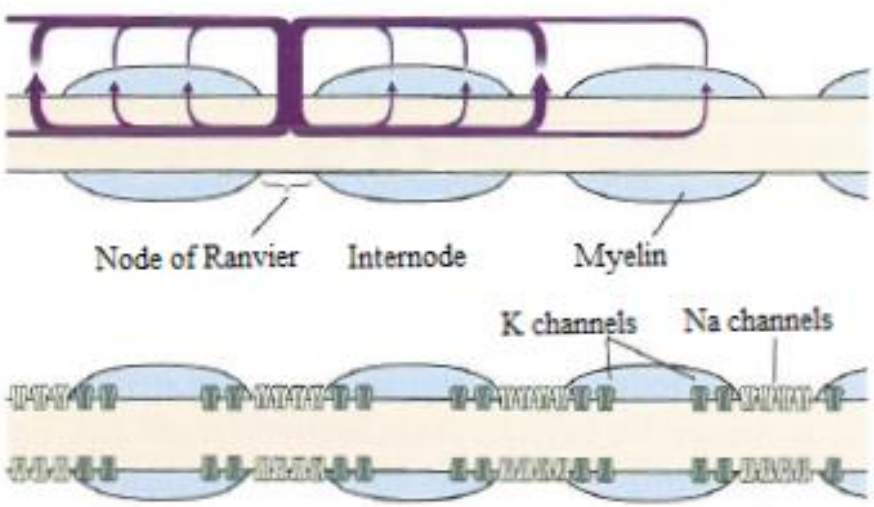

Figure 13. Myelinated axon

Unlike neurons Schwann cells are non-excitable cells. The non-excitability is determined by two factors. The first is the low density of Na channels, approximately 100-10000 times lower than that of the neurons. The second is the high K^+ permeability, which prevents the generation of regenerative action potentials. Schwann cells present both voltage-gated and non-voltage-gated channels, as well as receptor-operated channels. Voltage-gated channels are of particular interest for this work since they can be studied by patch clamp experiments. The main types of voltage-gated ion channel expressed by Schwann cells are K^+, Cl^-, Na^+, and Ca^{2+} channels.

The resting membrane potential for mammalian Schwann cells in culture is around -40 mV, mainly determined by potassium channels [21].

Schwann cells express both TTX-sensitive and TTX-resistant Na channels, activated by changes in the extracellular sodium concentration. In culture, they express Ca^{2+} channels with properties of L-type and T-type channels. The physiological role of Ca^{2+} channels in Schwann cells is unclear, although it has been suggested that they could contribute to the control of myelination. K^+ channels are the most abundant in glial cells, thus the K^+ conductances dominate over all other ion conductances. The main types of potassium channel are listed below [21].

1. *Inward rectifier K^+channels (Kir)* that conduct K^+ into the cell in response to hyper-polarizing voltage stimuli.
2. *Voltage -activated channels,* represented by *delayed rectifier (K_{dr})* and *inactivating channels (K_A)*.
3. *Ca^{2+}-activated K^+ channels.*

At least two types of K_{dr} were recognized. These channels are characterized by a linear I-V relation at potential more positive that the activation threshold of the channels. The two types, $\mathrm{K_{dr}^{fast}}$and $\mathrm{K_{dr}^{slow}}$, differ in voltage dependence, kinetic of activation (fast and slow) and sensitivity to α-dendrotoxin. These two types of channels are involved in the determination of the resting potential of the cell: cells that express only $\mathrm{K_{dr}^{slow}}$ channels show a resting of about -24 mV, while those that express $\mathrm{K_{dr}^{fast}}$ have a resting potential of -44 mV [21], [22] . Furthermore, there is some evidence that $\mathrm{K_{dr}^{slow}}$ could be involved in the regulation of Schwann cells proliferation. The family of inward rectifier $\mathrm{K^+}$channels undergoes a variety of intracellular regulations. These channels effectively contribute in forming a $\mathrm{K^+}$ leakage conductance in the cell membrane, and are expected to contribute to setting the resting potential.

1.5 Stem Cells.

The advances in medicine and biology have opened the possibility to use stem cells for different purposes thanks to their therapeutic potential. Nowadays, stem cells are used for gene therapy, cell therapy, and drug screening.

Stem cells are cells that have the potential to differentiate into many different types of cells in the body during early life and growth. In addition, in many tissues they serve as a sort of internal repair system, dividing essentially without limits to replenish other cells as long as the person or the animal is still alive. Stem cells can also divide through mitosis to produce more stem cells.

Stem cells are distinguished from the other types of cells by two important characteristics: the *self-renewal ability*, which is the ability to generate daughter cells identical to their mother while maintaining the undifferentiated state, and the ability to produce progeny with more restricted potential (*differentiated cells*). Another functional parameter that should be included in the definition of a stem cells is the *potency,* which describes the potential to produce differentiated cells. The self-renewal and differentiation abilities are attributed to the signals that the stem cells receive from their microenvironment, the *stem cell niche*. The stem cell niche is a restricted locale in an organ that supports the self-renewing division of the stem cells and so prevent them from differentiation [23].

According to the differentiation potential, stem cells are classified as *totipotent, pluripotent*, *multipotent*, and *unipotent.*

Totipotent stem cells are cells derived from embryos at the 4-8 cell stage (around 1-3 after the fertilization), which can differentiate into any and all human cells. After four days of embryonic cell division, the cells begin to specialize into pluripotent stem cells.

Pluripotent stem cells are embryonic cells at the blastocyst stage (4-14 days after fertilization). These cells are able to differentiate in the three germ layers of the embryonic tissue: ectoderm, mesoderm, and endoderm.

Multipotent stem cells are cells at the stage of gastrula. As well as the adult stem cells have the ability to multiply and renew in culture only a limited number of time, and they can differentiate into different tissues of the same embryonic package.

Unipotent stem cells constitute the stem cells population that resides in the adult tissue. They are able to self-renew, but can differentiate only into cell types of the original tissue, ensuring its repair and maintenance. Therefore, are also called *progenitor cells*.

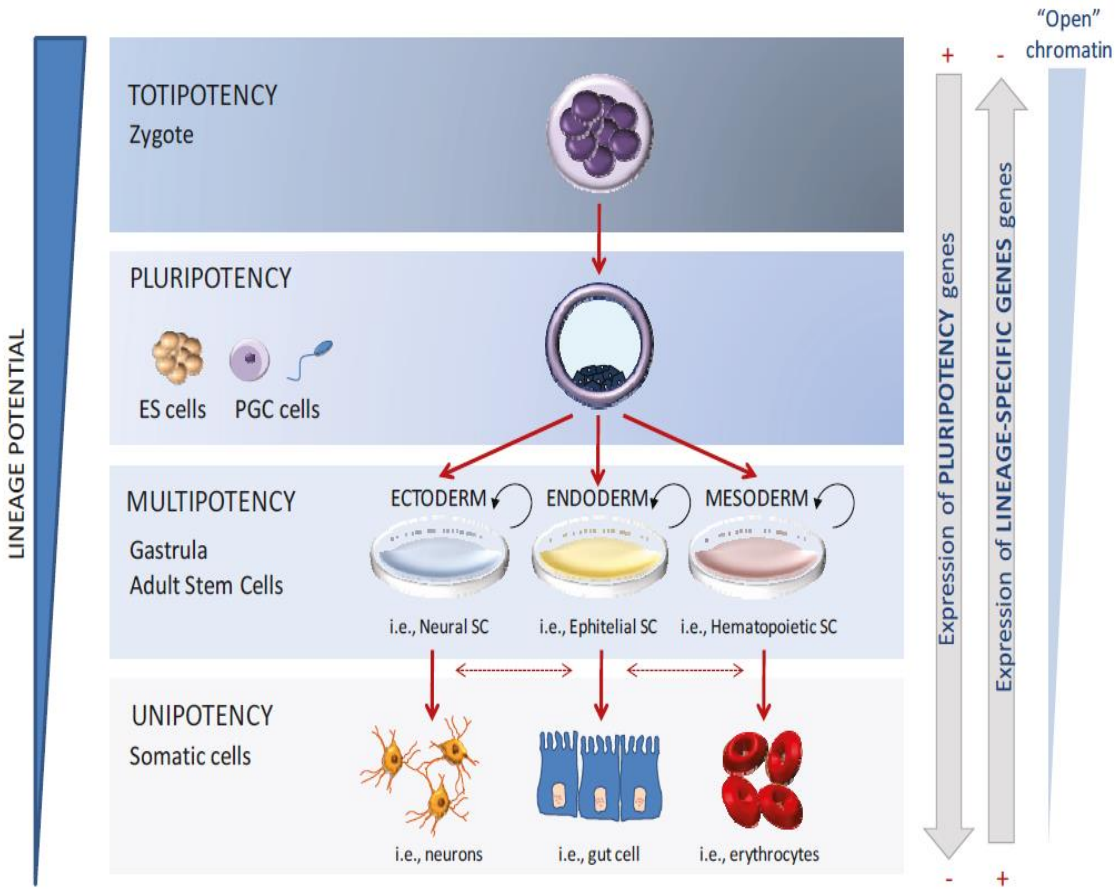

Figure 14. Stem cells classification [24]**.**

Stem cells can be, also, classified, according to their tissue of origin, as: *embryonic stem cells (ESCs)*, *mesenchymal stem cells (MSCs)*, and *skin derived precursors (SKPs)*.

Embryonic stem cells are pluripotent stem cells derived from the inner cell mass of the blastocyst, from which the embryo itself will originate. ESCs can give rise to cells from any of the three germ layers: ectoderm, endoderm, and mesoderm.

Skin derived precursors are multipotent Neural Crest (NC)-like stem cells distinct from MSCs, arising in mid-embryogenesis and persisting in lower number in the adulthood.

Mesenchymal stem cells are multipotent stem cells that belong to the mesodermal lineage and can be isolated from mesenchymal tissue, such as umbilical cord, dermis, adipose tissue, and peripheral blood.

Cell-based therapy on MSCs gave an important relevance in regenerative medicine because they can be induced to differentiate in a broad spectrum of cells (Figure 15) for the replenishment of lost cells. Thanks to this capability to differentiate in a wide variety of cells, MSCs are become an attractive cell source, making simple the generation of a very realistic model of different diseases. Mesenchymal stem cells extracted from skin exhibit mesenchymal as well as neuroglial potential if grown in media specialized for neural precursors propagation. For this reason, they represent a realistic therapeutic alternative to other sources as bone marrow, since the extraction from dermis is less invasive and more accessible respect to the other sources.

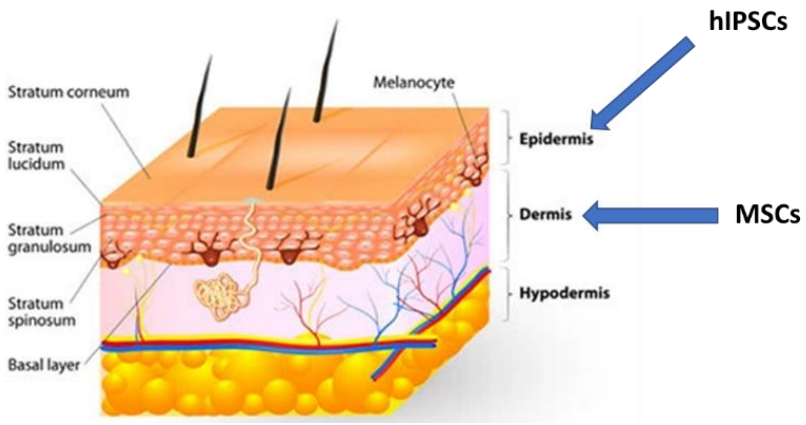

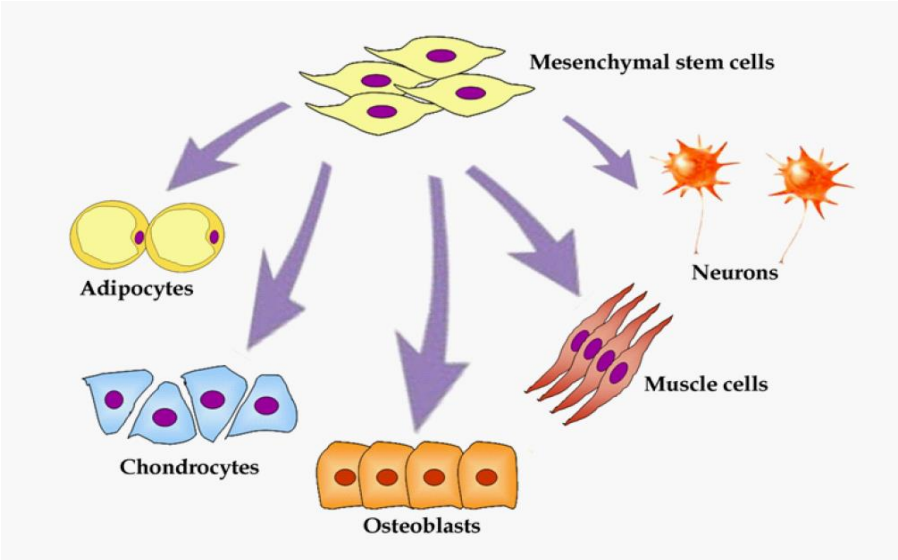

Figure 15.Origin and Differentiation potential of MSCs. *MSCs can differentiate in a large variety of human tissues including osteogenic, chondrogenic, adipogenic, and neuronal lineages. Recently, it was also demonstrated the presence of MSC-like cells in adult skeletal muscle*

Induced pluripotent stem cells (*IPSCs*) are derived by expressing pluripotency genes in differentiated adult somatic cells. This process reprograms the cells back in time, to embryonic-like pluripotent state. These pluripotent cells can be differentiated in almost any cell type of the human body. Furthermore, when taken from patients with specific neurological diseases they can be used to create powerful *in vitro* models to study the molecular basis of the disease and to test pharmacological approaches. The first iPSCs were obtained by Shinya Yamanaka in 2006, who showed that the introduction of four specific genes encoding transcription factors (Oct4, Sox2, c-Myc, and Klf4) could convert adult cells into pluripotent stem cells. The first human iPSCs were obtained by fibroblasts in November 2007.

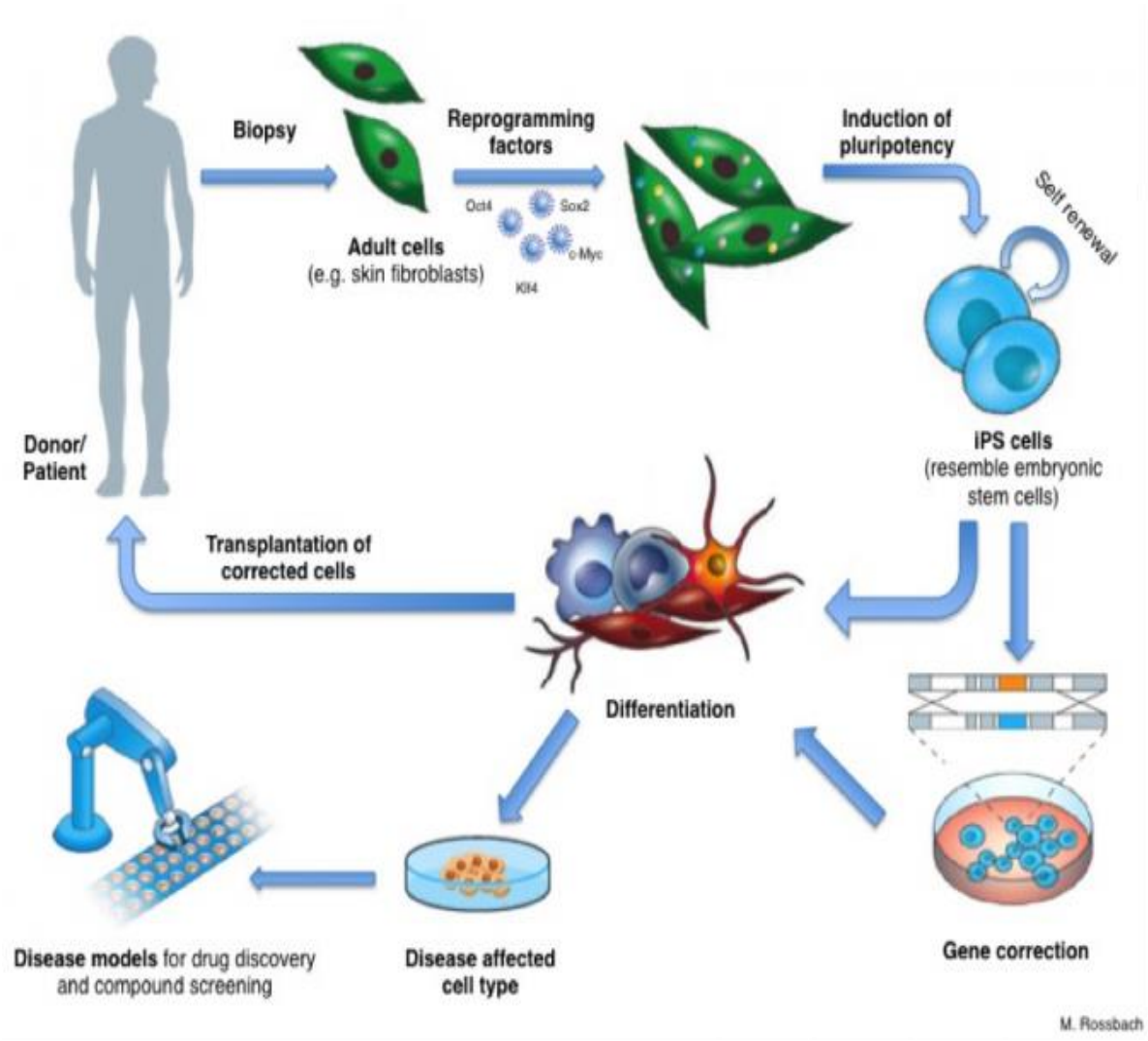

Figure 16. Potential applications of induced pluripotent stem cells (IPS) .

One of the most important advantages of iPSCs compared to the ESCs is that the fibroblasts needed to produce iPSCs can be obtained with a simple skin biopsy. Thanks to their ability to differentiate into all somatic cells type, iPSCs bear a promise to advance biomedical research and regenerative medicine. Transplantation of functional cells to replenish lost tissue has been proposed as a strategy to treat neurodegenerative diseases. For this kind of therapies, the use of patient-derived cell generated by the reprogramming is an advantage, as autologous cells are predicted to avoid immune system rejection after transplantation.

2. MATERIALS AND METHODS.

The first section is dedicated to the theoretical description of microscopy techniques. The middle part describes fundamentals of the patch-clamp technique, and the setup used for patch-clamp experiments. The final part describes briefly the procedures used for the cell culture and preparation, more detailed information about this argument can be found in the Appendix A and B, where the detailed protocols are reported.

2.1 MICROSCOPY TECHNIQUES.

2.1.1 DIFFERENTIAL INTERFERENCE CONTRAST (DIC) MICROSCOPY.

Differential Interference Contrast microscopy, also known as Normanski Interference Contrast microscopy, is an optical microscopy technique used to enhance the contrast in unstained, transparent samples. DIC works on the principle of interferometry to gain information about the optical path length of the sample, to see otherwise invisible features.

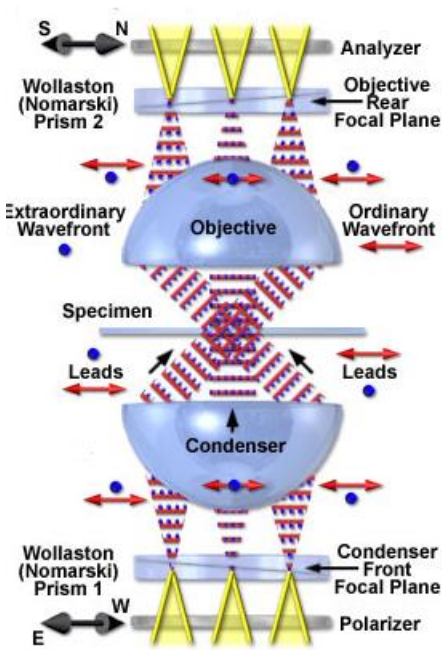

Figure 17. Schematic representation of a DIC microscope.

The light produced by a source encounter a polarizer in front of the condenser which produces plane polarized light. The plane of vibration of the E vector is oriented horizontally on an east-west or right-left line when looking into the microscope. The polarized light travels through a condenser Wollaston prism mounted close to the front aperture of the condenser, that acts as a beam splitter. Every incident ray of polarized light entering the prism is split into O and E rays. After refraction by the condenser, the O and E rays travel parallel to each other separated by about 0.2 µm in the so called *shearing direction*. An objective DIC prism mounted close to the back aperture of the objective lens recombines the two beams in the objective back aperture. The action of this prism is essential for interference and image formation. Equally essential is the analyser, which "analyses" rays of plane and elliptically polarized light coming from the objective and transmits plane polarized light that is able to interfere and generate an image in the image plane. It is located near the objective back aperture with its vibrational plane oriented vertically in a north-south or top-bottom orientation when facing and looking in the microscope.

When undisturbed by the presence of a specimen, the coherent ray pairs experience identical optical path differences between the specimen and image planes and arrive at the objective rear focal plane having the same phase relationship as when they left the condenser. The prism located behind the objective recombines the rays in the objective focal plane to generate linearly polarized light having an E vector vibration orientation identical to that of the condenser polarizer transmission axis. Linearly polarized light exiting the objective prism is blocked by the analyser, which has a transmission axis oriented perpendicular to that of the polarizer. As a result, the image background appears very dark or black, a condition referred to as extinction. In the event that paired rays encounter a phase gradient present in the specimen while passing from the condenser to the objective, the waves will undergo a phase shift along the shear axis (although no change in polarization occurs). Upon arriving at the objective prism, the phase-shifted paired wavefronts are recombined and generate elliptically polarized light (in contrast to the linearly polarized light produced in the absence of a specimen). The component of the elliptically polarized light that is parallel to the transmission axis of the analyser will pass through the analyser and will ultimately be able to generate intensity in the image plane.

2.1.2 FLUORESCENCE MICROSCOPY.

The fluorescence microscopy is one of the most widely used techniques, since it permits the identification and the study of subcellular structures, using particular molecules, called fluorophores, that bind to the site of interest in the cell and emit fluorescence light when excited with a proper wavelength.

Spontaneous fluorescence emission is a radiative de-excitation mechanism through which a molecule, excited to high energy level S_1 by absorption of a quantum of light, can return to its ground state S_0. When a fluorophore absorbs energy from light, it is usually excited to a higher vibrational energy level of an excited state, such as S_1, before rapidly relaxing to the lowest excited energy level $S_1(0)$. This event is termed *vibrational relaxation* or *internal conversion* and occurs in about 1 ps or less. The excess energy of the excited vibrational mode is transferred to the kinetic modes in the same molecule or to the surrounding molecules. An excited molecule may dwell in the lowest excited singlet state $S_1(0)$, for periods on the order of few nanoseconds before finally relaxing to the ground state. If relaxation from this long-lived state is accompanied by the emission of a photon, the process is known as *fluorescence*. The emission of fluorescence light is not the only way for the de-excitation of an excited molecule, for example an alternative way is the intersystem crossing, which is a process that involves transitions between a singlet state S_1 and a triplet state T_1. This transition is, in principle forbidden because it involves the spin reversion of the excited electron. In practice, the probability is not negligible when the vibrational levels of the two excited states overlap. The result of this process is that the energy became trapped in the triplet state with only classically forbidden transition available to return to the lower energy state S_0. These transitions, although forbidden, will occur anyway with some non-zero probability, giving rise to *phosphorescence* emission. However, being kinetically unfavourable, phosphorescence progresses at significantly slower time scales then fluorescence emission. Typically, an excited molecule may dwell in the triplet state for several milliseconds or, for some compounds, for minutes or even hours.

The spectrum of fluorescence emission wavelengths depends on the energy gap between final and initial states the electron experiences in the transition. The emission wavelength is always longer than the excitation wavelength, since some of the absorbed energy is lost during vibrational relaxation. This fact causes a relative shift, named *Stokes shift*, between the absorption and emission spectra of a molecule, whose size can range from few to hundreds nanometers (Figure 19).

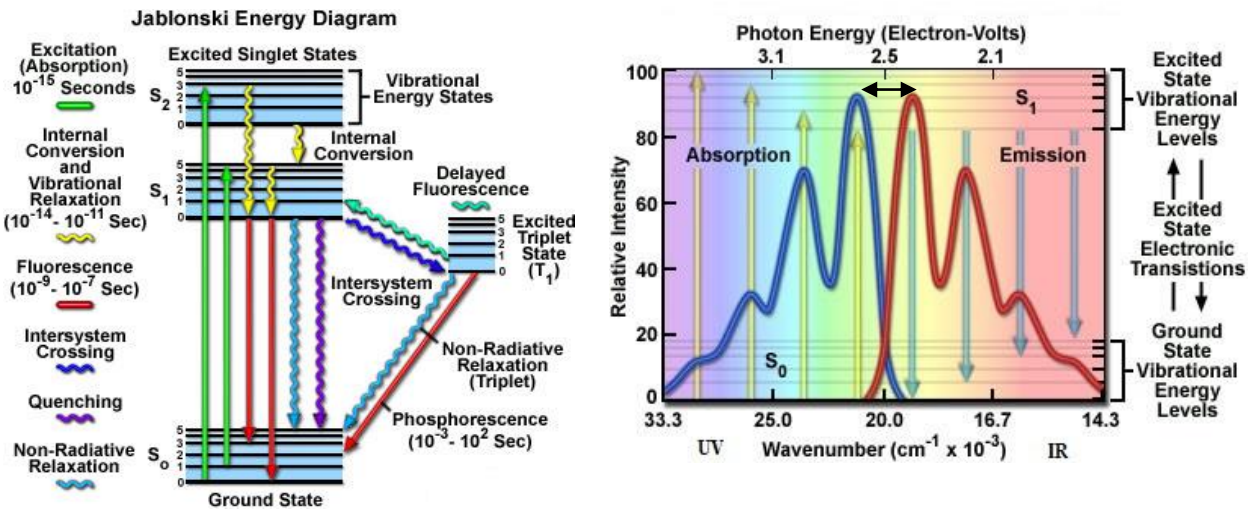

Figure 18.Jablonski energy diagram (left) for a fluorophore and its excitation and emission spectra (right).

The difference between emission and absorption spectra allows the construction of the fluorescence microscope. The working principle of this type of microscope is to irradiate the specimen with a wavelength in the absorption spectrum and collect fluorescence light, separating the two by means of a combination of dichromatic mirror, also called beamsplitter, and filters. In a properly configured microscope, only the emission light should reach the eye or the detector so that the resulting fluorescent structures are superimposed with high contrast against a very dark background. The limits of detection are generally governed by the darkness of the background, as the excitation light is typically several hundred thousand to a million brighter than the emitted fluorescence.

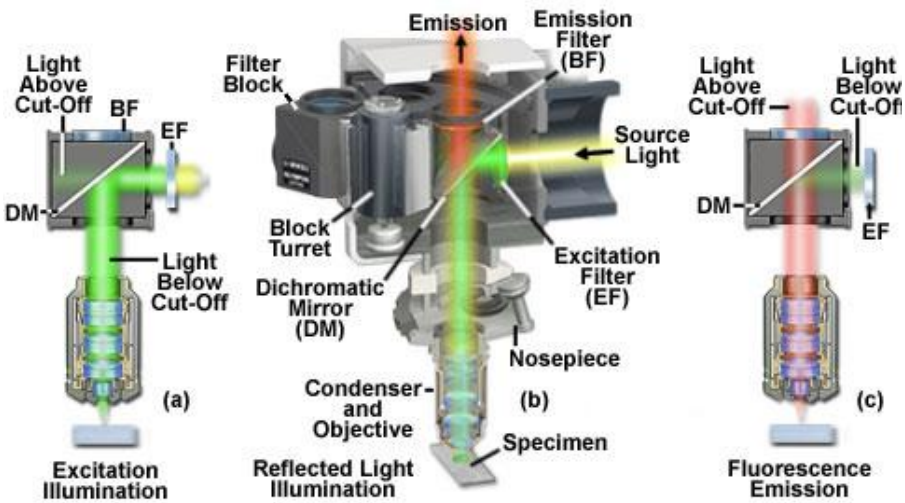

Figure 19. Schematic representation of a fluorescence microscope.

The excitation filter selects a narrow band of excitation wavelengths from the illumination beam in entrance to the mirror. The dichromatic mirror, mounted at a 45° angle with respect to the optical axis, reflects short excitation wavelengths at 90° towards the specimen and transmits along the optic axis long

fluorescence wavelengths collected by the objective. Longer fluorescence wavelength crosses the objective again, that behaves also as a condenser. The fluorescence light than travels along the optical axis reaching again the beamsplitter by which is transmitted and then passes through the emission filter for a finer selection. After the filtered fluorescence light, proceeding along the axis to the ocular and detector.

2.1.3 CONFOCAL MICROSCOPY.

The main problem of the widefield fluorescence microscopy derives from contributions of out of focus sample regions, producing unwanted light that is collected by the objective. This problem can seriously compromise the ability to resolve the specimen details, and it is normally referred as *axial blurring*.

The axial blurring problem was resolved in 1955, with the invention of the *confocal microscope* by Lee Minsky. Today confocal microscopy is a widely used optical imaging technique for increasing optical resolution and contrast by means of a spatial pinhole at the confocal plane of the lens to eliminate out-of-focus light. To avoid the axial blurring the object has to be illuminated and image point-by-point through the use of two pinholes, one placed at the exit of the source of a collimate light beam, called *source pinhole*, and the second positioned just before the photodetector, called *detector pinhole*. Thus, the illumination and the detection are confined to diffraction limited spots, which are optically conjugated. The confocal microscopy presents a high intrinsic capability of removing almost completely the axial blurring effect. Furthermore, the resolution (defined as the FWHM of the imaged PSF) is improved by a factor of $\sqrt{2}$ compared to a traditional microscope.

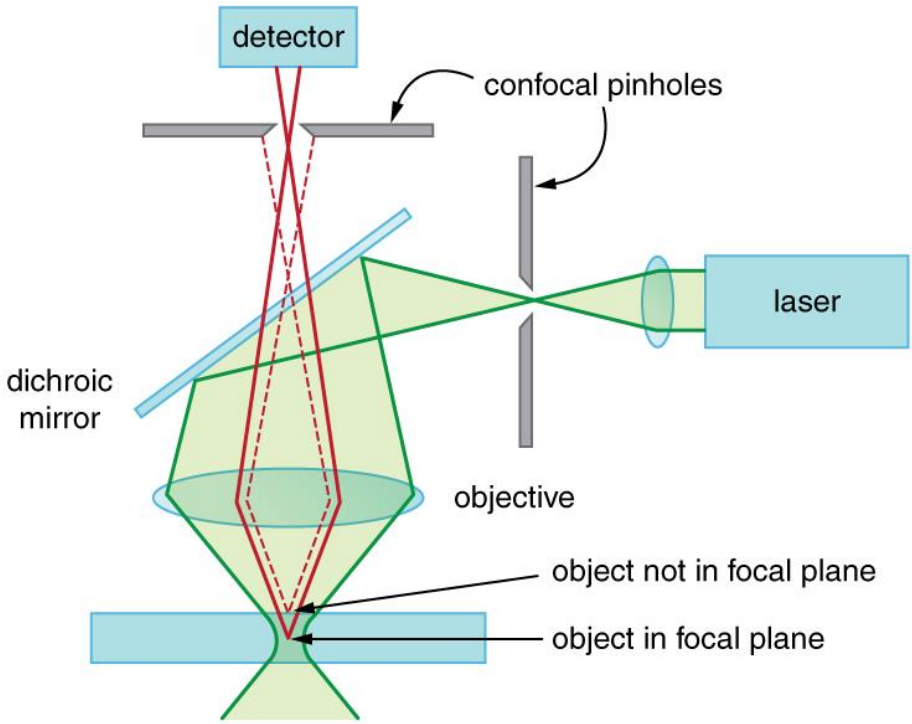

Figure 20. Scheme of a confocal microscope.

Immunofluorescence pictures reported in this thesis are taken with LEICA TCS SP5 and ZEISS LSM700.

2.2 THE PATCH-CLAMP TECHNIQUE.

The patch clamp technique is an extremely powerful and versatile method for studying electrophysiological properties of biological membranes. This technique was developed by Erwin Neher and Bert Sakmann in 1976, and caused a revolutionary advancement of many research areas in both cellular and molecular biology. This technique permits to experimentally control and manipulate the voltage of membrane patches or of the whole cell (*voltage clamp*); therefore, allowing the study of the voltage dependence of ion channels. Alternatively, it is possible to monitor the changes in membrane potential in response to currents flowing across ion channels (*current clamp*). For these reasons the main targets of patch-clamp investigations are membrane ion channels such as, voltage-dependent, receptor activated, and second messenger-activated channels [25].

The basic approach to measure small ionic currents in the picoAmpere range through single channels, requires a low-noise recording technique. This is achieved by tightly sealing a glass micropipette onto the plasma membrane of the intact cell, thereby isolating a small patch. The currents flowing through the channels enclosed by the pipette tip within that patch are measured by means of a patch-amplifier. This is the *cell-attached* configuration (Figure 21.A), which is the precursor of all the other possible configurations in which is possible to perform patch-clamp experiments.

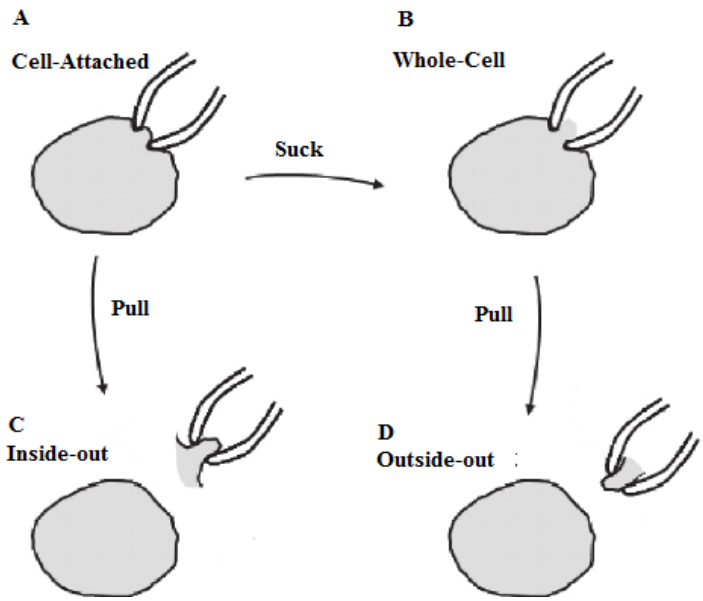

Figure 21. Patch-clamp configurations.

The resistance between pipette and plasma membrane is critical for determining the electrical background noise from which the channel currents need to be separated. The seal resistance should typically be around or more than 10 GΩ, forming the so called *gigaseal.* However, there is another important reason for requiring a high seal resistance in the cell-attached configuration: the higher is the seal resistance, the more complete is the electrical isolation of the membrane patch. The cell-attached configuration is normally used for the recording of the currents through a single, or a few, ion channels within the patch. This configuration leaves the cell intact, and is therefore the most "physiological "configuration to study single channels. Anyway, it does not allow easy manipulation of the media on either side of the membrane, and the membrane resting potential remains unknown.

The *whole-cell* configuration (Figure 21.B) is reached when the cell-attached patch is ruptured by applying a pulse of suction through the patch pipette, thereby creating a hole in the membrane and gaining access to the cell interior. This configuration is characterized by a low-resistance access to the cell interior through the pipette tip, so larger currents can be injected quicker, allowing current-clamp recordings. A patch pipette tip is sufficiently large to allow washout of the cytoplasm by the pipette-filling solution; thus the composition of the intracellular fluid can be considered equal to that of the pipette-filling solution because the volume of the cell is negligible compared with that of the patch pipette.

There are two configurations that do away with the cell altogether by excising a patch of membrane from the cell and studying it in isolation. The *inside-out* (Figure 21.C) patch can be obtained from the cell-attached configuration by withdrawing the pipette from the cell. This usually retains the gigaseal pipette-patch assembly and allows the study of ion channels in the excised patch. The inside-out configuration enables easily to change the cytosolic side of the patch. For this reason, this method is used to study the second-messenger-activated channels at the single channel level. The *outside-out* (Figure 21.D) configuration can be reached from the whole-cell configuration by withdrawing the pipette from the cell. This generally result in resealing of both plasma membrane of the cell and the patch at the pipette tip. Thus, the geometrical orientation of the patch results in the outside of the membrane facing the bath solution. This configuration allows to easily change the extracellular side of the patch; it is therefore often used to study receptor-operate ion channels.

In this work the most used technique used for the study of HeLa cells and differentiated neurons is the whole-cell patch clamp, which is described more in detail in section.

2.2.1 THE WHOLE-CELL CONFIGURATION.

The whole-cell recording method allows to record from cells and modify their internal environment by using a patch-clamp pipette. This has become the most commonly used patch-clamp configuration. This configuration is obtained by disrupting the patch of the membrane under the pipette in a cell-attached patch configuration by a pulse of suction or voltage. In the whole-cell configuration the integrity of the plasma membrane is lost and the pipette electrode has direct contact with the cell cytoplasm.

The equivalent circuit for the whole-cell patch configuration can be seen Figure 22

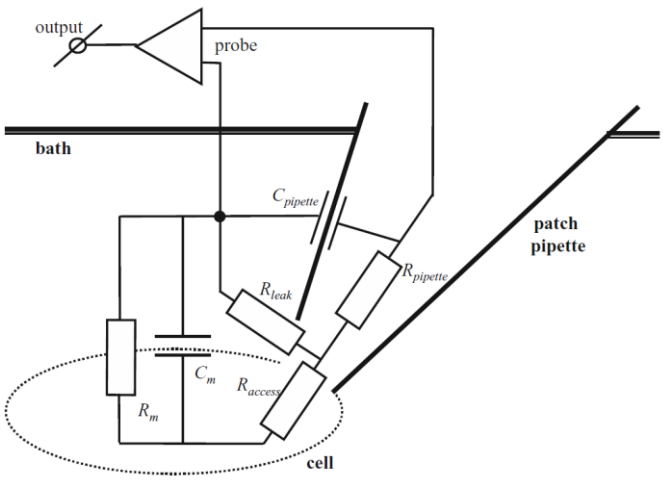

Figure 22. Equivalent electrical circuit for the whole-cell configuration

The series circuit consists of the pipette resistance $R_{pipette}$, the access resistance R_{acces} , and the membrane resistance R_m . The latter is the largest resistor, so this configuration allows the observation of

currents through R_m. These currents are the sum of currents through all the activated channels of the cell, for this reason they are called whole-cell currents or macro-currents. Parallel to the circuit is the leak resistance R_{leak}, which should be as high as possible. The membrane capacitance C_m plays an important role in the whole-cell recording because it affects the voltage-clamp time characteristics. Any change in holding potential will be delayed because the access resistance and the pipette resistance in series with C_m form a significant RC circuit; so special methods are required in order to quantify and minimise the effects of this RC circuit [1].

To obtain this configuration during the experiments only isolated cells were selected, because paired cells may express gap-junction channels, thus complicating the equivalent circuit.

CELL PARAMETERS ESTIMATION.

$$R_{acces} = \frac{V}{I_{peak}}, \tag{2.1}$$

$$R_m = \frac{V}{i} - R_{acces}, \tag{2.2}$$

$$C_m = \frac{\tau}{R_{acces} + R_m}. \tag{2.3}$$

In the whole-cell configuration the cell parameters (C_m, R_{acces} , and R_m) can be estimated from the current response to rectangular voltage step of about +10 mV or -10 mV.

Where V is the step amplitude, I_{peak} is the amplitude of the current peak, τ is the time constant of the exponentially decay current, and *i* is the stationary state current. A good estimation of the cell parameters is necessary for the analysis of the data, and for monitoring the state of the cell during the experiments. Thus, is fundamental to measure currents as precisely as possible to reduce errors in the parameter estimation. The major source of errors is the presence of noise. In the most general case, noise can be defined as any disturbance that interferes with the measurements of the desired signal. In electrophysiological measurements, such disturbances can arise from the preparation itself, the electrodes that couple the preparation to the measurement instrument, the electronic instrumentation and interference from external sources. Therefore, it is convenient to record data with high signal-to-noise ratio (SNR) to improve parameters estimation. To improve SNR, Axopatch 200B amplifier is mounted with an analogical 4-pole low-pass Bessel filter. The bandwidth of the filter is selected to reduce noise to acceptable levels so that the desired signal can be adequately observed. The correct parameters of the cell are, then calculated taking in account the presence of the filter.

2.2.2 PATCH-CLAMP SETUP.

There is a wide variety of patch-clamp setups, used in various laboratories. Each setup is adapted to meet specific experimental requirements, but there are some basic features shared by all the patch-clamp setups. In its simplest form, a patch-clamp setup may consist of a microscope placed on a vibration isolation table within a Faraday cage, a patch clamp amplifier and a pulse generator for voltage-clamping the cells, a micromanipulator holding the amplifier probe for positioning the attached patch pipette, a perfusion system, and data-recovery devices. In additions instruments for pipette fabrication (puller and

microforge) are needed. In this section is described in detail the setup used for the experiments in this thesis.

OPTICS.

The microscope is a fixed stage Olympus BX51WI placed in anti-vibration table. This microscope is made up of the combination of an epi-fluorescence and a Differential Interference Contrast (DIC or Normanski by its inventor) microscope.

The transillumination light sources are a green (520 nm) and red (660 nm) leds used under Köhler illumination in the objective plane. These light sources are used to record transmission images of the samples directly by the oculars. The objective is a water immersion Nikon Fluor 40x/0.8w, DIC M, WD 0.20. The emission light produced by the sample is collected by the objective lenses and recorded by a PCO-edge camera (PCO.EDGE 5.5) this camera allows to record very fast frames, till 10 ms/frame. To improve the visualization in this procedure, DIC microscope is used. In the following table reports the configurations of dichroic and emission filters used in the experiments.

The epi-fluorescence light sources are 470 nm, 365nm, 385nm, 565 nm, and 460 nm leds, which can be used to excite fluorescence emission in the samples. The emitted fluorescence light is collected by a digital camera.

Depending on the experimental needs, different dichroic mirrors and emission filters are used to filter light. All the parts of this setup (cameras, leds, laser, shutters....) are controlled by Roboscope, a custom software built in VIMM laboratories, which permits also to design specific protocols for imaging experiments.

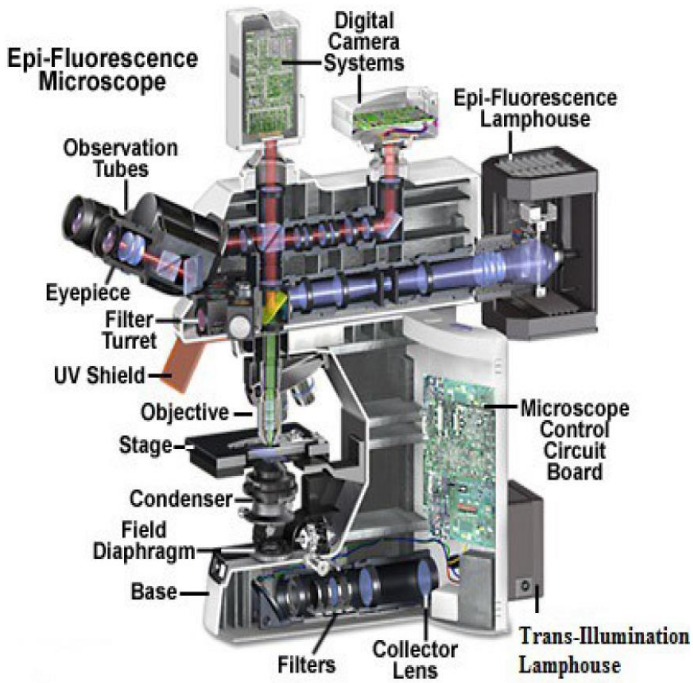

Figure 23. Scheme of an upright fluorescence microscope.

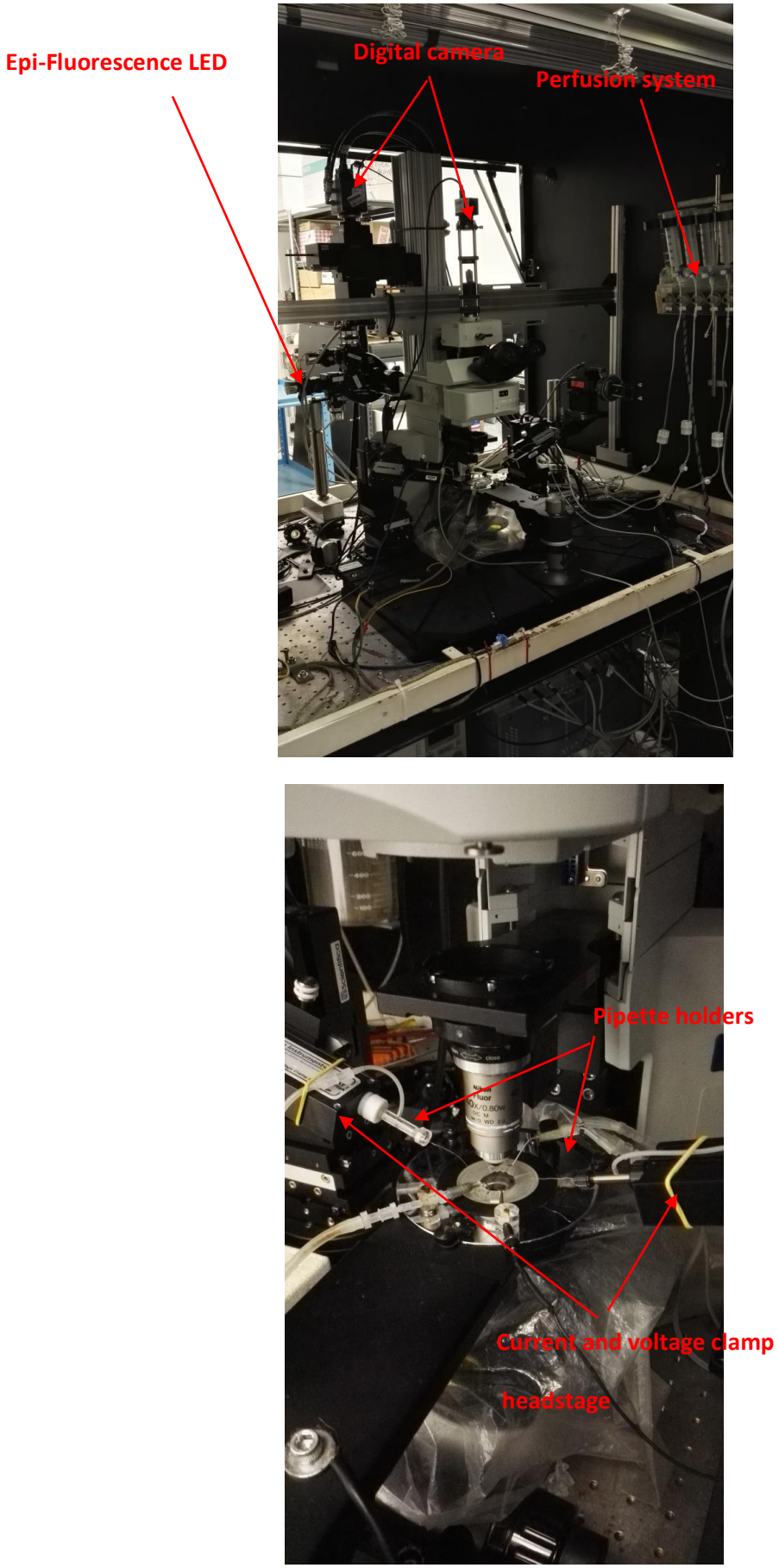

Figure 24. The complete patch-clamp setup

PERFUSION SYSTEM.

During a patch-clamp experiment the glass coverslip in which the cells are grown is placed in a small chamber which is filled with a suitable solution, prepared in order to keep the cells healthy and to point out the specific aspects to be studied. The perfusion system is fundamental every patch-clamp setup, since it permits not only a continuous change of the solution in the chamber, but also, allows to change the solution with a different one during the experiment, thus permitting to study the cell response to changes in the extracellular environment (e.g. changes in Ca^{2+} extracellular concentration).

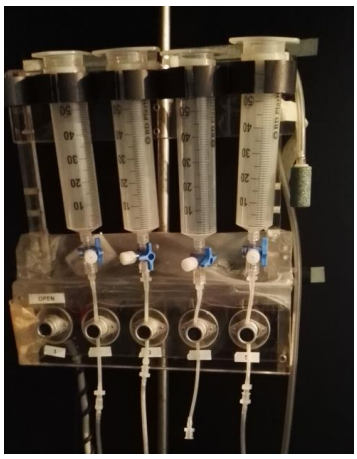

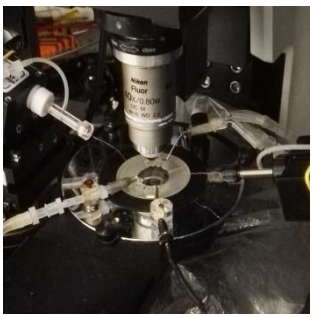

Figure 26. Chamber for the samples

Figure 25. Perfusion system controller.

Figure 27. Syringes of the perfusion system.

The perfusion system used is made up of four 50 ml syringes, which are connected to the chamber via thin plastic tubes. The flux of solution through the tubes can be manually regulated, while the opening and closing of different ducts can be done with the control system showed in Figure 25. At the opposite side of the chamber is placed a nozzle which draws the excess solution from the chamber, thus ensuring continuous renewal of the solution in which the cells are immersed.

PIPETTE HOLDERS AND HEADSTAGES.

As can be seen in Figure 24 the microscope is in a fixed position, while the other parts of the setup (the plate with the chamber and pipette headstages) are placed in a platform, which can be moved by means of manipulators that allow both macro and micro-movements. This configuration allows to change the position of the objective with respect to the centre of the chamber where the samples are placed.

Pipette holders and headstages (Current Clamp and Voltage Clamp Headstage, CV-7B, Axon Instruments) can be moved with respect to the platform with manipulators. The manipulators allow both macro and micro-manoeuvres for refine placements of the pipette respect to the cell. The headstage is connected to the amplifier (MultiClamp700B MOLECULAR DEVICES) by means of a BNC cable. The amplifier is designed specifically for patch voltage-clamp or highspeed current-clamp recording with the same headstage. The amplifier can be controlled from a computer using MultiClamp and Axon Clampex software.

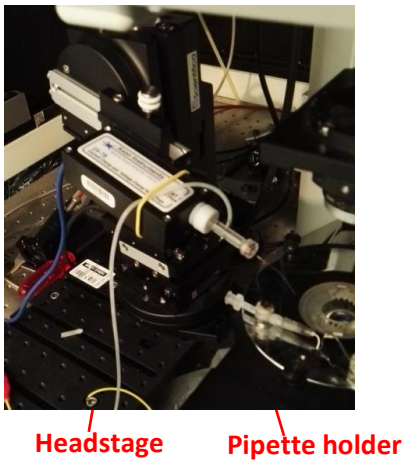

Figure 28. Pipette holder, headstage and patch-clamp amplifier.

DATA ACQUISITION SYSTEM.

Data acquisition is performed with Axon DigiData 1550A (MOLECULAR DEVICES), which is a low-data acquisition system equipped with a HumSilencer, an advanced technology that learns the local-line frequency harmonics and removes them from the incoming signal in a filter-free way.

PATCH PIPETTES AND ELECTRODES.

There are many types of patch pipettes, which can differ in size and material. Depending on which patch clamp configuration is used, and also on the size of the cells to be patched, an optimal adjustment of the size, shape, glass type, and coating of the patch pipette is necessary.

Patch pipette fabrication involves two steps: pulling and heat polishing of the tip. Patch pipettes can be pulled from glass capillary tubes. This is a two-step process performed with a vertical microelectrode puller and standard heating coil supplied with it (Figure 29).

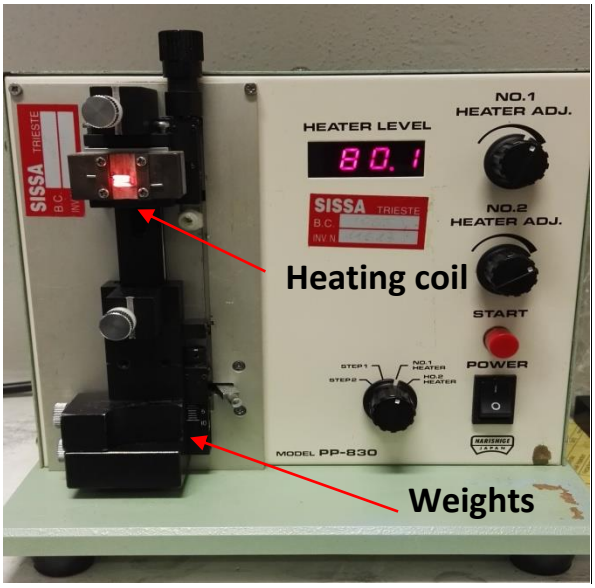

Figure 29. Vertical puller.

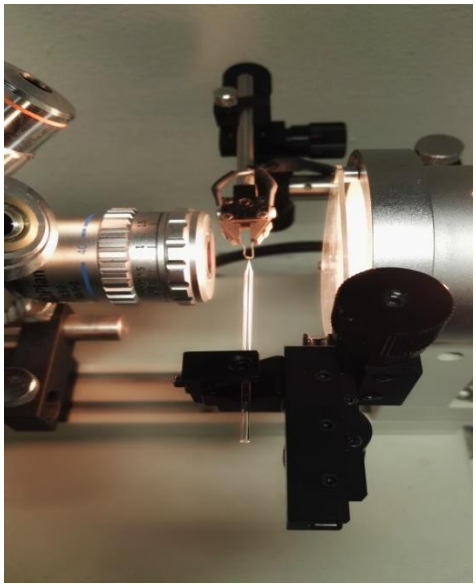

Figure 30. Microforge.

In the first pull the capillary is heated and thinned over a length of 7-100 mm to obtain a minimum diameter of 200 μm. The capillary is then recentered with respect to the heating coil and in the second pull the thinned part breaks, producing two pipettes. The temperature of the two pulls should be properly chosen depending on the type of glass and the desired tip size and shape of the pipette.

The tips of the two pipettes are then polished with a microforge (Figure 32). The heat is supplied by a platinum filament. The tip of the pipette is placed within 10-20 μm from the filament for a few seconds.

For electrophysiological recordings on HeLa cells the following capillary tubes were used: Patch glass-thin wall, OD =1.5mm, ID =16 mm, length = 10 cm (WARNER INSTRUMENTS). The pipettes obtained from these capillaries have a diameter of 1-3 μm and a resistance of 5-7 M Ω when immersed in the bath solution.
For the experiments with neurons sodaglass R6 type were used, OD = 1.5 $\pm$ 0.05 mm, ID = 1.10 $\pm$ 0.05 mm, length = 1000 $\pm$ 3 mm (GARNER GLASS). Pipettes made with this glass do not require the polishing of the tip with the microforge, and have a resistance of 3-5 MΩ when immersed in the bath solution, with a tip diameter of 1-3 μm.

Patch pipettes were filled with specific intracellular solutions, which provide the fluid connection from the cell to the electrode. The electrodes have the function to convert the ionic current in solution into electron currents in the wires. The most common type is a Ag/AgCl interface, which is made up of a silver wire coated with silver chloride. For this electrode chloride ions react with the Ag to produce AgCl plus an electron, or an electron reacts with AgCl to produce Ag plus Cl^{-}. Thus, the current carried by chloride ions in solution is converted into electrons according to the following reversible reaction:

$$Cl^{-} + Ag \rightleftharpoons AgCl + e^{-}$$

2.2.2 SOLUTIONS FOR PATCH CLAMP.

The main aim of a patch-clamp experiment is to study the electrophysiological characteristics of the cells, e.g. their resting potential and the ability of generating action potentials in the case of neurons. In order to do this, is fundamental to choose accurately the extracellular solution in which the cell would be immersed during the experiment, and the intracellular solution, with which the pipettes are filled in whole cell recordings.

The extracellular medium must mimic the ionic composition of the physiological extracellular fluid in the body. Thus, the extracellular solution (ECS) is mostly based on sodium chloride. Intracellular solution (ICS) is generally more rich in potassium. PH and osmolarity of the solutions are critical in maintaining the cells in good conditions during the experiment. Most vertebrate extracellular environment is set to the physiological pH of about 7.4 and it is important to be consistent throughout a series of experiments because even small changes in acidity can influence channel behaviour. Typically, the ICS is a little more acidic than the ECS, with a pH of about 7.2-7.3 to obtain the correct pH, NaOH was added to the ECSs and KOH to ICSs. EGTA and BAPTA in the ICSs are used to maintain the $[Ca^{2+}]_i$ low. Ca^{2+} is restrained by the endoplasmic reticulum and, under certain conditions, it can be released in the cytoplasm altering the normal gating of ion channels, hemichannels and connexons. HEPES is used to maintain the pH constant. The absolute osmolarity and the difference between osmolarity of ICS and ECS are critical for the success of the experiments. The osmolarity difference between the media inside and outside the cell determine the volume of the cell and the osmotic force on the membrane. All the solutions are obtained by dissolving

different substances in bidistillated water. In the following tables are reported the compositions of the various intracellular and extracellular solutions.

In the experiments with MSCs and IPSCs, sometimes amino acids and vitamins were added to the ECS in order to keep the cells in good condition and to increase their survival outside the incubator.

CHANNELS BLOCKERS.

Blockers are fundamental for the electrophysiological characterization of the cells, since they are able to suppress the contribution of a specific class of ion channels. Adding different blockers to the extracellular solution makes possible to study the behaviour of the different types of channels that populate the cell membrane. For example, in the case of neurons the action potentials are the result of the combined action of sodium and potassium channels, and it is not possible to study separately the contributions of these channels to the total current across the membrane without adding specific inhibitors for these channels in the extracellular solution. Potassium channel blockers are also required in experiments on untrasfected and transfected HeLa cells, because the contribution of this class of this class of channels to the measured currents cannot be distinguished from that of the connexin hemichannels. In order to reduce this contribution different blockers for the K-channels were added to the ECs. Summarizing, the channel blockers serve two main functions: the first is the reduction of the parasitic currents, with a consequent increase of the membrane resistance, and the second is to block specific channels, allowing the study of the contributions of the others.

In general, a blocker is a molecule which is able to inhibit the function of a specific type of ion channels. A blocker could not alter a physiological function without having molecular interactions with one or several tissue components. The sites of interaction are called receptors. The simplest way to understand how a blocker acts on channels is to suppose that the blocker molecule binds reversibly to a single class of sites; and that binding to one receptor site blocks a fixed fraction of the function without influencing the binding of the other blocker molecules to the other receptors. Like any bimolecular reaction, the binding of a blocker to receptor could be characterized by an equilibrium dissociation constant $\mathrm{K_d}$, defined in terms of the forward and backward rate constants of the reaction $\mathrm{k_1}$, and $\mathrm{k_{-1}}$

$$\mathrm{T+R} \underset{\mathrm{k_{-1}}}{\overset{\mathrm{k_1}}{\rightleftharpoons}} \mathrm{TR} \qquad \mathrm{K_d} = {}^{\mathrm{k_1}}/_{\mathrm{k_{-1}}} = {}^{[\mathrm{T}][\mathrm{R}]}/_{[\mathrm{TR}]} \ . \tag{2.4}$$

Where $\mathrm{K_d}$ is the equilibrium dissociation constant of the blocker-receptor complex. At the equilibrium, the fractional occupancy *y* of receptor is a saturating function of [T]:

$$y = \frac{[\mathrm{TR}]}{[\mathrm{TR}] + [\mathrm{R}]} = \frac{1}{1 + \mathrm{K_d}/[\mathrm{T}]} \tag{2.5}$$

When the blocker-receptor complex is reached, conformational changes of the ion channel occur and lead the occlusion of the pore [5].

As discussed above the most widely used blocker for the experiments in this thesis are blocker for sodium and potassium channels. They are listed below, with their functions.

- TetraEthylAmmonium (TEA), non-selective blocker for the voltage-gated K-channels;
- Cesium chloride (CsCl), blocker for voltage-gated K-channels;

- 4-AminoPyridine (4-AP), non-selective blocker for the voltage-gated K-channels;
- TRAM-34, which is potent and highly selective blocker for the Ca^{2+}-activated K-channels;
- UCL-1684, highly potent blocker for the Ca^{2+}-activated K-channels.
- Tetrodotoxin (TTX) to block voltage-dependent sodium channels;
- Nickel chloride ($NiCl_2$-$7H_2O$) to block voltage-dependent Ca^{2+}-channels.

EXPERIMENTS WITH IPSCS.

			PH=7,3; mOsm=290
Name	Weight (g/mol)	Molarity (mM)	g/l
NaCl	58.44	127	7.42188
K_2PO_4	136.086	1.2	0.16333
KCl	74.56	1.9	0.14166
$MgSO_4$	120.37	1.4	0.168518
$NaHCO_3$	84.01	26	2.18426
Glucose	180.2	10	1.802
$CaCl_2$	110.99	2.2	0.24398

Table 3. Extracellular solution used for IPSCs.

			PH=7.3; mOsm=277
Name	Weight (g/mol)	Molarity (mM)	g/25ml
K-Glu	234.5	125	0.732
KCl	74.56	5	0.01
CaCl_2	110.99	0.2	/
ATP-Mg	507.18	2	0.025
HEPES	238.1	10	0.06
EGTA	380.35	10	0.01
GTP	523.18	0.2	0.003
KOH	56.11		

Table 4.Intracellular solution used for IPSCs.

These solutions were used also in the experiments with Schwann cells obtained from IPSCs.

EXPERIMENTS WITH MSCs.

			Ph=7.4; mOsm=322
Name	Weight (g/mol)	Molarity (mM)	(g/l)
NaCl	58.44	140	8.18
KCl	74.56	5	0.373
$CaCl_2$	110.99	2	0.222
$MgCl\text{-}6H_2O$	203.3	2	0.407
HEPES	238.31	10	2.383
Glucose	180.2	10	1.802
NaOH	40		

Table 5. Extracellular solution used for MSCs.

The ICS is the same used for the experiments with IPSCs.

2.4 IMMUNOFLUORESCENCE.

Immunofluorescence is a broadly applicable method generally used to assess both the localization and endogenous expression levels of proteins of interest. This technique is based on the use of specific antibodies which have been chemically conjugated to fluorescence dyes. The fluorescence emitted by these dyes, when illuminated with a proper wavelength, can be observed with a fluorescence microscope.

There are two classes of immunostaining: primary, or direct, which used only a single antibody, and secondary, or indirect, which requires the use of two different antibodies. In this work immunostaining of samples is performed with the indirect technique.

Indirect immunostaining uses two antibodies. The primary antibody specifically binds the target molecule. This antibody is unlabelled and it is recognized by the secondary antibody, which also carries the fluorophore. Multiple secondary antibody can bind to a single primary antibody, allowing the staining of the sample with different primary antibodies at the same time.

Here this technique is used to evaluate the expression of the characteristics proteins during the different stages of differentiation of hIPSCs and MSCs into in neurons and Schwann cells.

To perform immunostaining, first the cells are washed with PBS one time, then fixed with 4% PFA at room temperature for 10-15 minutes. After the PFA removal, the cells are washed two times with PBS and placed in the blocking solution (FBS 0.5%, 0.3% TRYTON, PBS) at least overnight at 4°C, to block nonspecific antibody reactions. Next, the primary antibody, diluted in the blocking solution is incubated overnight at 4°C. After that the primary antibody is removed, the cells are washed with PBS and the secondary antibody is incubated for three hours at room temperature. Finally, when the secondary antibody solution is

removed, the staining with DAPI is performed (10 min. of incubation at room temperature). For mounting the coverslips MOWIOL® was used.

2.5 Cell culture and preparation.

In this thesis are presented the results of the experiments performed with different types of cells: HeLa cells, used for learning the patch clamp technique, neurons and Schwann cells derive from hIPSCs, neurons derived from MSCs. In this paragraph the culture and differentiation protocols, carried out by the biologists of the laboratory, are described briefly. Further information can be found in the Appendix.

2.5.1 Induced Pluripotent Stem Cells.

MIFF1 (mRNA induced foreskin fibroblast clone 1) iPSC cells are got from the laboratory of Stem Cell Biology of Professor Peter Andrews (Department of Biomedical Science of the University of Scheffild, UK). In the Prof. Peter Andrews lab, human foreskin fibroblasts transfections are performed on sequential steps with the modified mRNA for: OCT4, SOX2, KLF4, cmyC and LIN28.

At the time of shipment, cells are maintained in hESC medium on Mouse Embryonic Fibroblasts (MEF) prior to freezing. Once arrived MIFF1 are quickly thawed and gently resuspended in hESC-medium supplemented with 10 µM of Rock-Inhibitor; then seeded ($1\times10^6/\text{well}$) of feeder cells. IPSCs are fed with daily changed hESC medium and passaged with collagenase IV. Cells are expanded in MEF, and when a good number is reached some of them are cryopreserved in freezing medium 1 and some of them are adapted in feeder-free culture. Cells in feeder-free environment are daily fed with Essential 8™ Medium, a xeno-free and feeder-free medium specially formulated for the growth and expansion of PSCs. MIFF1 are passaged with EDTA solution. When adaptation is complete, the cell number is expanded in order to cryopreserve a part of them in freezing medium 2 and the other is used for further purposes.

Moto-neuron differentiation protocol.

The differentiation protocol of neural crest cells into motor-neurons is composed of six steps, carried out by application of small molecules. This protocol is a modified protocol respect to which described in [26] having 90 % efficiency. The steps of the protocol are reported in the scheme below. The detailed protocol and compositions of different media used for differentiation can be found in the Appendix B together with some pictures at different stages of differentiation

Phase	Neural Induction	MN Specification	Expansion	MN Pre-Maturation	Neuronal Maturation
Time Interval	D1 –D6 (NEP)	D7 – D12 (MNP)	D13 – D18 (MNP)	D19– D24	D25 – D35
Culture Condition	Chir+SB+DMH	Chir+SB+DMH+RA+Pur	Chir+SB+DMH+RA+Pur+VPA	RA+Pur	RA+Pur+Compd. E
Positive Markers		Olig2	Olig2		Tuj1, MAP2, GAP43,HB9

Schwann cells differentiation protocol.

The first stage to obtain mature Schwann cells is the differentiation of MIFF1 IPSCs into neural crest cells (Appendix A). The differentiation is verified with immunohistochemistry and RT-PCR. After neural crest phase the cells are sorted with FACS for P75 marker; then cultured with Mesenpro supplemented with Neuregulin-1 [27] until day 40.

Phase	Neural Crest Cells	P75+ Sorted NC Cells	Schwann Cell Maturation
Time Interval	D1-D7	D8	D9-D40
	SB431542+Chir		Mesenpro + Neuregulin-1
Positive Markers		p75	

2.5.2 MESENCHYMAL STEM CELLS.

One of the most important possible advantages of using MSCs is that these cells constitute a small population of adult stem cells that resides in human skin. Cutaneous biopsies are obtained during plastic surgery from different region of the body of healthy donors (40-50 year; following the guidelines from the Clinic of Plastic Surgery, University of Padova, Italy) who has provided written contest collected by Dr. Vincenzo Vindigni (Unit of Plastic and reconstructive Surgery).

ISOLATION.

Skin biopsy is taken during a plastic surgery and steep in Eurocollins solution. After different washes in this solution, adipose tissue that is adherent to epidermis is removed and the biopsy is cut in small pieces of 6 mm^2. The strips of skin are left in the fridge for one hour with Eurocollins supplemented with antibiotic-antimycotic. After three washes in Eurocollins the strips are further cut in small pieces of 2 mm^2 and incubated overnight in a solution with DMEM/F12 and Worthington collagenase IV at 37°C with 5% CO_2 atmosphere.
The following day, the suspension is shaken by vortexing three times for 10 seconds, filtered by 70 µm cell strainer (BD Bioscience, Mississauga, Canada) and collected in a 50 ml tube.
After centrifugation for 7 minutes at 2500 rpm, the supernatant is removed, the pellet is resuspended in recovery medium, cells is plated in a 6-well plate and cultured at 37°C with 5% CO_2 atmosphere.

PROLIFERATION.

Skin derived cells are cultured in adhesion in pre-coated (with Matrigel) flasks with proliferative medium Half medium is changed every day for 2 weeks splitting the cells with TrypLE incubation once 95-100% confluence is reached (usually after two days).

At the end of the proliferative period, which lasts from day 0 to day 28, SKD cells are quantified and seeded with Rock inhibitor at 100.000 cells/cm^2 density in german glass coverslips pre-coated with LPL or Geltrex. Cells are left for 1 day in recovery medium.

DIFFERENTIATION.

Since an efficient protocol of differentiation of MSCs into neuron-like cells is still not defined, different protocols are carried on in parallel, in order to establish the best one. The protocols are based on the idea to apply small molecules (i.e Chir, DMH1, TGFβ inhibitor, retinoic acid, and puromorphamine), known to induce neuronal differentiation in IPS cells.

The cells are plated in coverslips, with a density of 50000 cells/ cm^2, previously coated with Matrigel (1/100). The following diagram shows a summary of the different protocol tried on the skin sample received the 22nd of December 2016. The plating phase was started the 3rd of February 2017. The composition of the media used in each the phases are reported in the Appendix B.

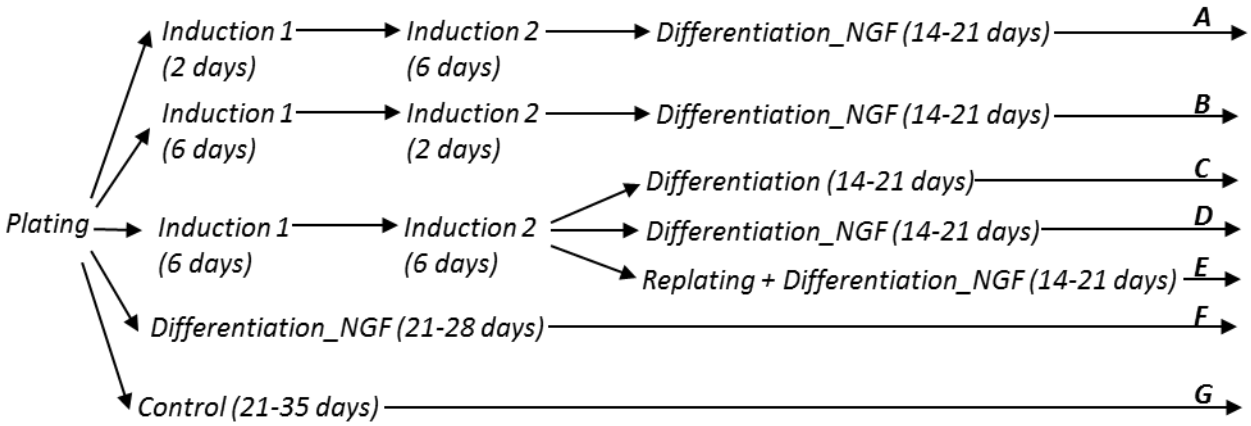

Figure 31. Differentiation protocols for MSCs.

In Appendix B are reported some pictures showing the cells at different stages during the differentiation protocol: 3,10,20, and 30 days, starting form 2nd February 2017. Further pictures of mature cells are reported in 3.3.

The cells were tested with patch clamp and immunofluorescence assays ate different stage of differentiation.

3 RESULTS.

3.1 EXPERIMENTS WITH INDUCED PLURIPOTENT STEM CELLS.

The IPSCs differentiated with the protocol described in 2.3.2 were tested with patch clamp experiments. The purpose of this analysis was to determine the resting potential and the electrophysiological properties of the cells. Moto-neurons and Schwann cells were tested separately in order to study their individual characteristics.

The ICS and ECS used are reported in Table 4 and Table 3. TTX (0.5 µM) and TEA-Cl (5 mM) + 4-AP-(500 µM), were added to ECS to block respectively voltage-dependent Na^+channels and K^+ channels, allowing the study of their contributions to the total current.

MOTOR NEURONS.

Functional motor neurons are obtained at the end of the protocol described in Appendix A. As discussed previously this protocol is divided in five steps (see Appendix A). To verify that the differentiation was proceeding in the correct way, immunofluorescence analysis was performed at different stages. First, we verified that the hIPSCs were expressing the typical markers for pluripotency (Sox2, Oct4, Tra1-60, Tra1-81) (Figure 32). The second analysis was performed on Neuro Epithelial Progenitor (NEPs). Since the specific markers (PAX6 and Nestin) for this phase were not available in our laboratory in that moment; NEPs were stained for DAPI and Vimentin, to visualize the typical rosettes formed at this stage (Figure 33, left). The last immunofluorescence before the maturation was performed in MNs Differentiation phase I to confirm whether the cells are Olig2 positive (Figure 33, right). Finally, we tested mature neurons at 20 days of maturation for classic motor neuron markers: Olig2, HB9, NeuroFilament (NF), TUJ1, and GAP43 (Figure 38).

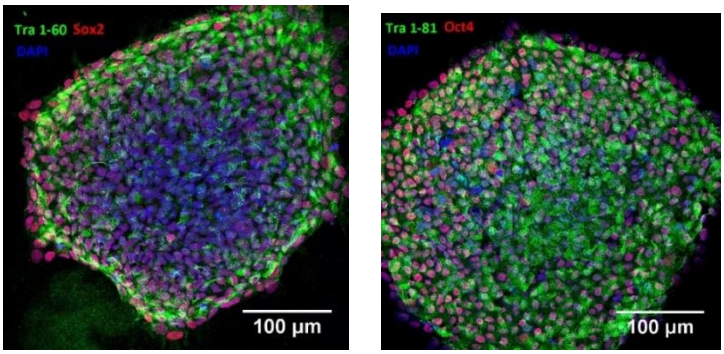

Figure 32. Pluripotency tests for MIFF1 hIPSCs.

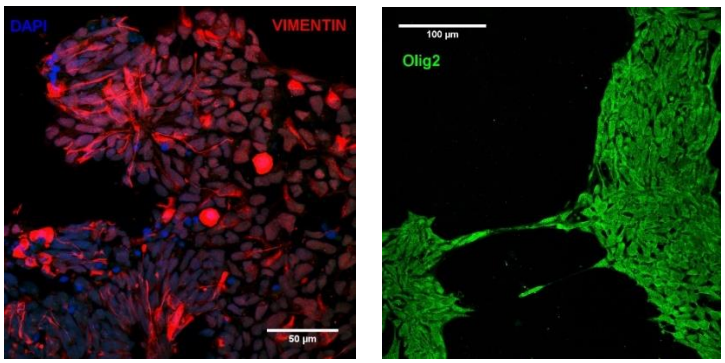

Figure 33. Immunofluorescence analysis of NEPs at day 7(left) and Olig2 positive cells during the expansion phase (day21) (right).

Patch clamp experiments were performed at two different time points: at 10 and 17 days of maturation. The cells were patched with soda-glass pipettes with a tip resistance 5-6 MΩ. Motor neurons and Schwann cells were tested with both voltage clamp and current clamp protocols. The voltage clamp protocol for testing active membrane properties consisted of a 200ms depolarizing -10 mV pulse from the holding potential, set equal to the resting potential, that preceded each depolarizing steps to remove inactivation. The -10 mV step was followed by series of 1s depolarizing steps with 10 mV increments, taking membrane potential form -50 mV to +50 mV respect to the resting potential. In the current clamp protocol cells were held at -40 pA for 1250 ms, than current pulses with 20 pA increments were injected through the patch pipette to examine whether the cells are capable of producing action potentials. The pulsed were lasting 100 ms, taking the membrane current for -50 pA to 90 pA.

At ten days we tested fourteen cells, but only three were able to fire action potentials during the current clamp, and produce sodium currents during the voltage clamp (Figure 34). Only three sodium currents were detected because the number of voltage sweeps was not enough. The mean cell parameters were:

V_m= (-70.3±0.3) mV,
R_m = (1.4 ±0.4) GΩ,
R_a = (27.8 ±1.9) MΩ.

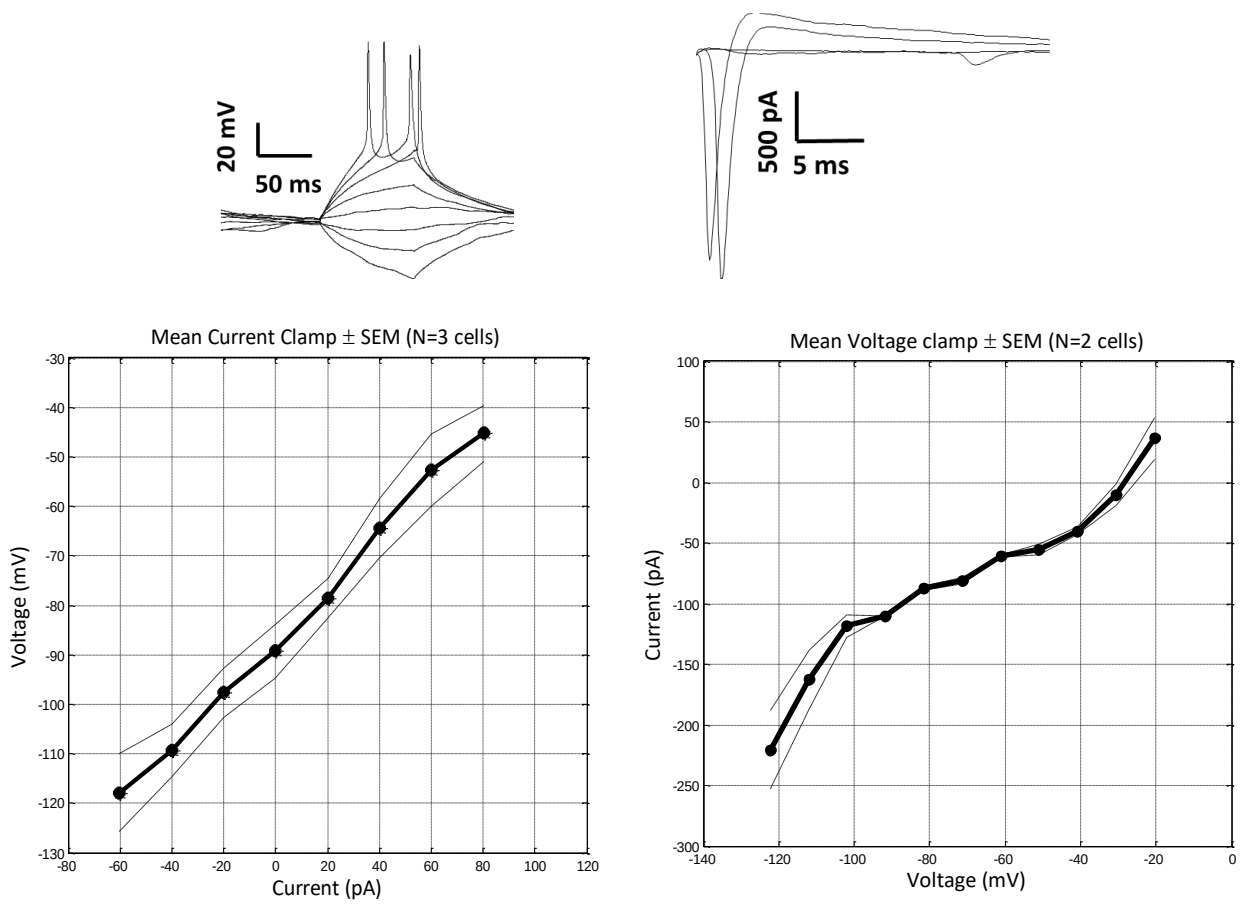

Figure 34. Patch clamp results at 10 days of maturation.

The cells were tested again at seventeen days of maturation. In this case the duration of current pulses in the current clamp was extended to 750 ms in order to allow the cells to fire multiple action potentials. In voltage clamp the total number of sweeps was maintained, but the number of negative steps was decrease

to two. In these experiments, we use TTX (0.5 µM) and TEA-Cl (5 mM) to block respectively sodium and potassium channels. Five cells were tested, and all of them were exhibiting neuronal activity, indicated that these cells can be considered completely functional neurons. TTX and TEA-Cl correctly suppress the action potentials during the current clamp. The mean values of the cell parameter were:

V_m= (-73.5±1.8) mV,
R_m = (2.2 ±0.3) GΩ,
R_a = (60.0 ±0.5) MΩ.

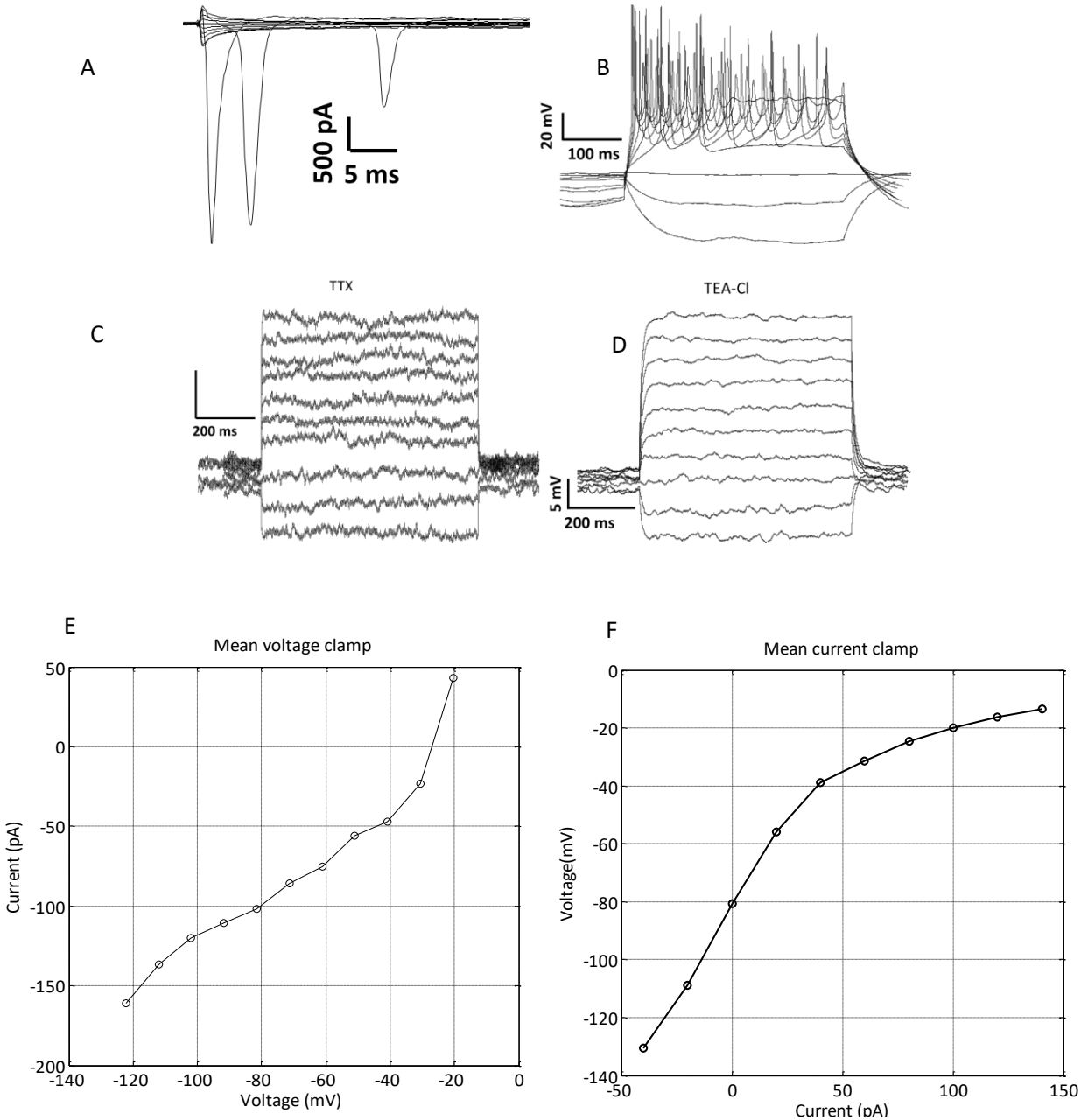

Figure 35. Patch clamp results at 17 days. *Sodium currents in the voltage clamp (A) and multiple action potentials recorded in the current clamp (A). Current clamp in presence of TTX and TAE-Cl (C, D). Mean I-V and V-I curves calculated from the data (E.F). Action potential recorded with a 20 pA current pulse (G).*

The last experiments were performed at 23 days in maturation (Figure 36). We used the same voltage and current clamp protocols of the previous experiments. In the voltage clamp, multiple sodium currents were produced when the voltage was higher than -40 mV. The mean resting potential was around -50 mV.

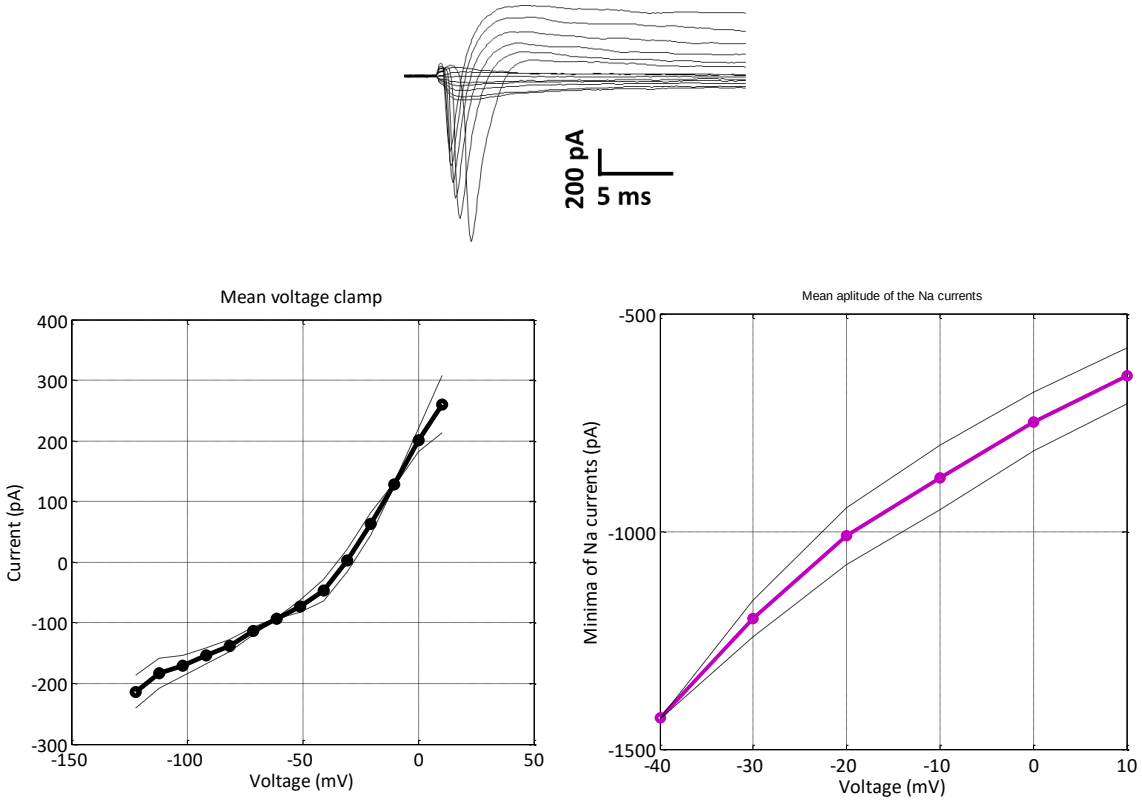

Figure 36. Patch clamp results at 23 days of maturation. Mean V-I relation calculated from the data (left) and mean amplitude of sodium currents (right).

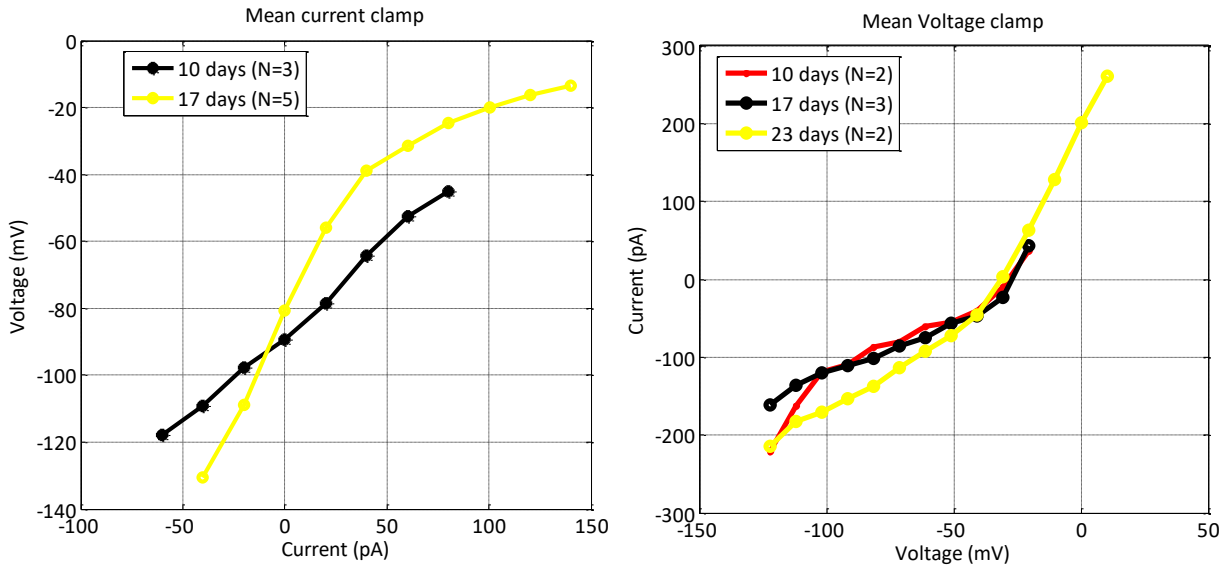

Figure 37. Comparison of current clamp I-V relation (left) and voltage clamp V-I relation (right) ate different stages.

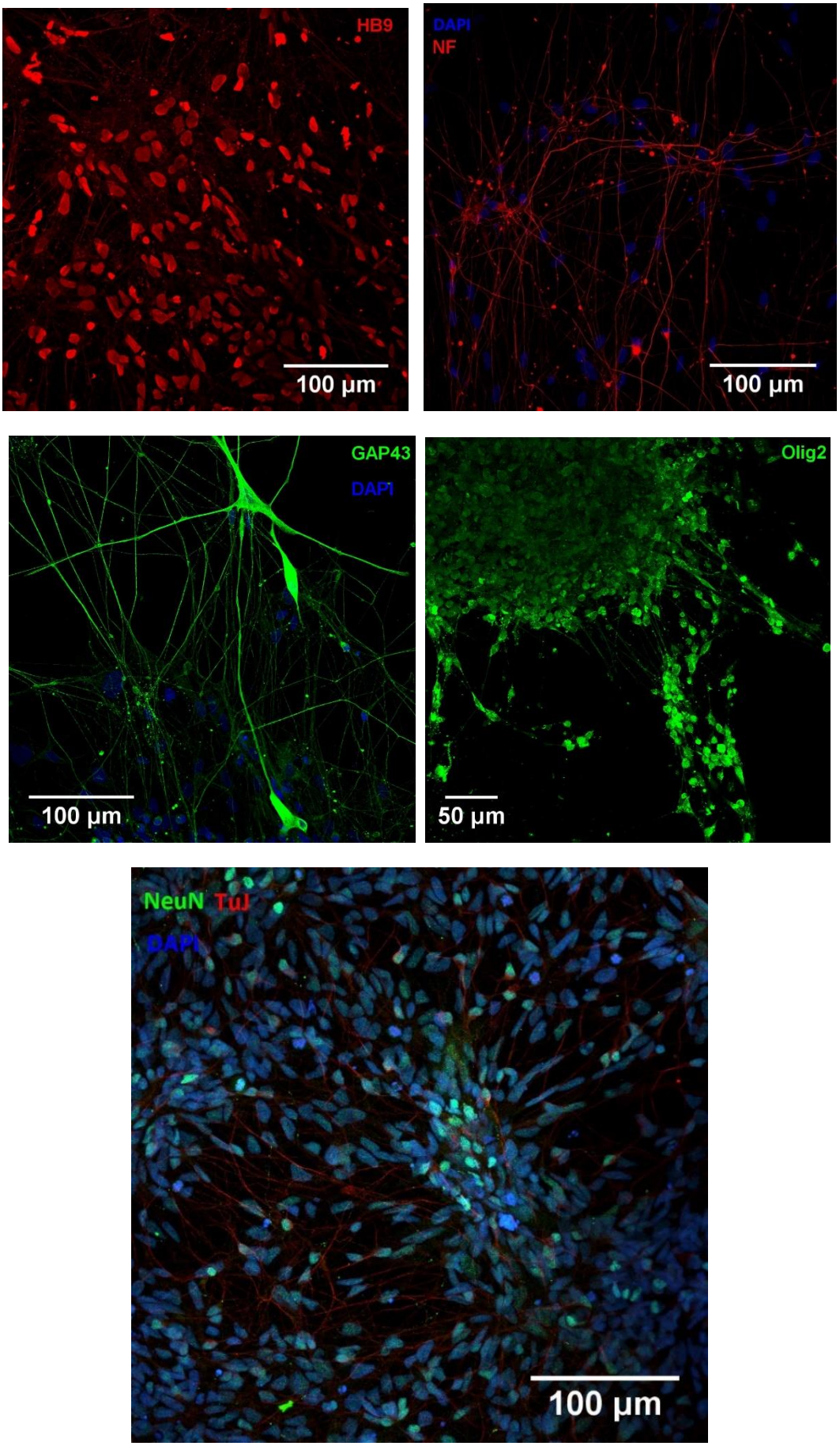

Figure 38. Immunofluorescence at 20 days of maturation.

SCHWANN CELLS.

For Schwann cells we used the same experimental protocols we used for iPSCs motor neurons. Immunofluorescence analysis on Schwann cells was performed at the neural crest stage, for P0, SOX10 and S100β as control, and again at the stage of mature Schwann cells, for P0, MBD, S100β and TUJ1 as negative control.

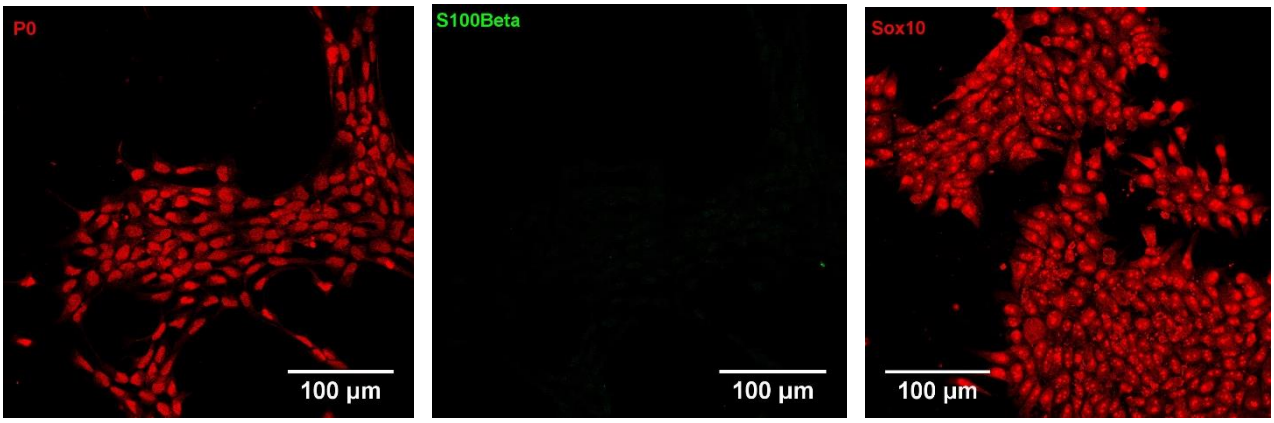

Figure 39. Immunofluoresceence of unsorted neural crest cells.

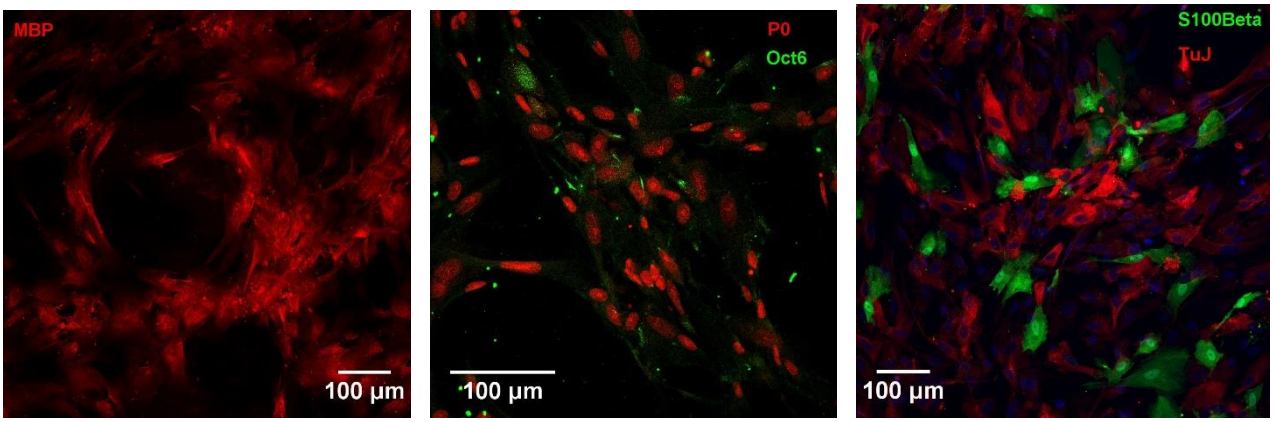

Figure 40. Immunofluorescence on mature Schwann cells

As expected at the neural crest stage the cells did not express S100β, which is a specific marker for mature Schwann cells, while they were expressing P0 and Sox10.

In mature Schwann cells were expressed the typical markers of mature Schwann cells: MBP, P0, and S100β. However, from these results were suggesting that we had a heterogeneous population of Schwann cells: some cells were expressing a typical neuronal marker TuJ1, used as negative control, and some others were expressing S100β.

Patch clamp experiments were performed on mature Schwann cells, at day 44 and 46 after neural crest differentiation (Figure 41). The experiments reported are relative to cells rescued from a contamination (probably fungal) by changing medium every day. The extracellular and intracellular solution were the same used for motor-neurons (Table 3 and Table 4). The experiments were performed with borosilicate glass pipettes with tip resistances 5-7 MΩ. The voltage clamp and current clamp protocols are same used for motor neurons at day 17.

The first experiments were performed just to verify whether the cells were behaving normally after the contamination. Thus, just voltage and current clamp experiments without channel inhibitors were performed. Once was established that the cells were showing the typical properties of Schwann cells, more detailed experiments were performed using TEA-Cl 2Mm and CsCl 2Mm, to block the potassium currents (Figure 41.D). Small action potential-like peaks were observed in the current clamp, probably related to the small fraction of sodium channels present in Schwann cells. More test with the application of TTX will be performed with the next differentiation.

The mean resting potential was Vm= (-36.4±1.6) mV, which is similar to the resting potential of sciatic nerve Schwann cells. The mean access resistance was R_a = (16.57 ±0.01) MΩ and the membrane resistance was R_m = (7.4 ±0.1) GΩ

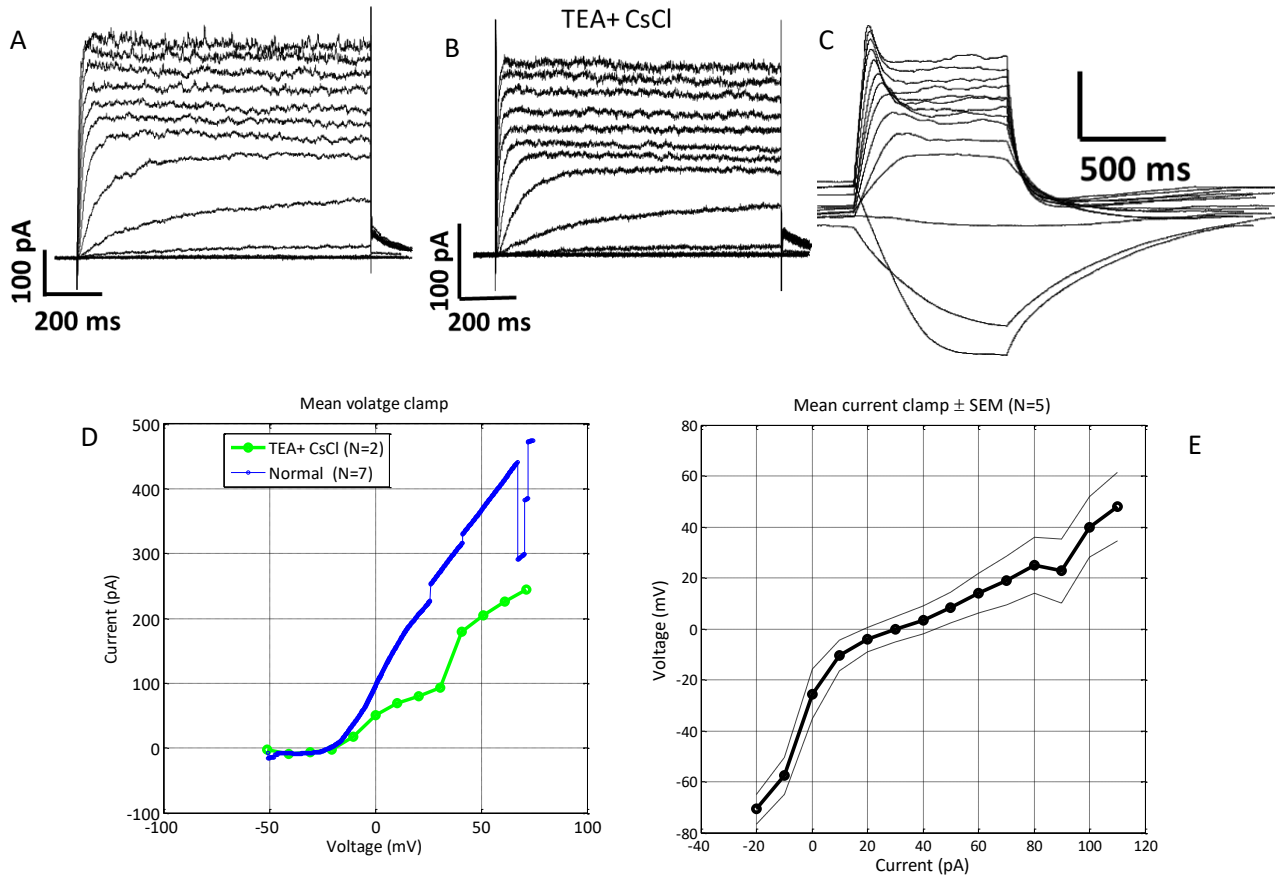

Figure 41. Patch clamp results for Schwann cells. *Voltage clamp traces with and without potassium channels blockers (A, B, and C), and current clamp (B, E).*

3.2. MESENCHYMAL STEM CELLS.

As discussed in 2.3.3, different protocols of differentiation of skin derived MSCs into MNs were tested at the same time. In this section are presented the results of the patch-clamp, and immunofluorescence experiments, at different stages of differentiation, performed on the cells that have undergone different protocols. These experiments have two main objectives. The first is the study of the characteristics of the cells in order to establish whether they are neurons or not. The second is to establish which protocol is the most efficient for the generation of neurons.

In the patch-clamp experiments the cells were tested with voltage and current clamp protocols. The voltage clamp protocol for testing active membrane properties consisted of a 200ms depolarizing -10 mV pulse from the holding potential, set equal to the resting potential, that preceded each depolarizing steps to remove inactivation. The -10 mV step was followed by series of 1s depolarizing steps with 15 mV increments, taking membrane potential form -15mV to +180 mV respect to the resting potential. In the current clamp protocol cells were held at 0 pA and current pulses were injected through the patch pipette to examine whether the cells were able to fire action potentials. The current increment (10-120 pA) between two steps was chosen separately for each cell in order to achieve an effective stimulation. Inhibitors were added to ECS to separate the contributions of the various types of channels to the total current flowing through the cell membrane in response to the stimuli. 0.5µM of tetrodotoxin (TTX) was used to block sodium channels, 500 µM of $NiCl_2$-$7H_2O$ to block the voltage-activated Ca^{2+}- channels, 500 µM of 4-aminopyridine (4-AP) and 5mM of tetraethylammonium (TEA) to block potassium currents. The extracellular solution is described in Table 5, and the intracellular in Table 4.

Immunofluorescence and RT-PCR were performed different stages of differentiation. Immunofluorescence pictures were collected with a confocal microscope ZEISS LSM700 by other colleagues of the lab.

PROTOCOL A.

The following diagram shows a summary of the differentiation protocol and the timeline of the patch clamp experiments. Immunofluorescence analysis was performed on the same coverslips used for patch clamp.

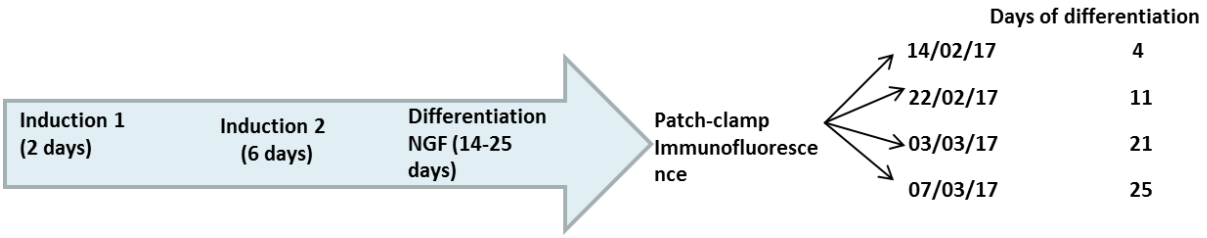

For each session of experiments the mean resting potential, membrane resistance, membrane capacitance, access resistance, and the I-V, V-I curves were computed from the experimental data.

The first experiments were performed 4 days after the beginning of the of the differentiation phase. Only five cells in the coverslip were showing neuron-like shape. We tested all these cells, but they did not show any action potential in the current clamp (Figure 44 C) or sodium currents in the voltage clamp (Figure 44 B), indicating that the voltage-gated Na^+ and K^+ channels are not yet developed in the cells. This is confirmed by the relation between current and voltage, which was ohmic (Figure 44 D and E). The mean resting potential was V_r = (-29.5 ± 3.5) mV and the mean membrane resistance was $R_m = (160.0 \pm 0.7)M\Omega$. The resting potential was considerably higher than the normal resting potential for a neuron (~ -70 mV). However, this fact is not so surprising since the cells are at the very beginning of the differentiation stage.

At 11 days of differentiation the voltage and current clamp traces were showing substantial differences with the recorded ones at 4 days of differentiation. In the voltage clamp there were small traces of voltage-activated currents (Figure 45). In addition to that, the I-V and V-I relations calculated from current and voltage clamp data are no longer linear as in the first experiments. Altogether, 8 cells were tested, but only two were considered for the analysis. The mean resting potential was more negative than before, V_r = (-44.0 ± 1.1) mV. Thus, we concluded that the cells are still premature, but they were proceeding in a good direction.

The third session of experiments was performed at 21 days of differentiation (Figure 46). 10 cells were tested. The mean resting potential V_r = (-46.0 ± 6.3) mV, was compatible with its estimation at 11 days. However, the voltage clamp traces were showing typical trend related to the voltage-gated potassium channels. In the current clamp there were small action-potential like peaks, but they were appearing under a very high stimulation: normally for neurons 20 pA steps taking the membrane from -20 pA to 100 pA maximum is enough to record action potentials, here 120 pA steps were applied, taking the membrane current from -120 pA to 1440 pA. This fact indicated that, probably, these peaks were related only to the opening of voltage-gating potassium channels rather than to sodium channels. It is also important to note that only one cell in ten (10%) was showing such characteristics that indicate an evolution towards neuronal-like behaviour.

The last electrophysiology experiments were performed at 25 days of differentiation (Figure 47). The voltage clamp protocol was the same used for the previous recordings, while the current clamp protocol consisted in 11 current sweeps taking the current form -10 pA to 110 pA, with 10 or 20 pA intervals depending on the specific cells. The voltage clamp traces were showing the typical pattern associated with voltage-activated potassium currents, and in the current clamp the 23% of the cells were showing small single AP-like peaks. The mean resting potential was V_r = (-44.7 ± 8.6) mV, still near the value at 11 days, and the membrane resistance R_m = (3.7 ± 0.1) GΩ. The cells cannot be considered mature neurons, but the fact that the peaks in current clamp were appearing at small stimulations was suggesting that probably a small fraction of sodium channels was developed, but not enough to permit the firing of action potentials.

Immunofluorescence analysis was performed at 11 and 21 days. The cells were stained for typical neuronal markers, as NeuN, and NeuroFilament (NF), both diluted 1:50. The nuclei were counterstained with DAPI. At 11 days many cells were expressing NeuN, but not all of them were expressing also Neurofilament Figure 42). At 21 days (Figure 43), the situation was almost the same: few cells were expressing both NueN and NF.

This results together indicated that we cannot consider the cells completely functional neuros, since these cells were showing voltage-activated potassium currents, but they did not develope not enough sodium channels to allow the generation of action potentials. Thus, even after 25 days of differentiation, which for hIPSCs are more than enough to produce functional neurons, we obtained only premature cells

In the following pages are reported the results of the experiments.

Days of differentiation	Resting potential (mV)	Membrane resistance (MΩ)	Number of cells
4	(-29.5 ± 3.5)	(160.0 ± 0.7)	5
11	(-44.0 ± 1.1)	(15.9 ± 0.1)	8
21	(-46.0 ± 6.3)	(77.6 ± 0.2)	10
25	(-44.7 ± 8.6)	(3.7 ± 0.1)	11

Table 6. Summary of mean cell parameters.

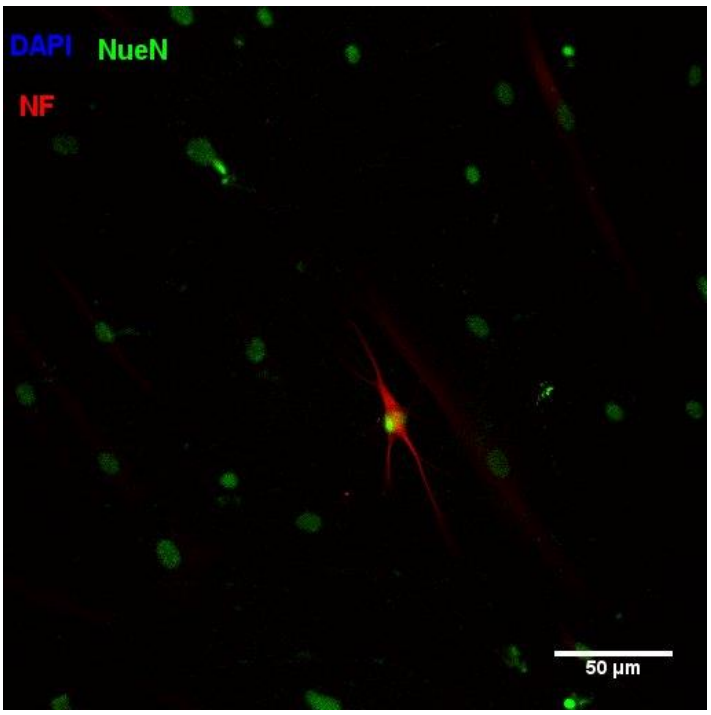

Figure 42. Immunofluorescence image at 11 days of neuronal differentiation.

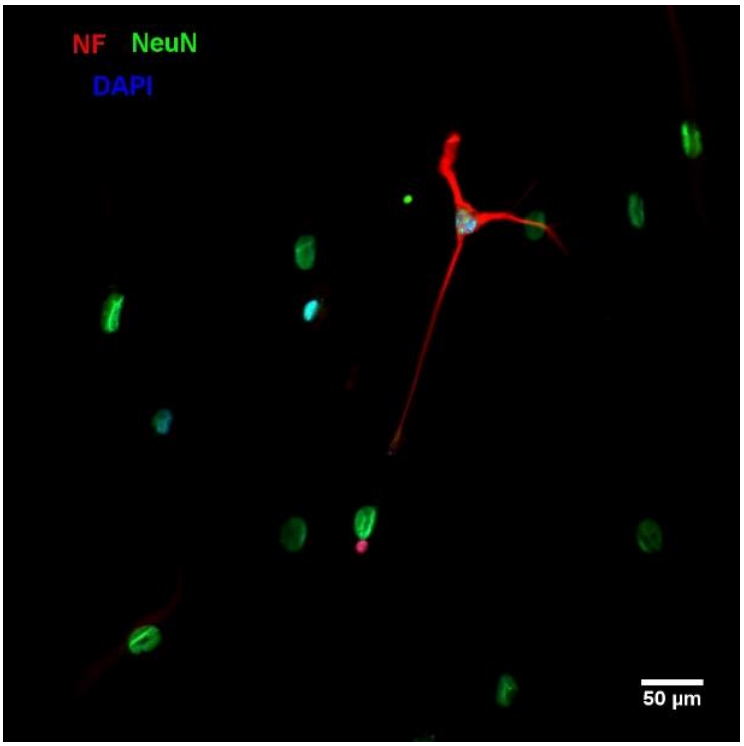

Figure 43. Immunofluorescence at 21 days of neuronal differentiation.

.

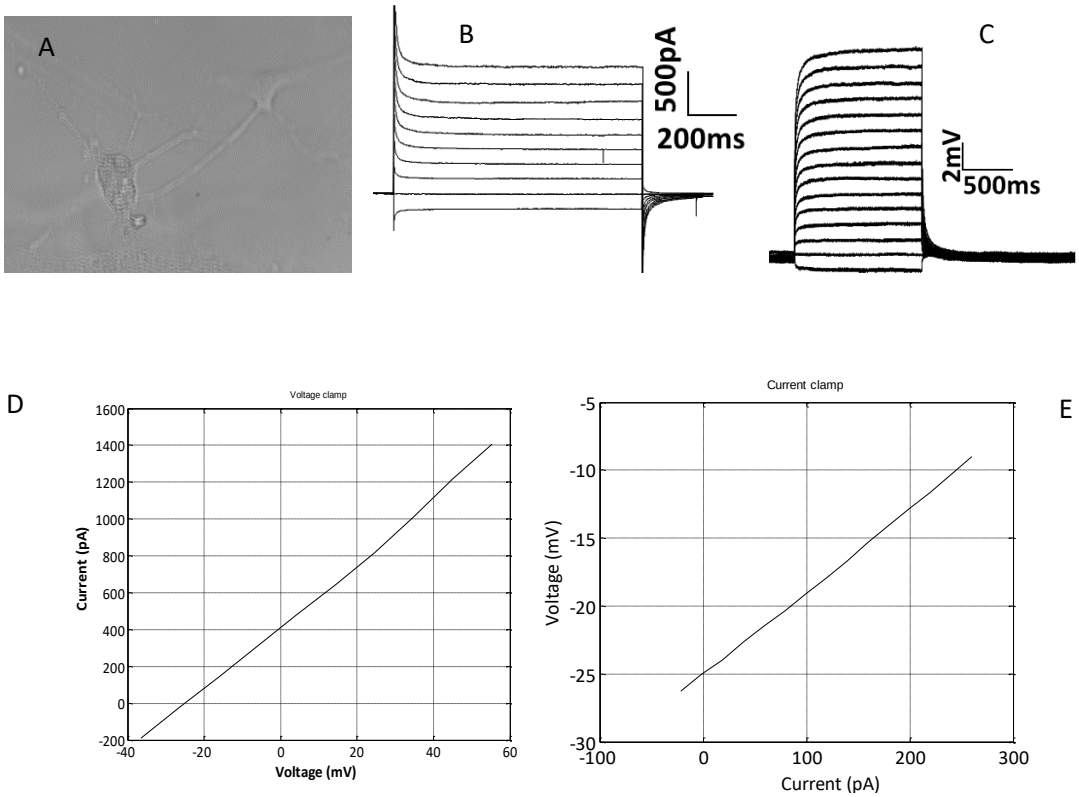

Figure 44. Patch clamp experiments at day 4. *Voltage clamp trace (B) and current clamp (C,20 pA steps); with respective V-I and I-V relation (D, E). The cell parameters were: Vr =-26 mV , Rm = 182±5 MΩ, and Ra=74±5 MΩ.*

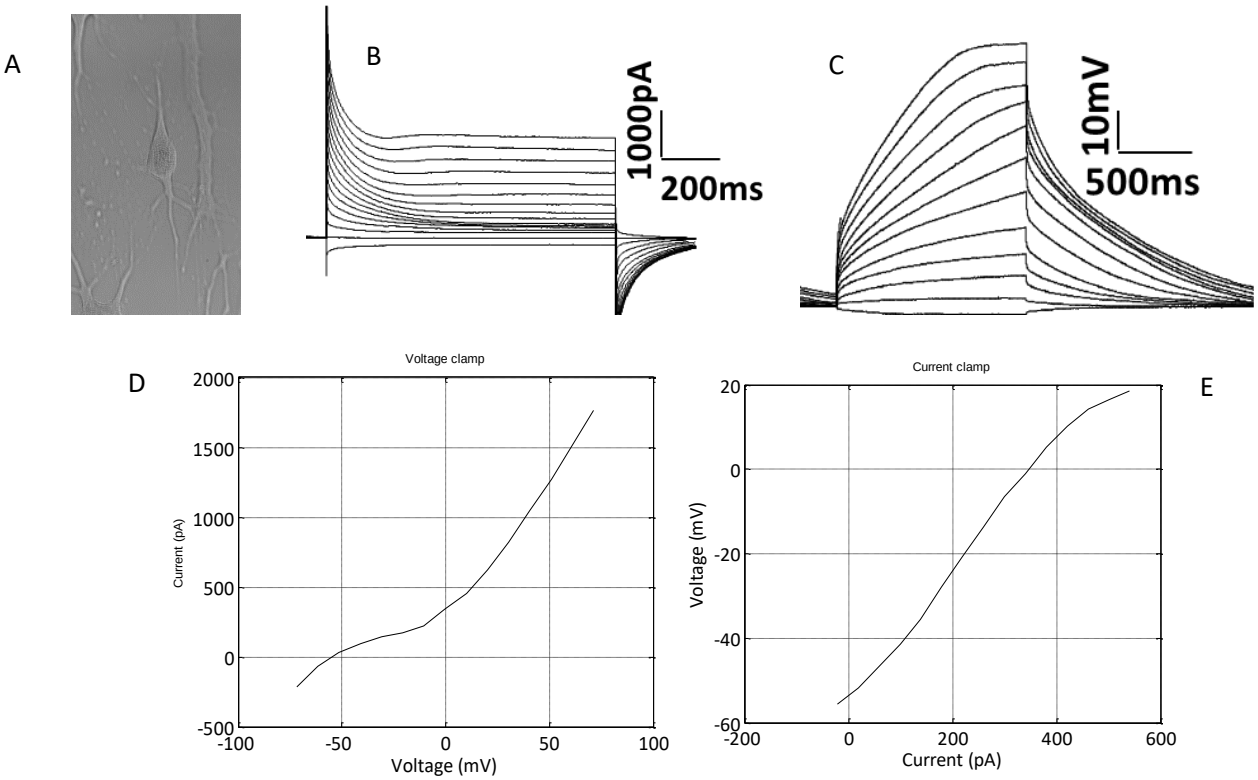

Figure 45. Patch clamp experiments at 12 days. *Voltage (B) and current (C, 20 pA steps) recorded traces, with V-I and I-V relations (D, E). The cell parameters were: Vr=-55 mV, Rm= 4.9±0.1 MΩ, Ra=45.2±0.1 MΩ.*

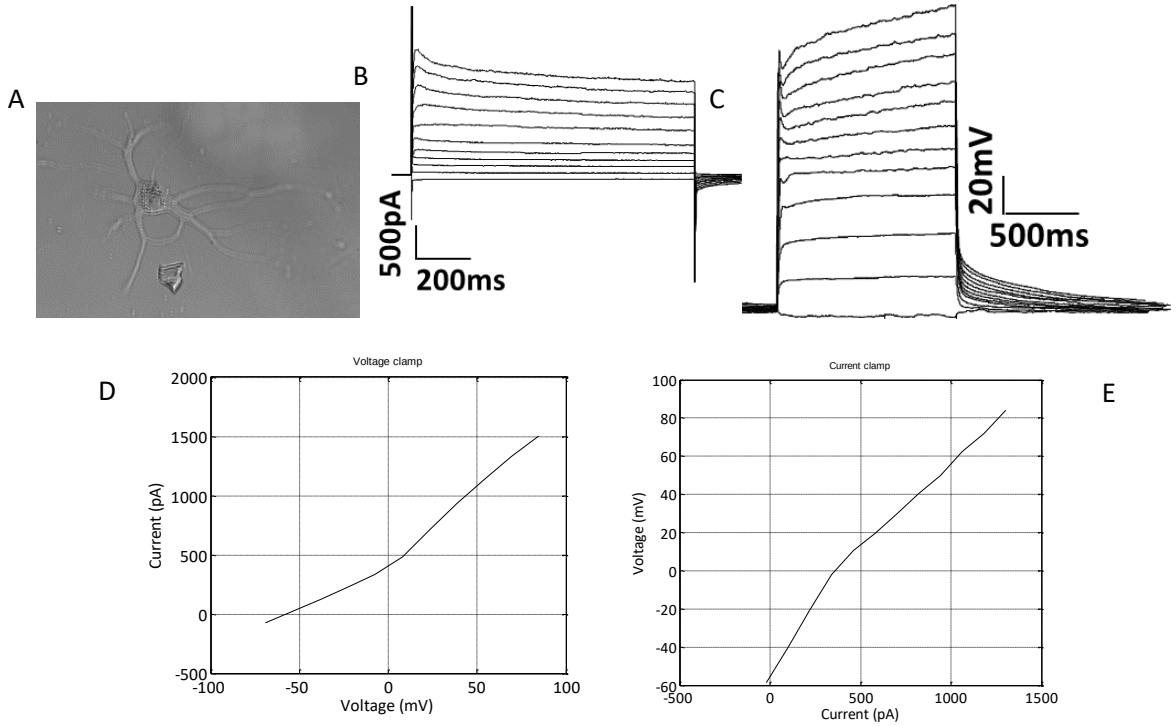

Figure 46. Patch clamp at day 21. *Voltage (B) and current (C, 120 pA steps) recorded traces, with V-I and I-V relations (D, E). The cell parameters were: Vr=-58 mV, Rm= 109.0±0.7 MΩ, Ra=35.9.2±0.3 MΩ*

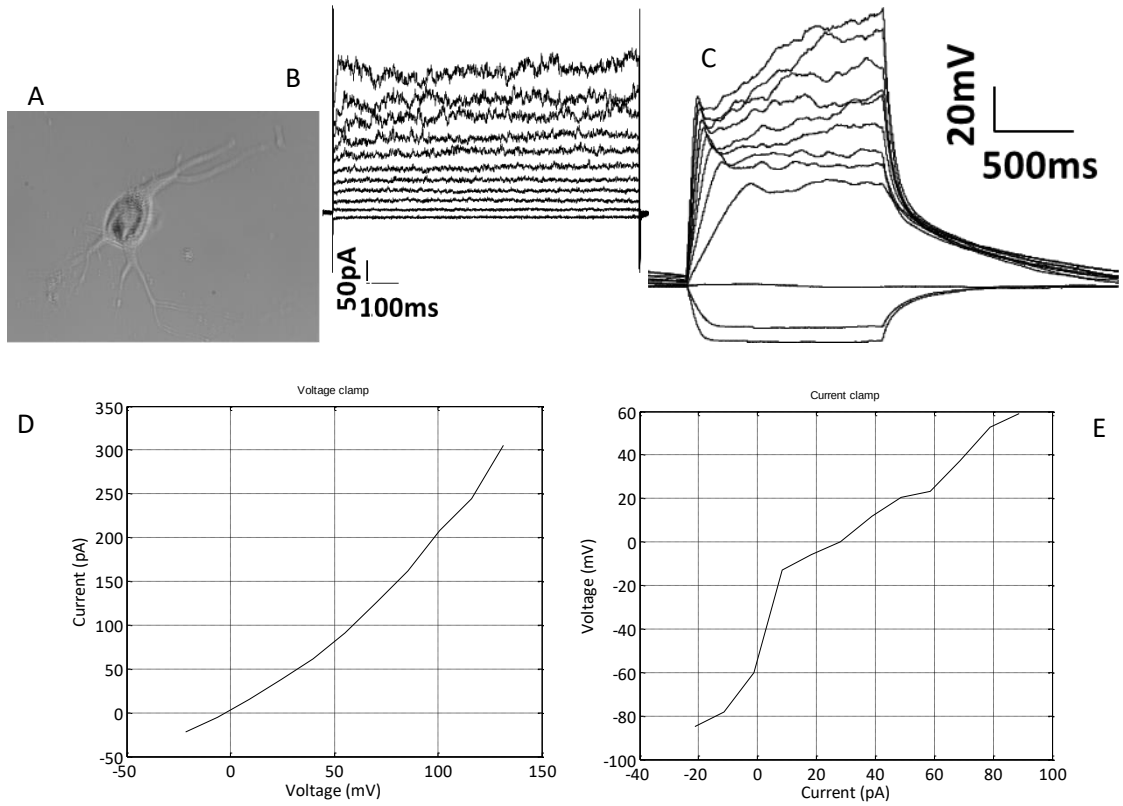

Figure 47. Patch clamp at day 25. *Voltage (B) and current C,10 pA steps) recorded traces, with V-I and I-V relations (D, E). The cell parameters were: Vr=-60 mV, Rm= 860.3±102.7 MΩ, Ra=13.14±0.08 MΩ*

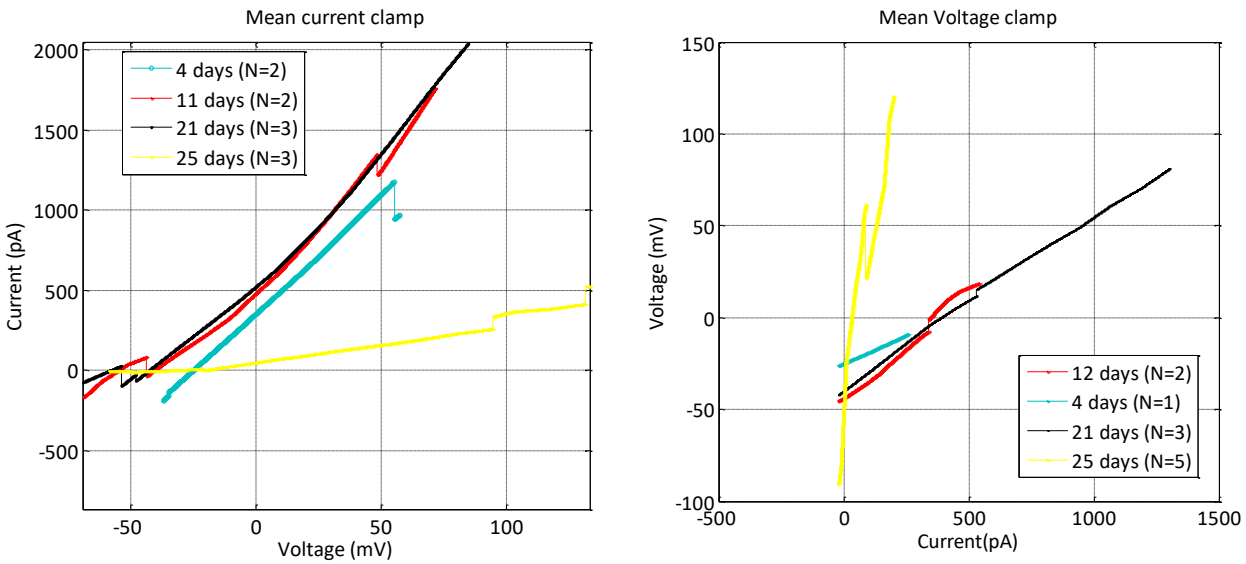

Figure 48. Mean current clamp I-V traces (left) and voltage clamp V-I traces (rigth)

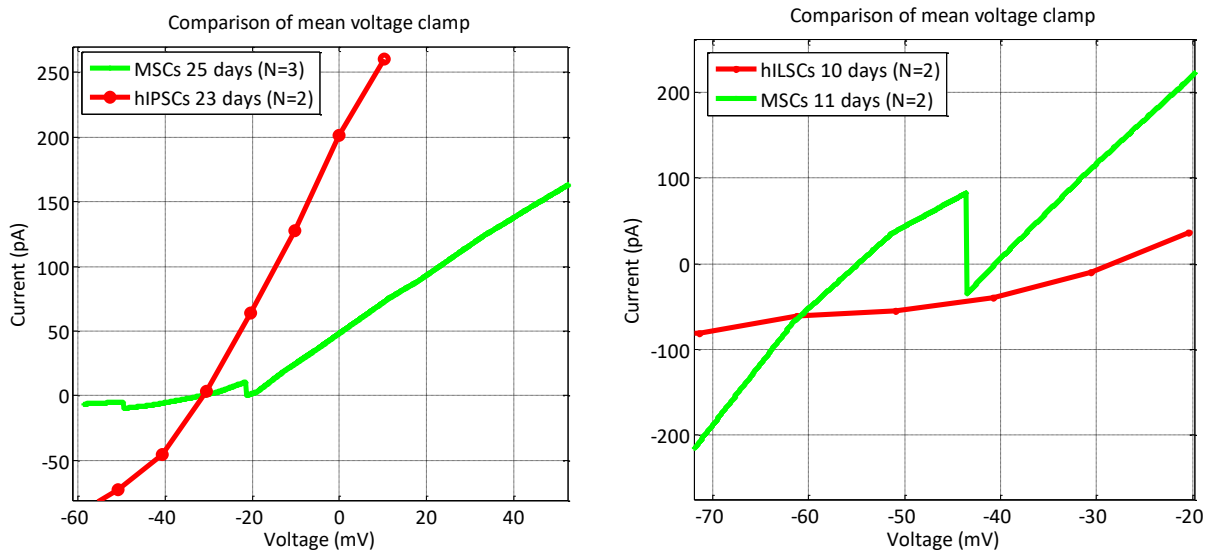

Figure 49. Comparison between MSCs and hIPSCs voltage clamp experiments

PROTOCOL B.

The following diagram shows a summary of the differentiation protocol and the timeline of the patch clamp experiments. Immunofluorescence analysis was performed on the same coverslips used for patch clamp.

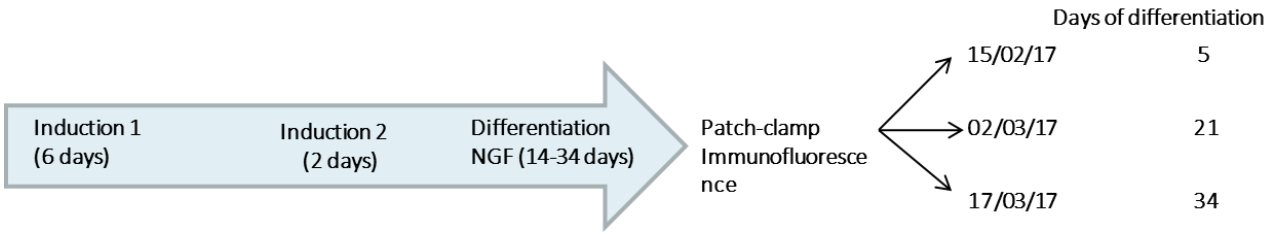

As before the cells were tested at different timepoints both with voltage clamp and the current clamp. In the coverslips used for patch clamp also immunofluorescence was performed.

At five days of differentiation the cells are not showing any action potential, but in the voltage clamp was found some evidence of voltage activated currents (Figure 50). In total nine cells were tested, and three were selected for the analysis. The mean resting potential was very low V_r = (-13.7± 0.5) mV compared to that of protocol A at the same stage, and even more to the typical value for neurons.

Since the cells that have undergone to differentiation with protocol A at 11 days were not showing particular neuronal activity, we decided to test again the cells differentiated with protocol B at 21 days, since the two protocols are very similar. At 21 days, the voltage clamp recordings were showing the presence of voltage-activated potassium currents (Figure 51). Also, in the current clamp we observed that the 36% of the cells were showing AP-like peaks. The mean resting potential was V_r = (-51.8± 3.1) mV, thus a little more negative than that of the protocol A at the same stage. However, the recorded currents and voltages were very similar in the two cases.

The last electrophysiology tests were performed at 34 days of differentiation (Figure 52). In total six cells were tested and only one was showing neuronal-like characteristics. In the current clamp, single AP-like peaks can be seen when positive voltage were reached. In this case the resting potential was -56 mV and the membrane resistance R_m = (3.0± 0.2) GΩ. Tests with three different inhibitors were performed to investigate the nature of these AP-like peaks in the voltage -clamp: TEA-Cl 5 mM + 4-AP 500 µM, TTX 0.5 Mm, and $NiCl_2$-$6H_2O$ 500 µM. The peaks in the current clamp were not disappearing with action of neither with TXX nor with $NiCl_2$-$6H_2O$. However, in the presence of TEA-Cl + 4-AP their height was reduced (this difference can be easily noticed form the V-I curves) indicating that these peaks may be related with the activation of voltage-gated potassium channels rather than voltage-activated sodium channels. The fact that the peaks in the current clamp with TEA-Cl and 4-PA were not disappearing probably is related with a too short time of inhibitor delivery. Together these observations were indicating that despite the fact that they were showing some typical neuronal potassium currents they were still immature even after 42 days. Therefore, the situation was very similar to that of the protocol A.

Immunofluorescence was performed on the same coverslips used for patch clamp for typical neuronal markers (NeuN, NF, GAP43, and MAP2) at 7 and 16 days of differentiations. As for protocol A at 7 days few cells were positive for both NeuN and NF, and the same situation is repeated for the staining at 16 days. Few cells were expressing both MAP2 and GAP43 (Figure 53).

Days of differentiation	Resting potential (mV)	Membrane resistance (MΩ)	Number of cells
4	(-13.7± 0.5)	(135.9 ± 0.3)	3
21	(-51.8± 3.1)	(181.7± 0.2)	8
34	-51	(3.0± 0.2) GΩ	10

Table 7. Summary of mean cell parameters

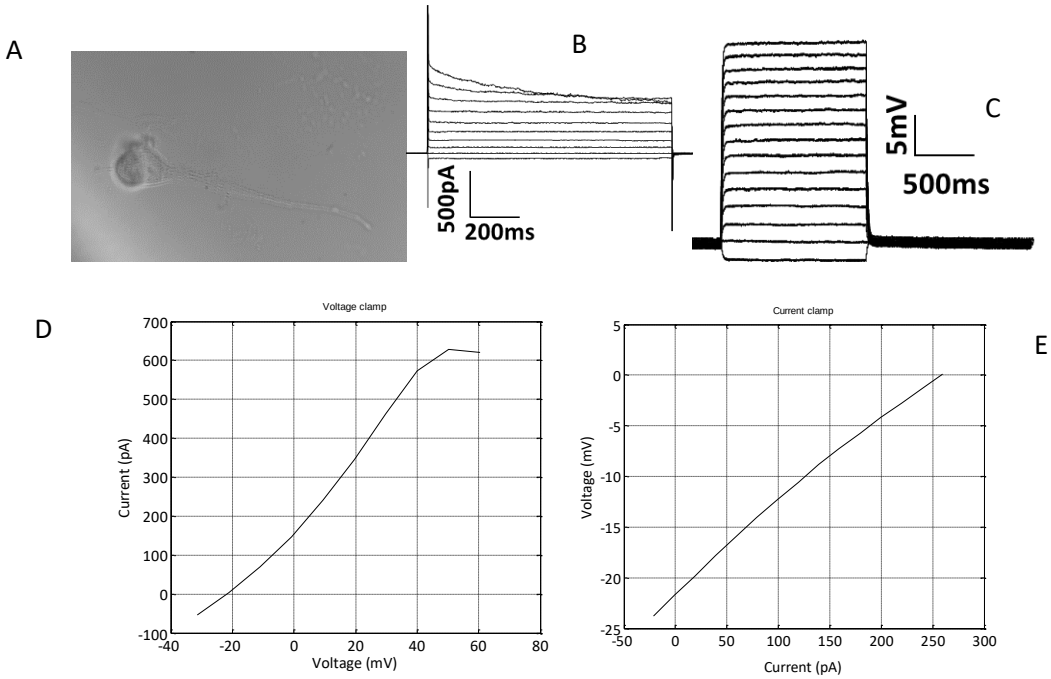

Figure 50. Patch clamp at day 5. *Voltage (B) and current (C,20 pA steps) recorded traces, with V-I and I-V (D,E). The cell parameters were: Vr=-14 mV, Rm= 160.7±4.7 MΩ, Ra=22.4±0.7 MΩ.*

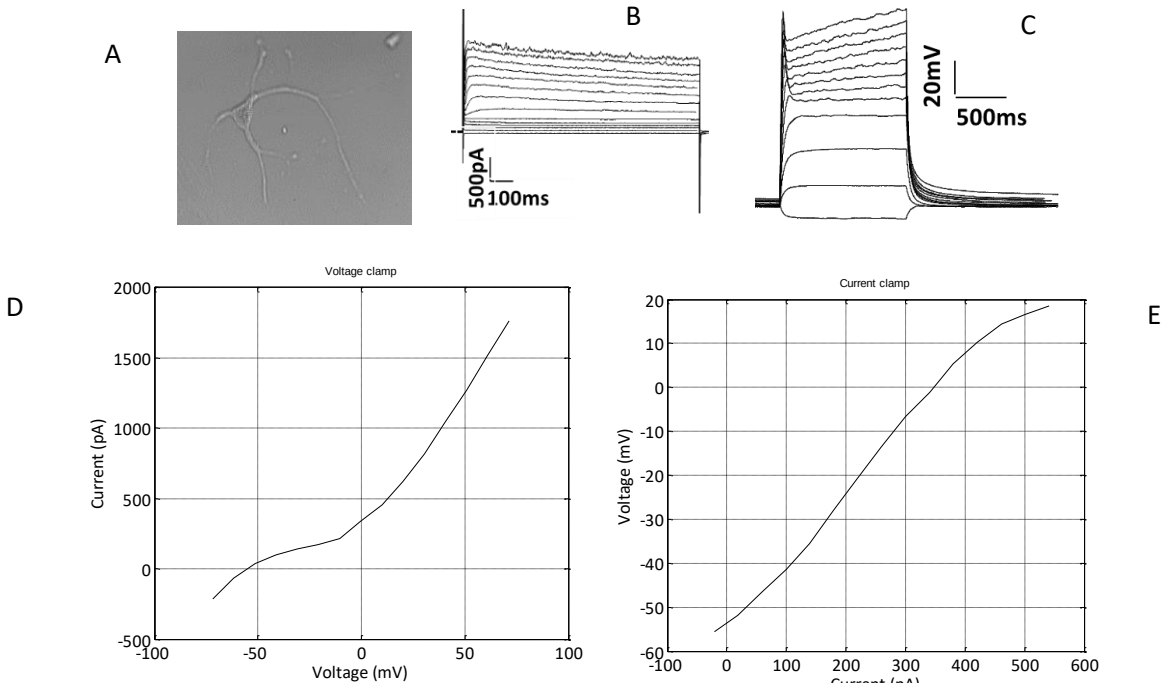

Figure 51. Patch clamp at day 21. *Voltage (B) and current (C,50 pA steps) recorded traces, with V-I and I-V relations (D, E). The cell parameters were: Vr=-50 mV, Rm= 21.8±0.2 MΩ, Ra=32.4±0.12 MΩ.*

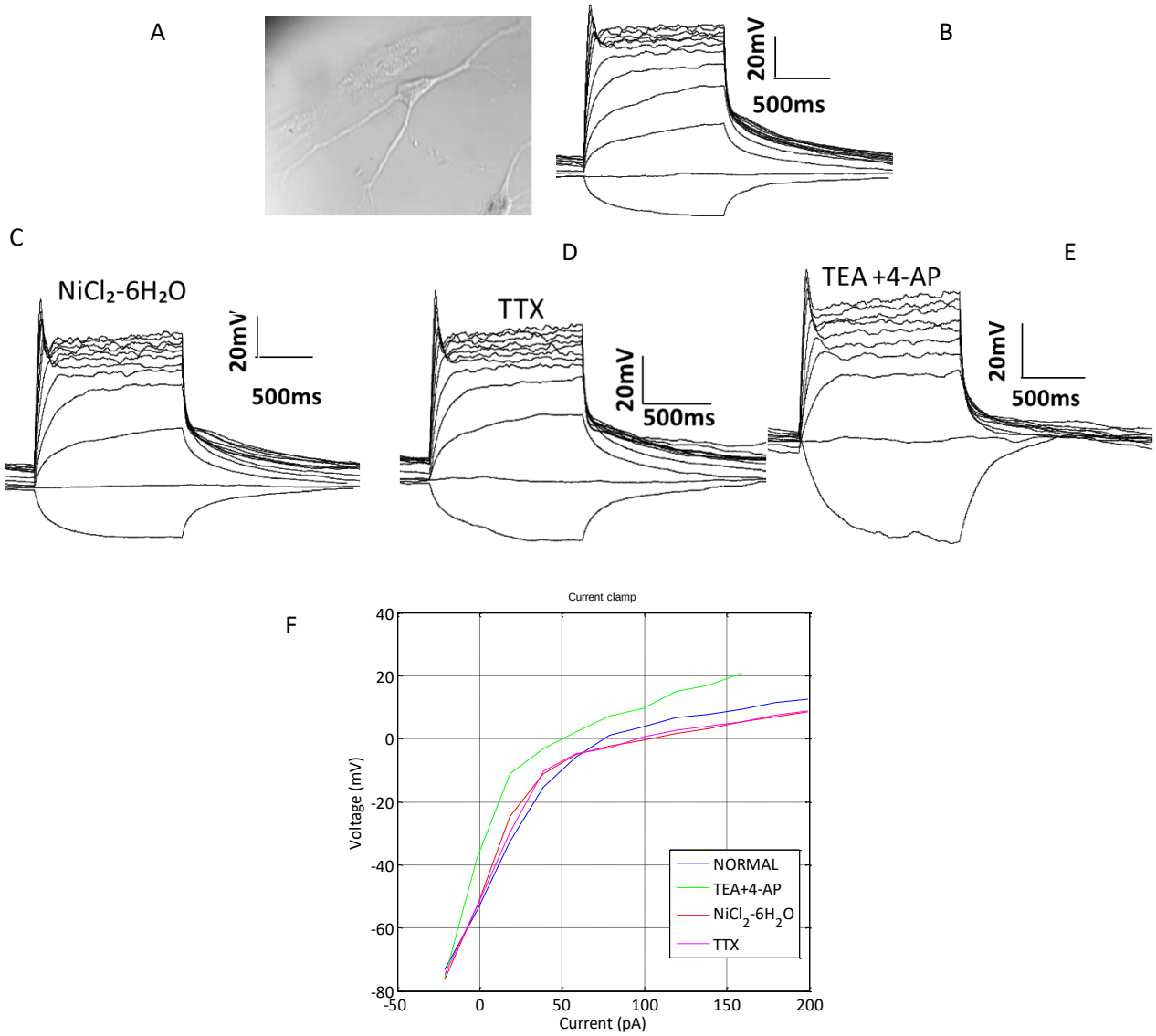

Figure 52. Patch clamp at day 34. *Current clamp (B,20 pA steps) traces in presence of TTX 1 µM (C), $NiCl_2$-$6H_2O$ 500 µM (D), and TEA 5 mM +4-AP 500 µM (E). The cell parameters were: Vr=-56 mV, Rm= 3.0±0.9 GΩ, Ra=15.64±0.0.03 MΩ.*

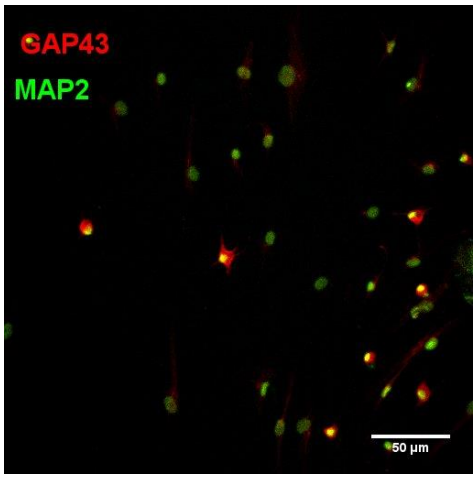

Figure 53. Immunofluorescence at 21 days

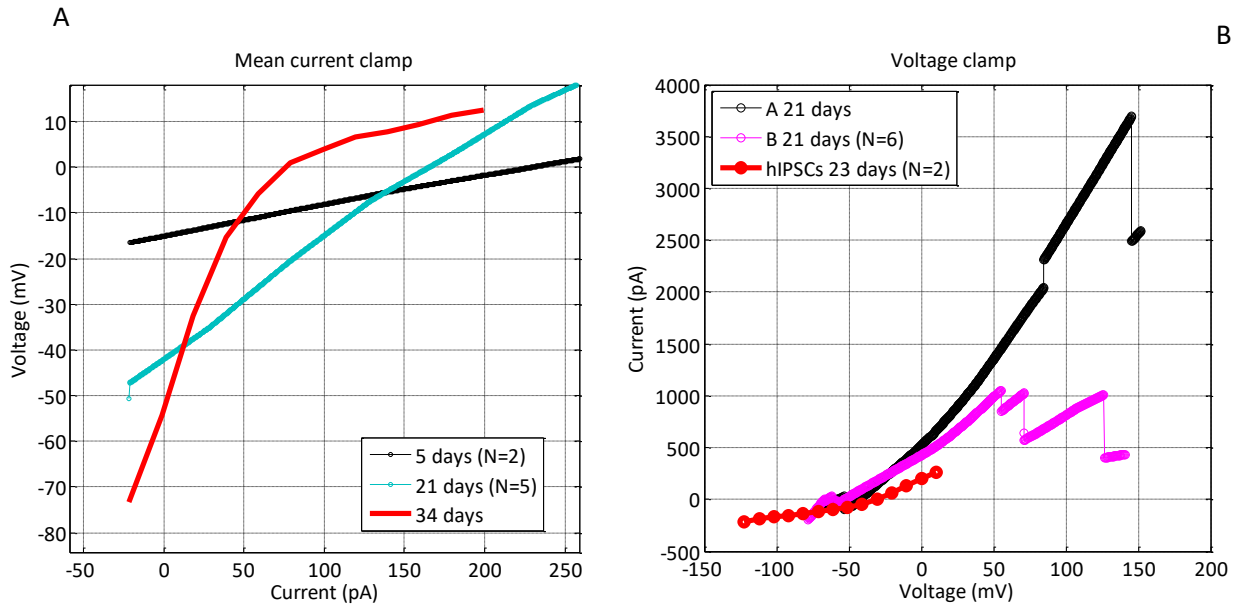

Figure 54. Comparison between I-V curves at different time points (A). (B). Comparison between protocol A, B and hIPSCs voltage clamp V-I curves.

PROTOCOL C.

The following diagram shows a summary of the differentiation protocol and the timeline of the patch clamp experiments. Immunofluorescence analysis was performed on the same coverslips used for patch clamp.

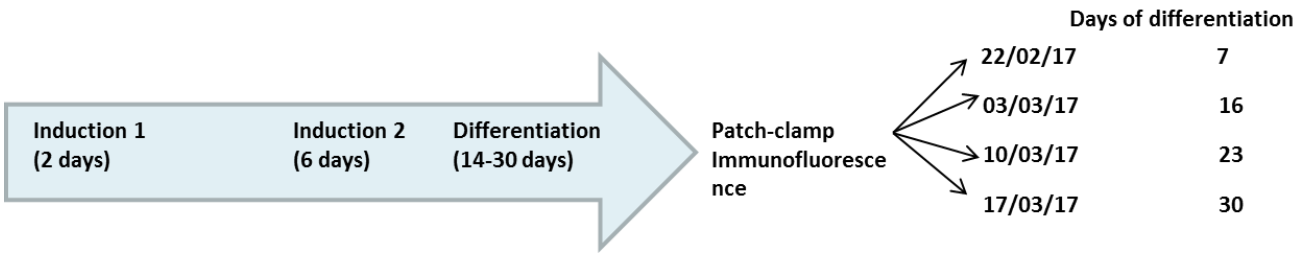

The electrophysiological tests were performed at 7,16,23, and 30 days of differentiation. At seven days of differentiation the mean resting potential was V_r = (-65.5± 0.5) mV, thus very closer to the expected value. However, no action potential or voltage activated currents were detected (Figure 56).

At 16 days, the situation in the current and voltage-clamp was the same (Figure 57), but with an increasing of the resting potential, V_r = (-55.3± 1.7) mV. We tested eight cells, and we found only one cell which was showing potassium currents.

The third test was conducted at 23 days (Figure 58). The mean resting potential was V_r = (-47.3± 2.4). Even though the resting potential was still increasing, in this case the 57% of the cells were presenting voltage-gated potassium currents, and one cell was showing also small voltage-activated sodium currents. In the current clamp, small AP-like peaks were observed. TTX was applied to verify whether the peaks in current clamp were disappearing. As shown in Figure 58. E the small peaks seemed to become sharper in presence of the blocker. In the I-V relation was observed a small shift in the curve, but it is related to a depolarization of the cell rather than to an effect of the blocker, since there was only a shift of the curve towards more

positive voltages, and not the expected rectification effect. We could explain this situation in two ways: the blocker was applied for a too short time to induce an observable effect, or the sharpening of the peaks is truly related to the inactivation of sodium channels.

The last experiments were performed at 30 days (Figure 59). In this case only one cells of seven was presenting neuronal-like characteristics. The resting potential moved to a value similar to the initial, it was -63 mV, but this time we detected potassium currents and the usual peaks in the current clamp. TEA-Cl and 4-AP were applied during the voltage clamp and leaded to the disappearing of potassium currents. In the current clamp TTX was applied but no significant effects were observed in the recorded traces, however a small effect of rectification in the I-V curve can be noticed in the presence of the blocker. Thus, probably the sodium channels contribution was too small to be distinguished directly in the recorded traces both in current and voltage clamp.

From Figure 61 we noted that the V-I relation derived from voltage clamp data is very similar for all the protocols around 21-25 days, and also, at lower voltages with the one of IPS cells.

Immunofluorescence was performed at 16 and 23 days. At 16 days (Figure 55) the cells were expressing both NueN and NF almost in the same ratio. Similar situation was found at 23 days for MAP2 and GAP43 (Figure 55). The number of cells expressing both markers applied was higher than that of protocols A and B.

Days of differentiation	Resting potential (mV)	Membrane resistance (MΩ)	Number of cells
7	(-65.5± 0.5)	(18.6± 0.1)	2
16	(-55.3± 1.7)	(23.87± 0.02)	8
23	(-47.3± 2.4)	(230.7± 1.8)	10
30	-63	(213.0± 3.7)	1

Table 8. Summary of mean cell parameters

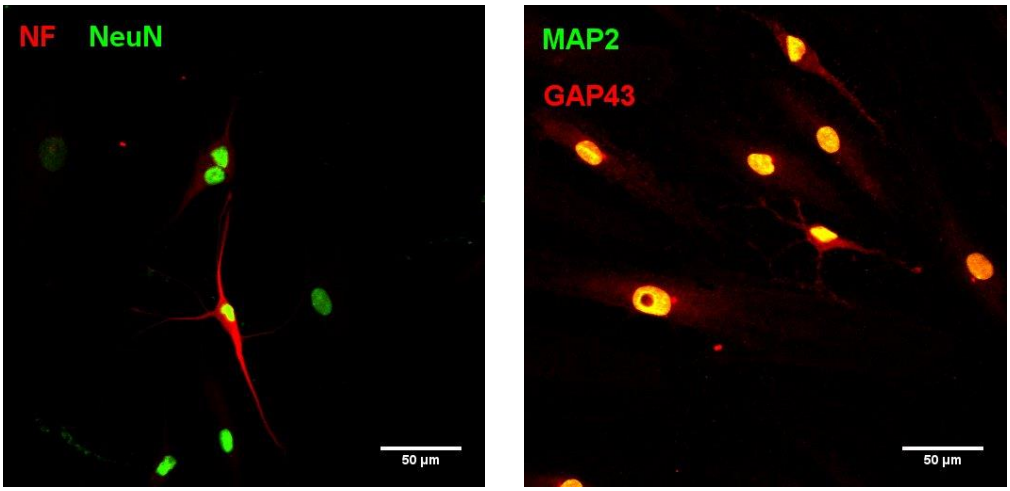

Figure 55. Immunofluorescence at 16 days (left) and at 23 days (right).

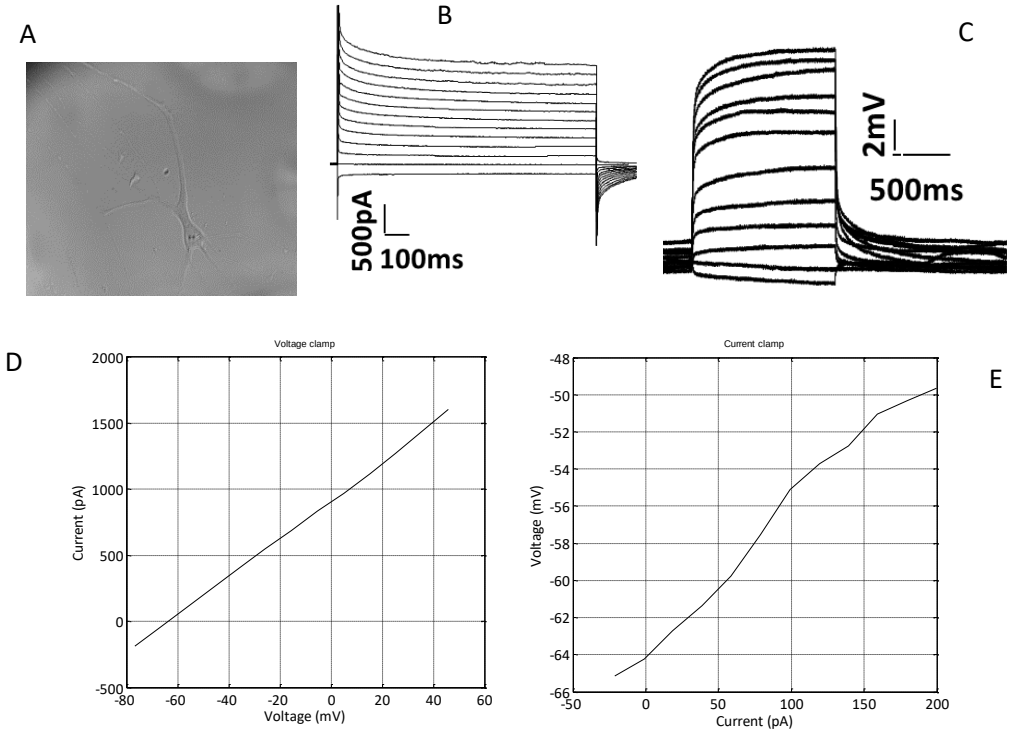

Figure 56. Patch clamp at 7 days. *Voltage (B) and current (C,20 pA steps) recorded traces, with V-I and I-V relations (D, E). The cell parameters were: Vr=-66 mV, Rm= 27.6±0.1 MΩ, Ra=31.15±0.08 MΩ.*

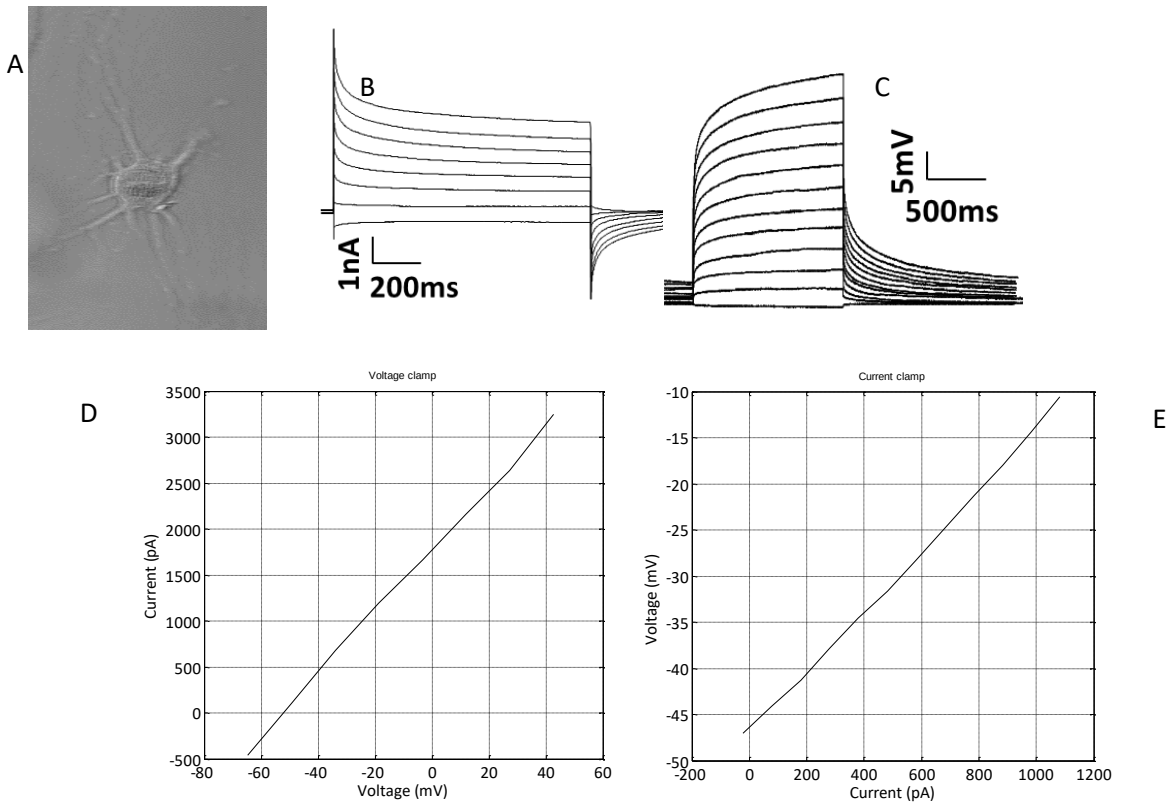

Figure 57. Patch clamp at 16 days. *Voltage (B) and current (C,20 pA steps) recorded traces, with V-I and I-V relations (D, E). The cell parameters were: Vr=-54 mV, Rm= 27.6±0.1 MΩ, Ra=31.15±0.08 MΩ.*

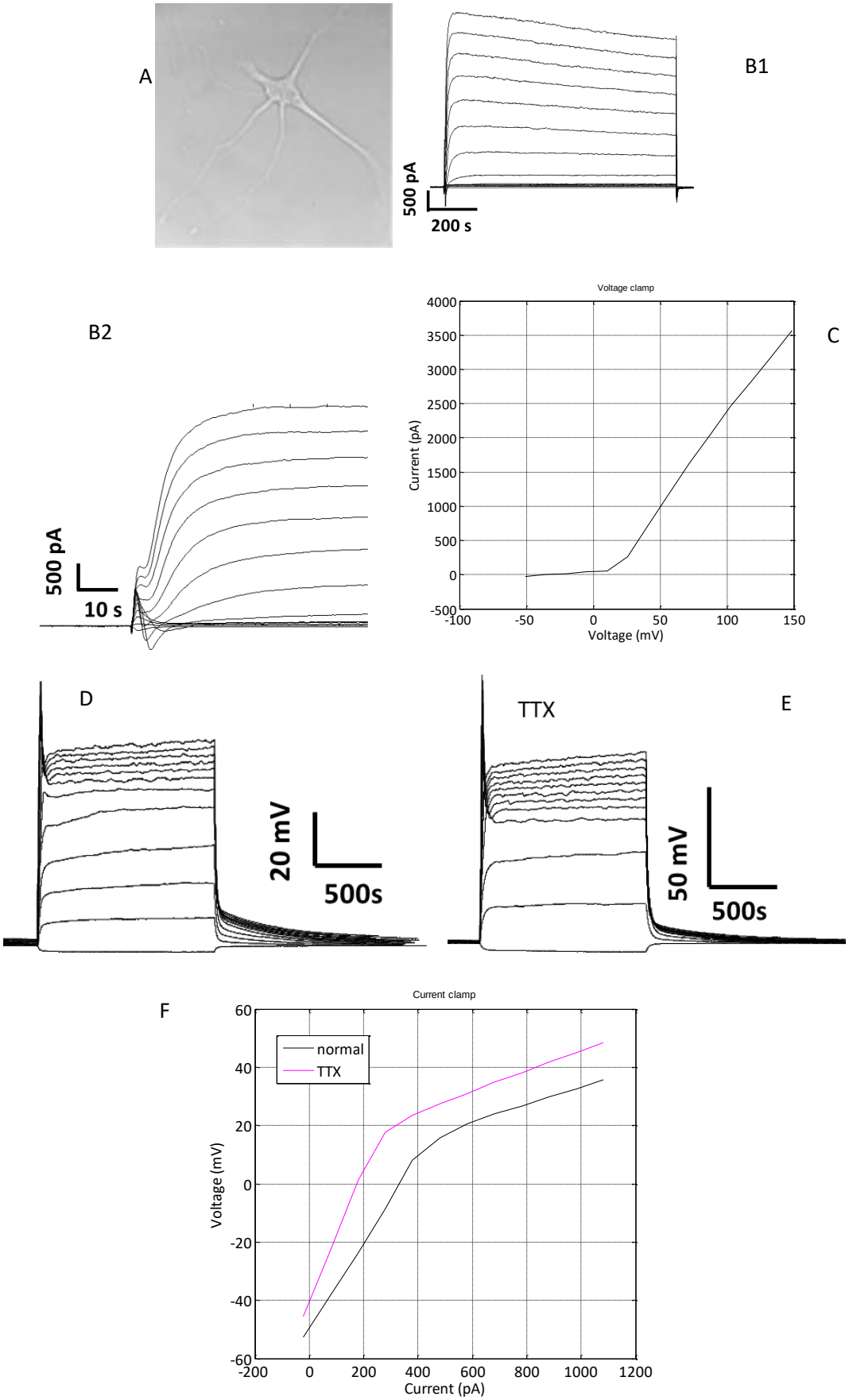

Figure 58.Patch clamp at day 23. *Voltage clamp (B1, B2) and current clamp (100 pA steps) with and without TTX 1Mm (D, E), together with V-I and I-V relations (C, F). The cell parameters were: Vr=-40 mV, Rm= 333.2±10.3 MΩ, Ra=22.9±0.4 MΩ.*

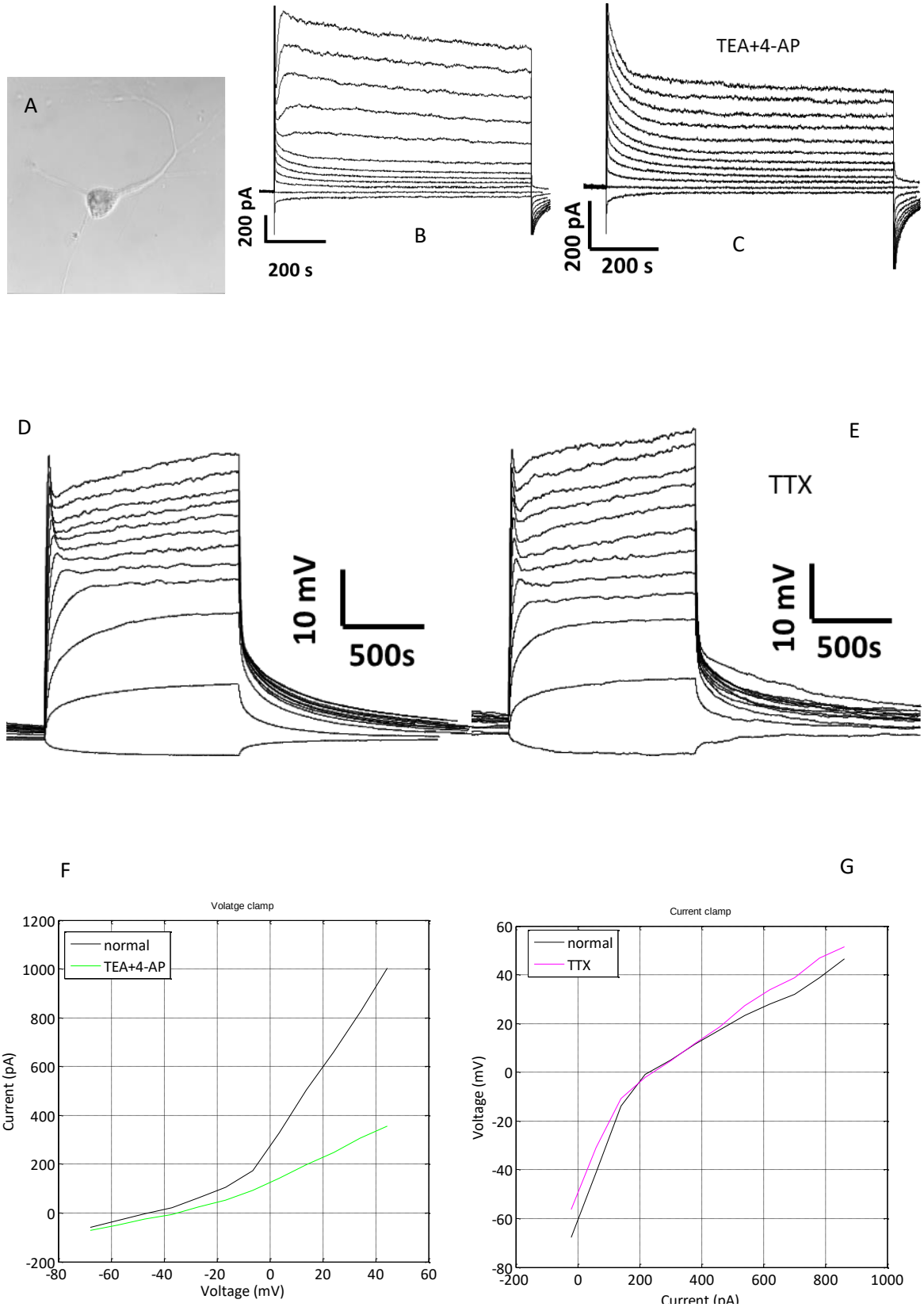

Figure 59.Patch clamp at 30 days. *Voltage clamp with and without TEA 5Mm +4-AP 500 µM (B, C) and current clamp (80 pA steps) with and without TTX 1µM (D, E), together with V-I and I-V relations (F,G) The cell parameters were: Vr=-63 mV, Rm= 213±4MΩ, Ra=24.8±0.3 MΩ.*

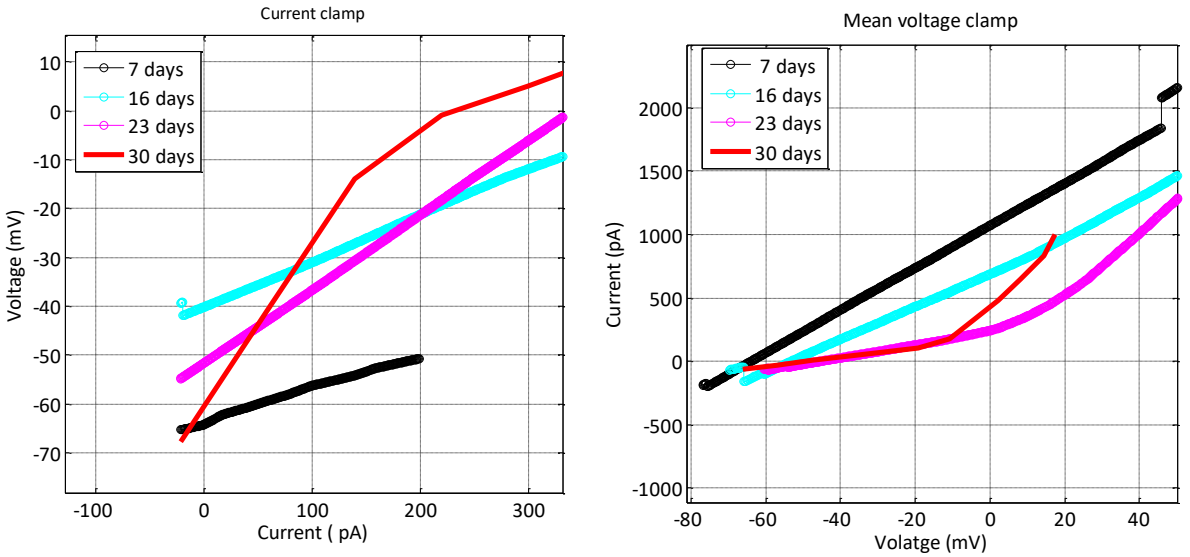

Figure 60. Man I-V (left) and V-I (right) curves at different stages.

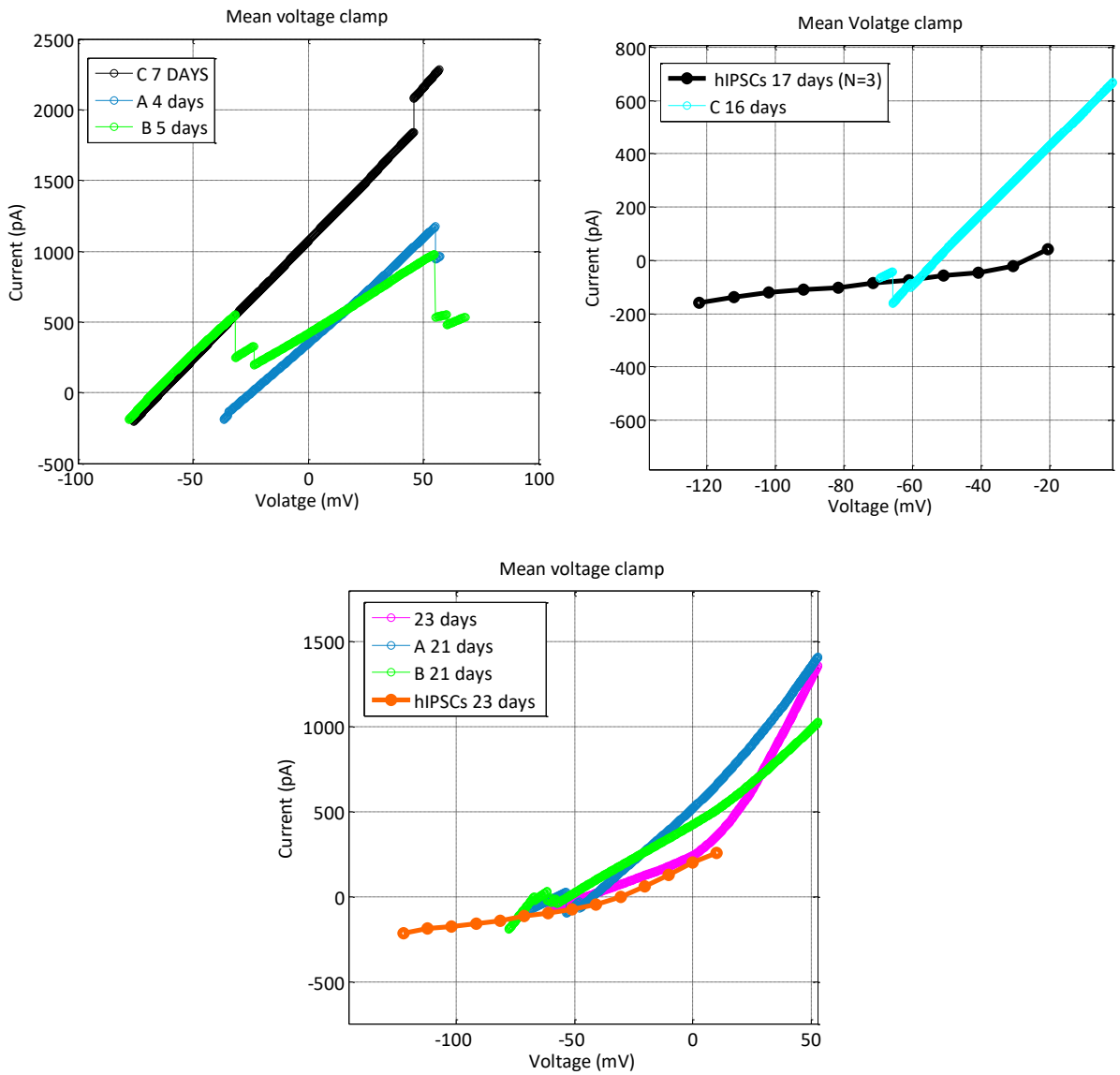

Figure 61. Comparison of the V-I curves between protocols A, B, C, and hIPSCs

PROTOCOL D.

The following diagram shows a summary of the differentiation protocol and the timeline of the patch clamp experiments. Immunofluorescence analysis was performed on the same coverslips used for patch clamp.

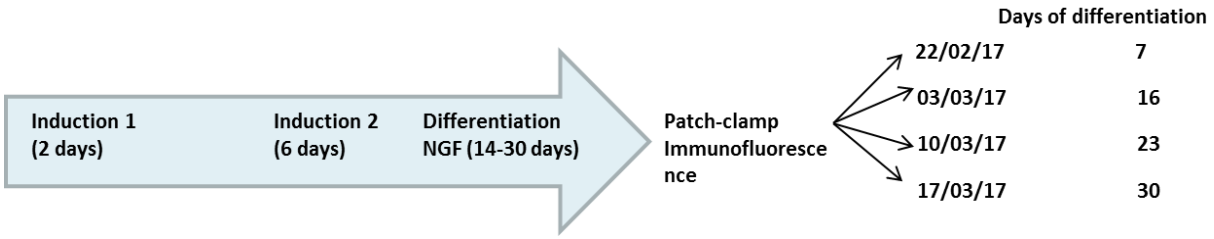

The duration of each phase of this protocol is the same of protocol C, the only difference was that the differentiation medium was not supplemented with NGF. The electrophysiological tests were performed at the same timepoints to compare the efficiency of the two protocols.

At seven days, the mean resting potential was V_r = (-46± 4) mV, thus very similar to that of protocol A and B at 4-5 days. We recorded only voltage clamp traces, because the cells detached from the pipette during the experiment due to problems with the perfusion system. In the voltage-clamp of both cells there were evidences of voltage activated potassium currents, in contrast with the ohmic behaviour observed in protocols A and B (Figure 64).

At day 16 the 57% of the cells were showing AP-like peaks in the current clamp (Figure 65), while in the protocol C at the same stage only 12% was showing this behaviour. The resting potential V_r = (-43.4± 8.0) mV is less negative than in the protocol C V_r = (-55.3± 1.7) mV.

More evident voltage activated currents and small AP-like peaks, under high current stimulations, were appearing at day 23 of differentiation (Figure 66). The mean resting potential was: V_r = (-51± 4) mV, again very similar to that of protocol A and B. TTX was tested in the current clamp, and as before the peaks were not disappearing. $NiCl_2$-$6H_2O$ applied during the current clamp did not lead to any significant effects neither in the trace nor in the I-V curves.

Other tests were performed at 30 days (Figure 67). Only one cell was showing the typical behaviour. The currents in voltage clamp were successfully blocked by TEA-Cl and 4-AP. $NiCl_2$-$6H_2$ was applied in the current clamp, however there were no evident effects, indicating that these cells were not expressing voltage-activated calcium channels, which are typical of premature neurons [28] [29].

No significant differences were observed during the time in the V-I curves (Figure 68) until day 30, when the curve became more similar to the V-I relation for hIPSCs at 23 days (Figure 69.D). As confirmed by the values of the resting potential the cells showed more similarity with that differentiated with protocols A and B than that of the protocol C. At low values of the voltage the curves were similar to that of the IPSC, despite the fact that the cells were not firing multiple action potentials.

We performed also immunostaining for NueN and NF after the patch at 7 and 16 days. At both stages the expression of the markers to that observed in protocols A and B (Figure 62, and Figure 63). The fraction of cells expressing NF was considerably low compared to that expressing NueN. In only few cells both markers were expressed.

Days of differentiation	Resting potential (mV)	Membrane resistance (MΩ)	Number of cells
7	(-46± 4)	(26.8± 0.4)	2
16	(-43.4± 8.0)	(22.8± 0.4)	7
23	(-51± 4)	(442.3± 1.7)	2
30	-63	(213.0± 3.7)	1

Table 9.Summary of mean cell parameters

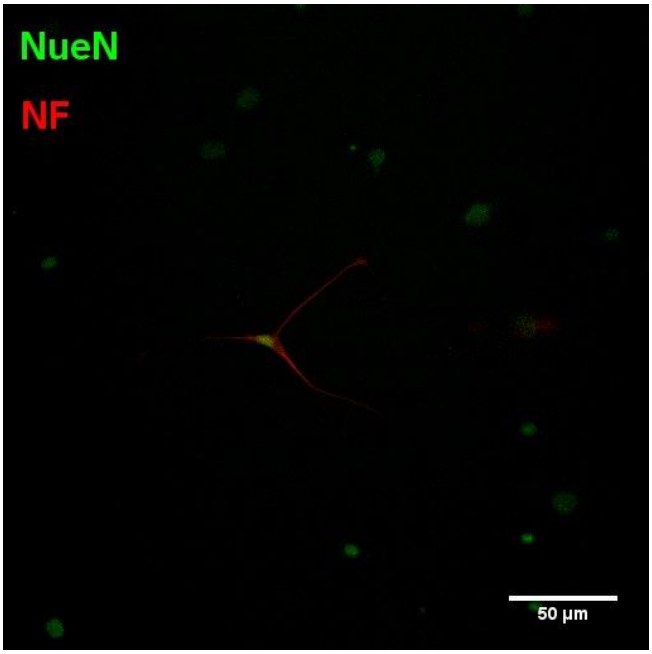

Figure 62. Immunofluorescence at 7 days.

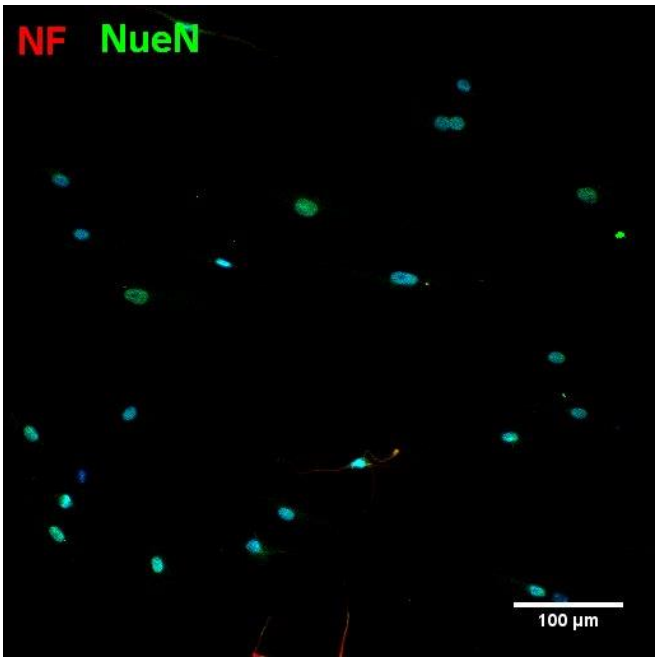

Figure 63. Immunofluorescence at 16 days.

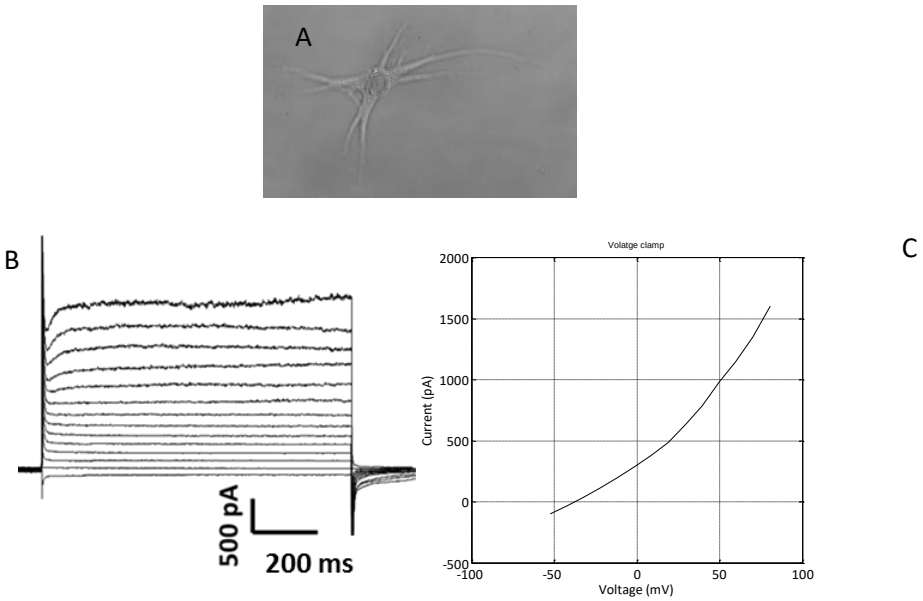

Figure 64. Patch clamp at 7 days. *Voltage clamp (B) with V-I relation (C). The cell parameters were: Vr=-50 mV, Rm= 23.4±2.4 MΩ, Ra=91.9±4.6 MΩ*

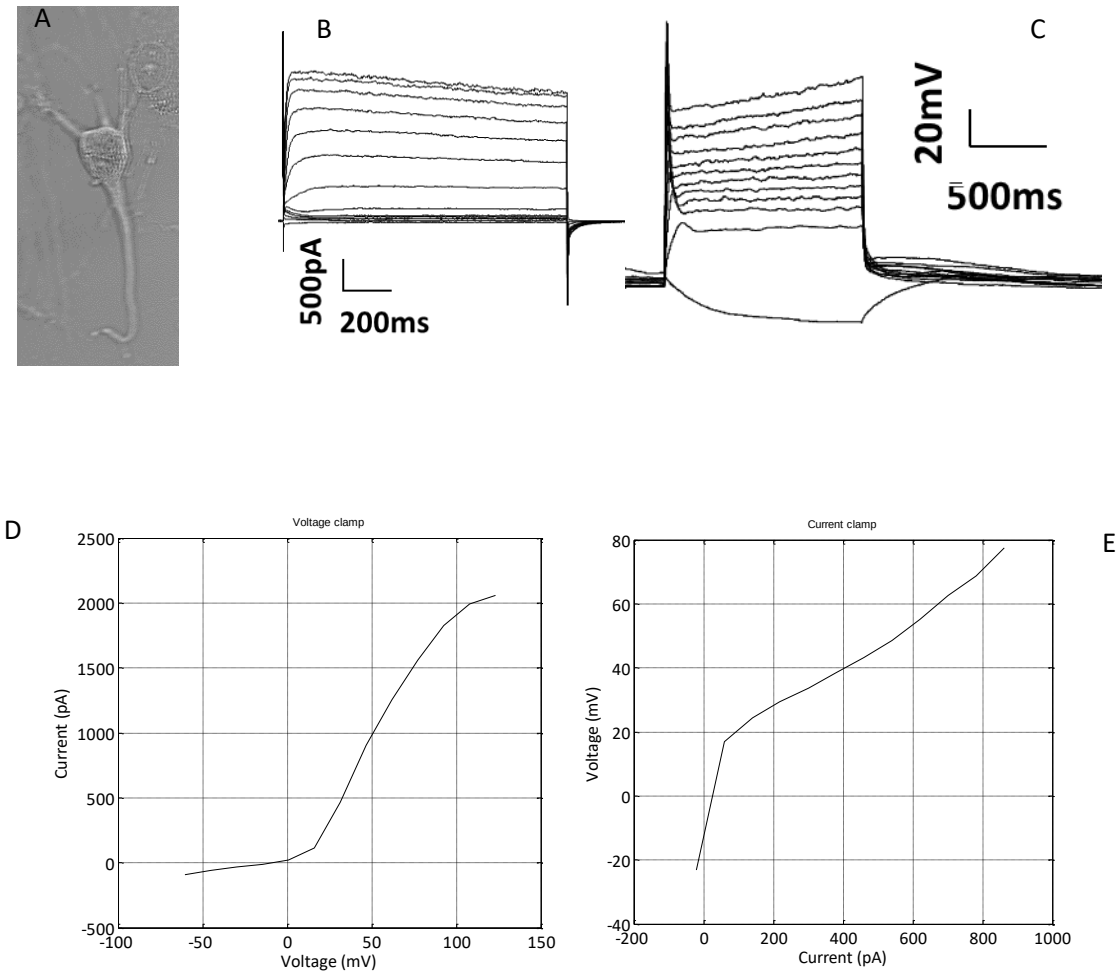

Figure 65. Patch clamp at day 16. *Voltage (B) and current (C row,80 pA steps) recorded traces, with V-I and I-V relations (D, E). The cell parameters were: Vr=-50 mV, Rm= 423.8±11.7 MΩ, Ra=36.4±2.6 MΩ.*

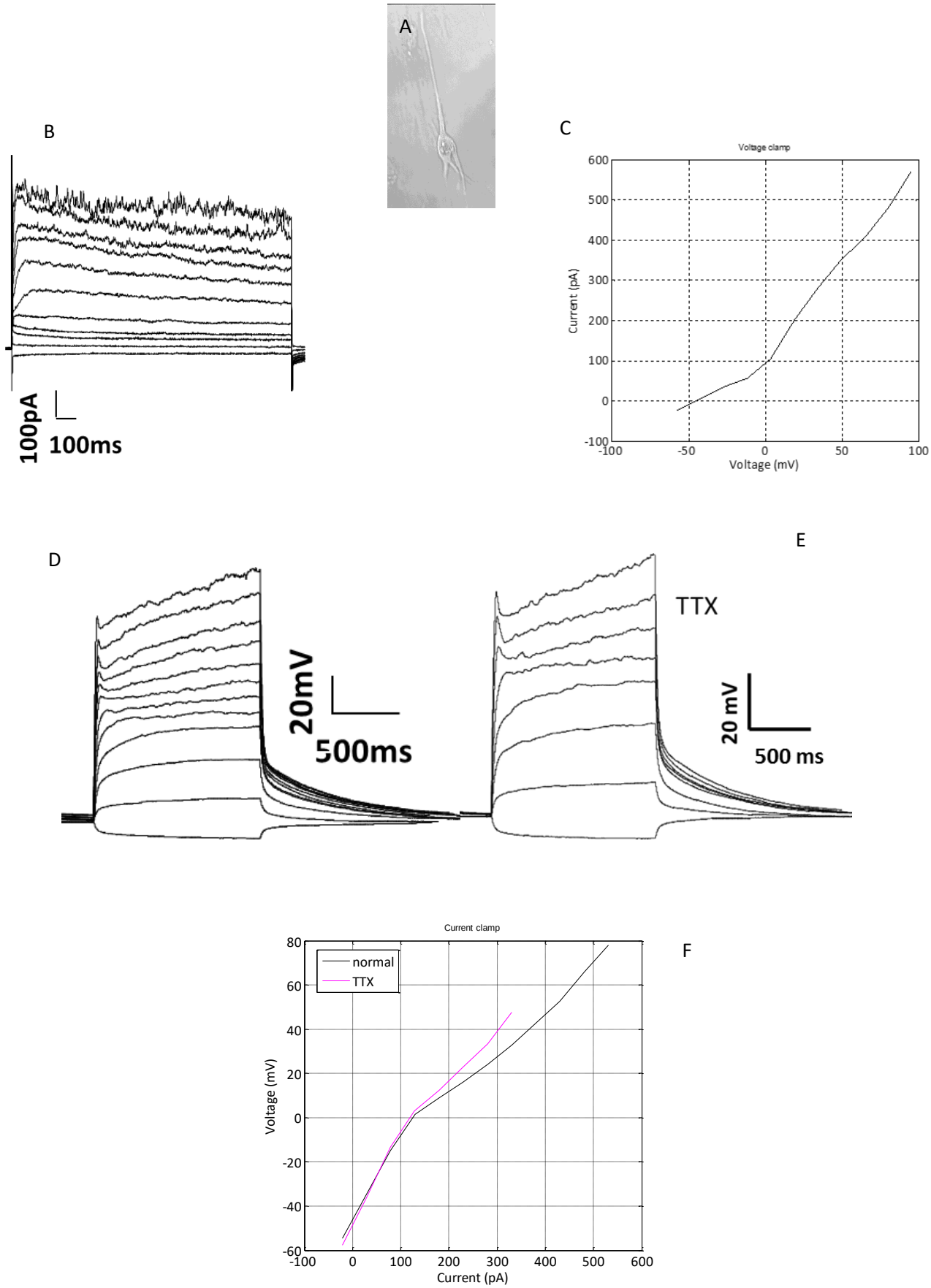

Figure 66. Patch clamp at day 23. *Voltage clamp (B) and current clamp (50 pA steps) with and without TTX 1Mm (D, E), together with V-I and I-V relations (C, F). The cell parameters were: Vr=-47 mV, Rm= 465.1±23.3MΩ, Ra=45.3±1.2MΩ.*

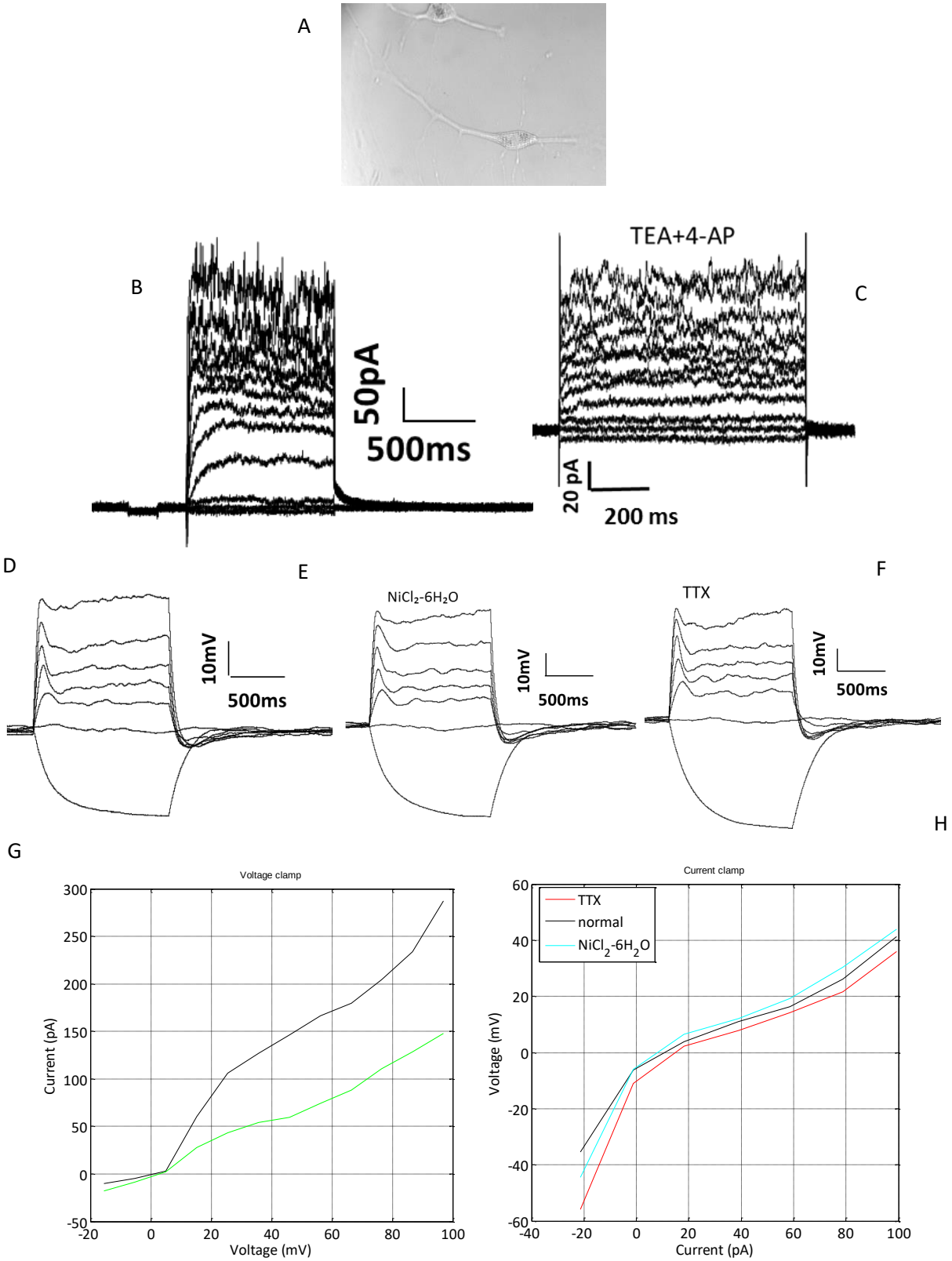

Figure 67. Patch clamp at day 30. *Voltage clamp with and without TEA 5Mm +4-AP 500 mM (B, C) and current clamp (20 pA steps) with and without $NiCl_2$-$6H_2O$ 500µM and TTX (D, E, F), together with V-I and I-V relations (G, H). The cell parameters were: Vr=-15 mV, Rm= 2.8±1GΩ, Ra=12.67±0.03 MΩ.*

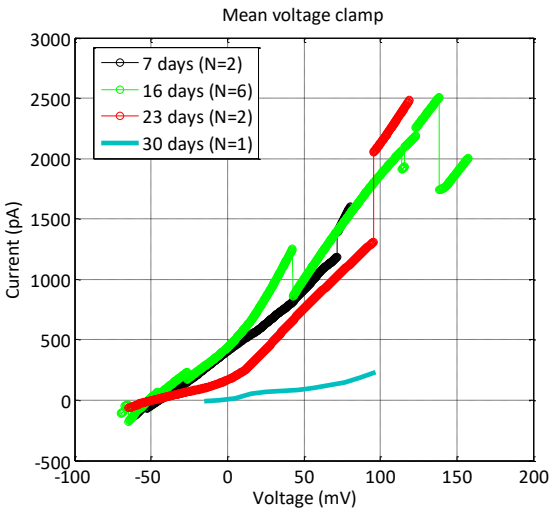

A

B

Figure 68. V-I curves at different time points.

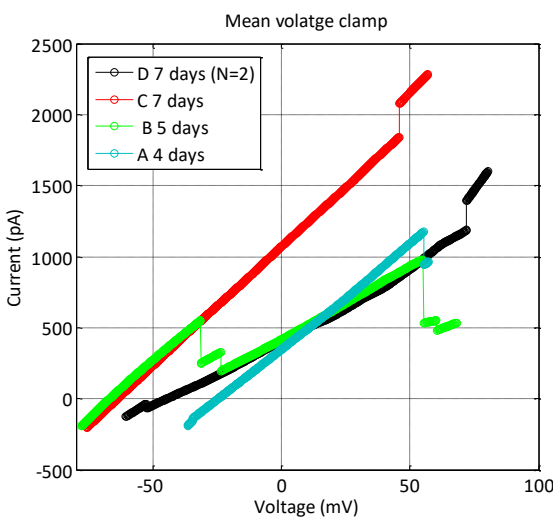

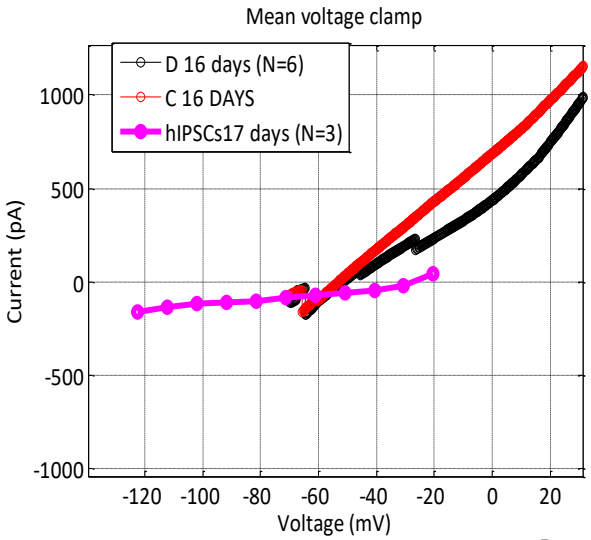

C

D

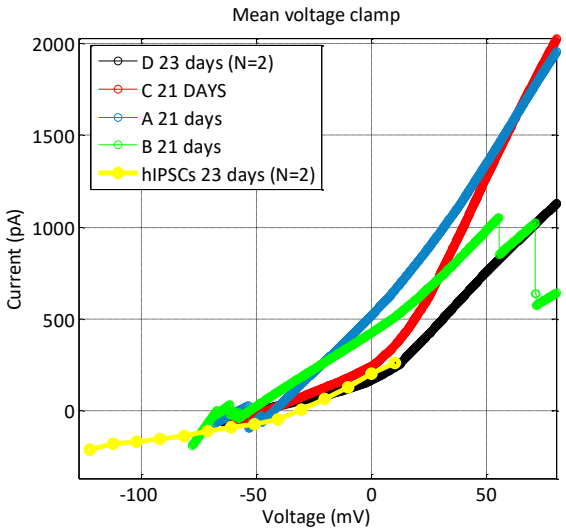

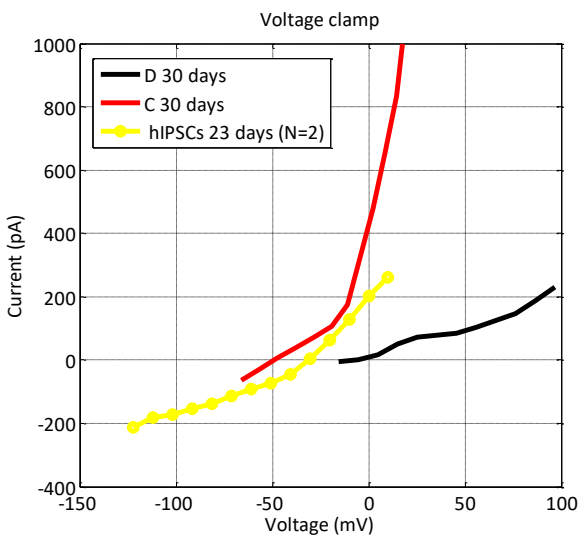

Figure 69. Comparison of the V-I curves for all the differentiation protocols for MSCs and hIPSCs at different stages.

PROTOCOL F.

The differentiation protocol for these cells consisted in direct differentiation with NGF. The cells were tested at 11, 19, and 28 days.

At 11 days, the cells were not presenting any neuronal property both in the voltage and current clamp (Figure 71). The average resting potential was V_r = (-48.7± 0.1) mV, and the membrane resistance was R_m = (268.3± 0.1) MΩ. In total five cells were tested in this phase.

Small sodium currents (Figure 72), like that observed in protocol C, were detected in only one cell at 19 days of differentiation (Figure 72). However, there was no corresponding action potential or the typical peaks in the current clamp. The mean resting potential at this stage was V_r = (-56± 4) mV.

The last experiments were performed at 28 days (Figure 73). The 45% of the cells was showing the typical features already detected in the cells that have undergone the other protocols: potassium currents in the voltage clamp and AP-like peaks appearing under very high current stimuli. We saw a little increasing of the resting potential V_r = (-44.9± 3.6) mV. In general, the values of the resting potential are similar to that of the protocol A, B, and D.

Form the patch clamp data we can conclude that the characteristics of the cells differentiated with protocol F were similar to that of the cell differentiated with protocols A, and B (Figure 75).

Immunofluorescence was performed after patch clamp at 28 days (Figure 70). Cells were stained for GAP43, and MAP2. The cells were expressing neuronal markers but they did not show electrophysiological properties of neurons.

Days of differentiation	Resting potential (mV)	Membrane resistance (MΩ)	Number of cells
11	(-48.7± 0.1)	(268.3± 0.1)	6
19	(-56± 4)	(423.1± 0.1)	3
28	(-44.9± 3.6)	(228.2± 0.3)	11

Table 10. Summary of mean cell parameters

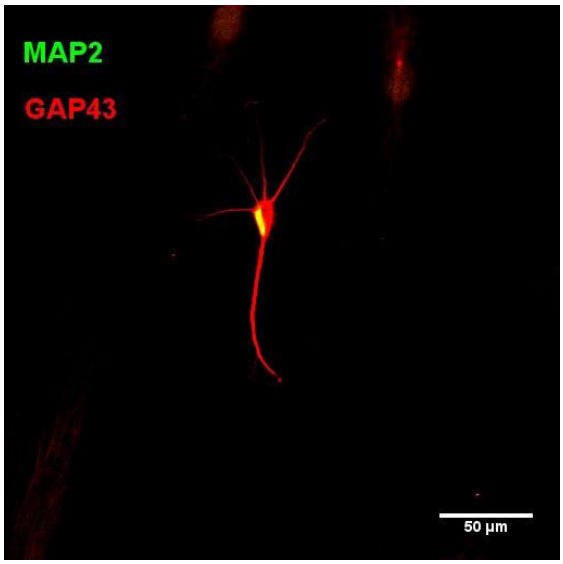

Figure 70. Immunofluorescence at 28 days.

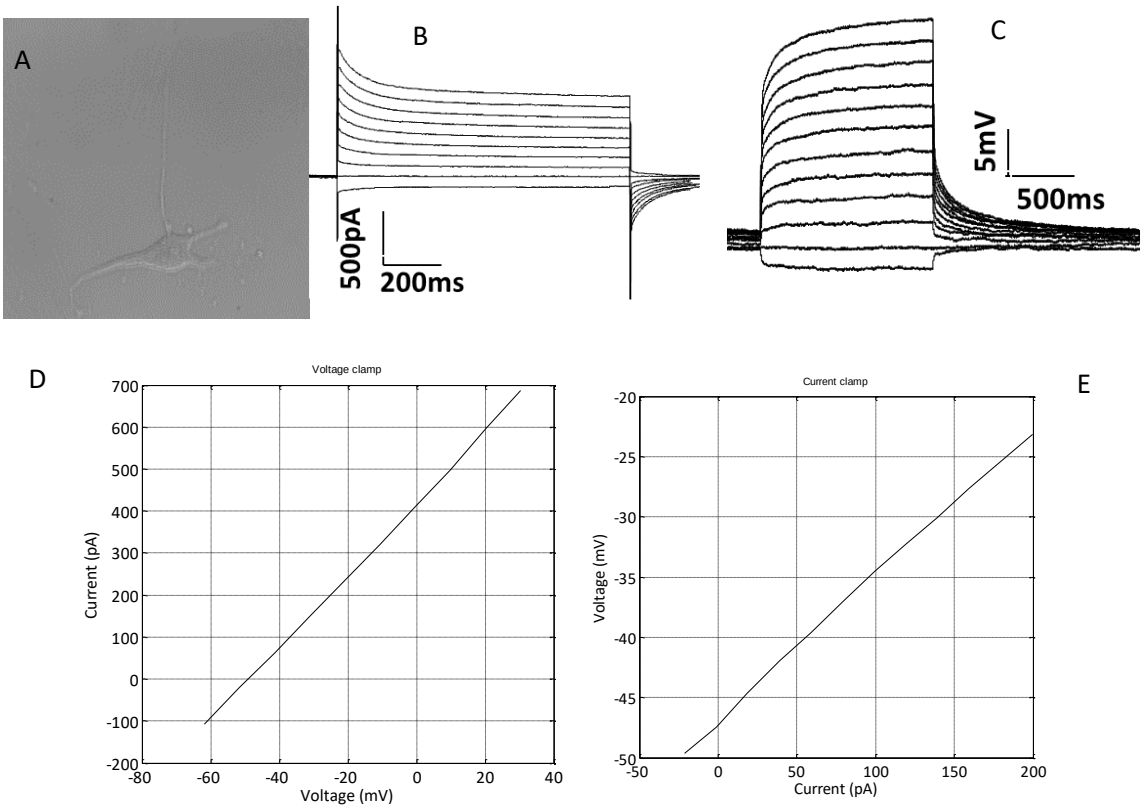

Figure 71. Patch clamp at day 11. *Voltage (B) and current (C,20 pA steps) recorded traces, with V-I and I-V relations (D, E). The cell parameters were: Vr=-51 mV, Rm= 39.6±2.7 MΩ, Ra=56.9±3.1 MΩ.*

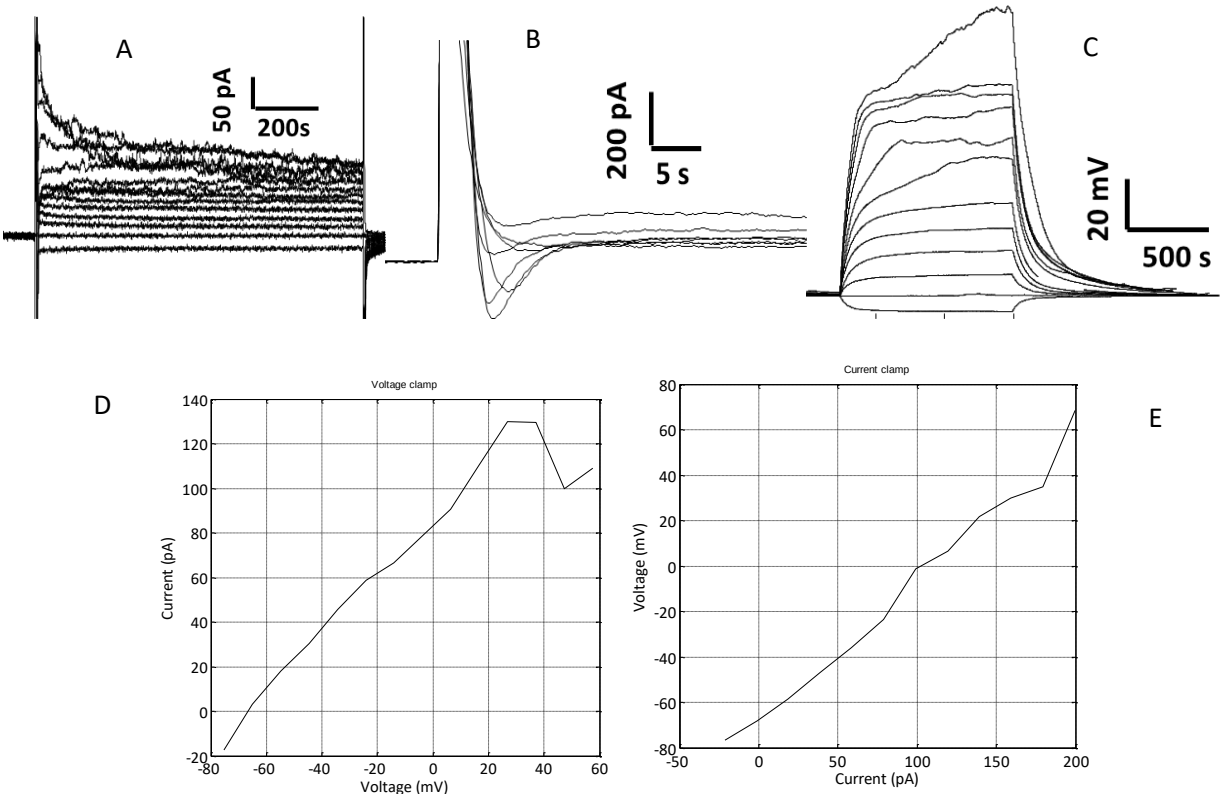

Figure 72. Patch clamp at 19 days. *Voltage (A, B) and current (C,20 pA steps) recorded traces, with V-I and I-V relations (D, E). The cell parameters were: Vr=-64 mV, Rm= 454.1±4.5 MΩ, Ra=10.5±0.2 MΩ.*

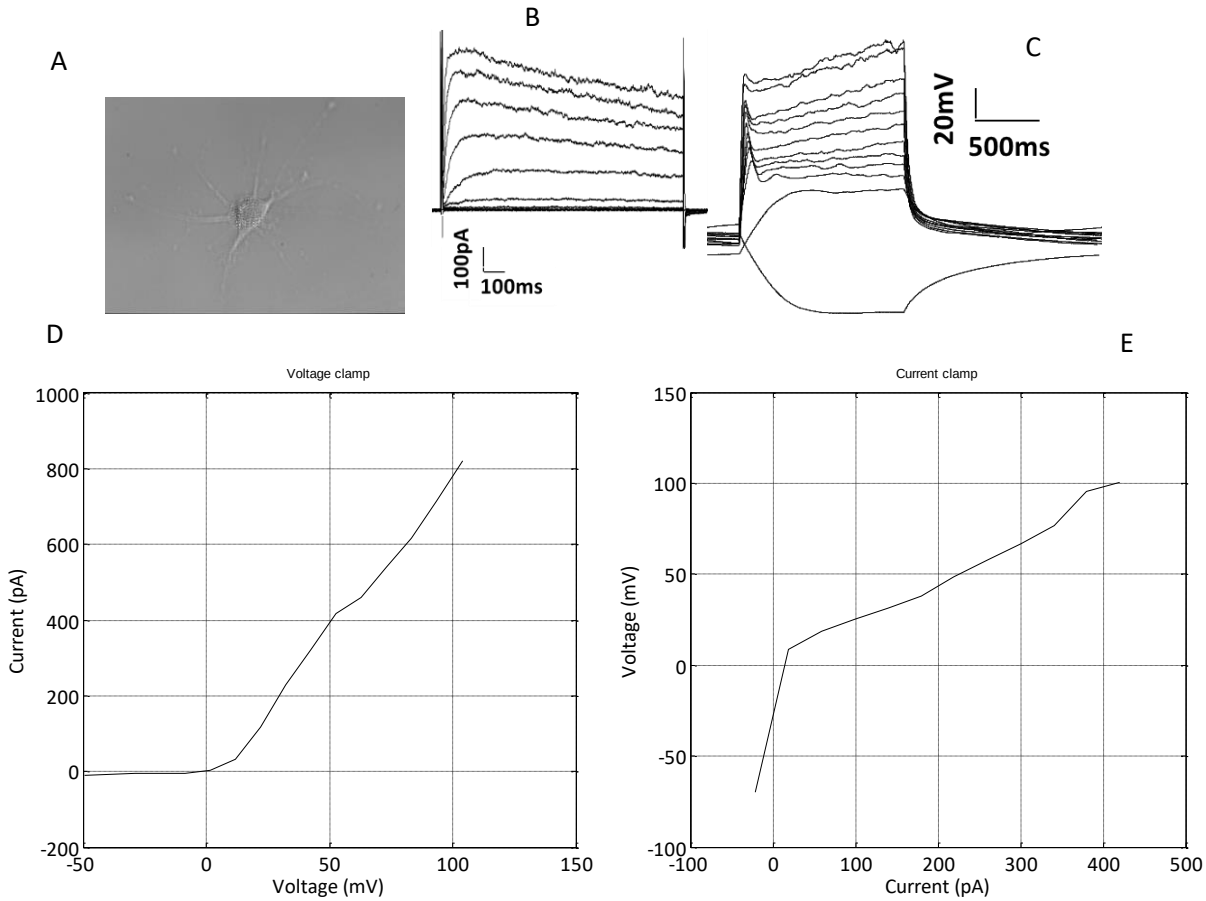

Figure 73. Patch clamp at 28 days. *Voltage (B) and current (C, 50 pA steps) recorded traces, with V-I and I-V relations (D, E). The cell parameters were: Vr=-39 mV, Rm= 32.9±0.3 MΩ, Ra=47.8±0.2 MΩ.*

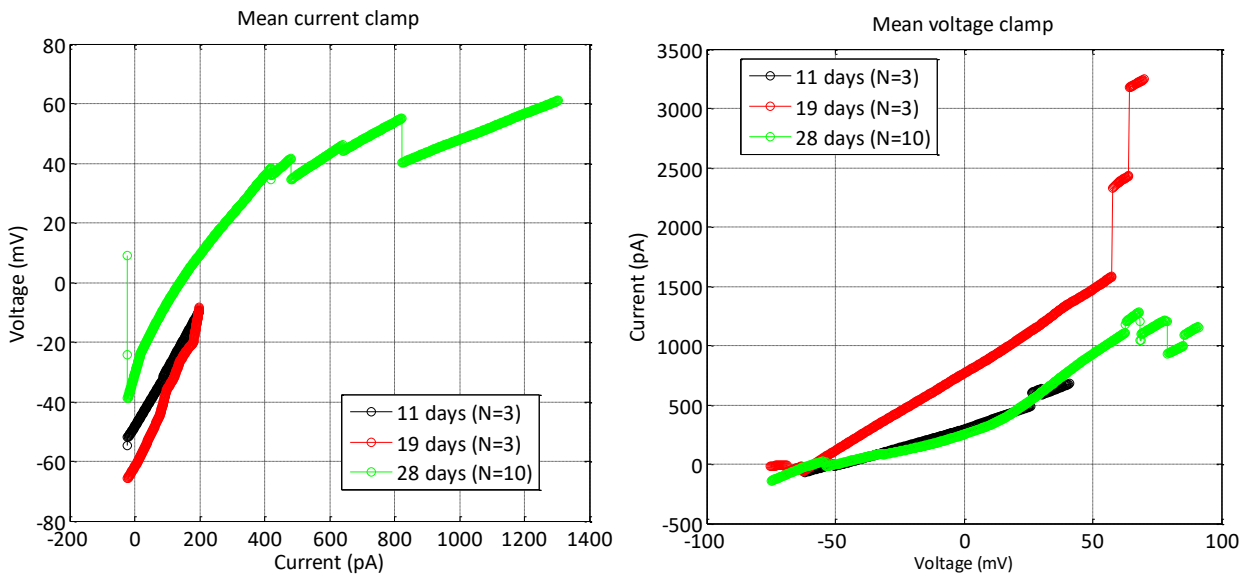

Figure 74. Mean I-V (left) and V-I (right) at different stages.

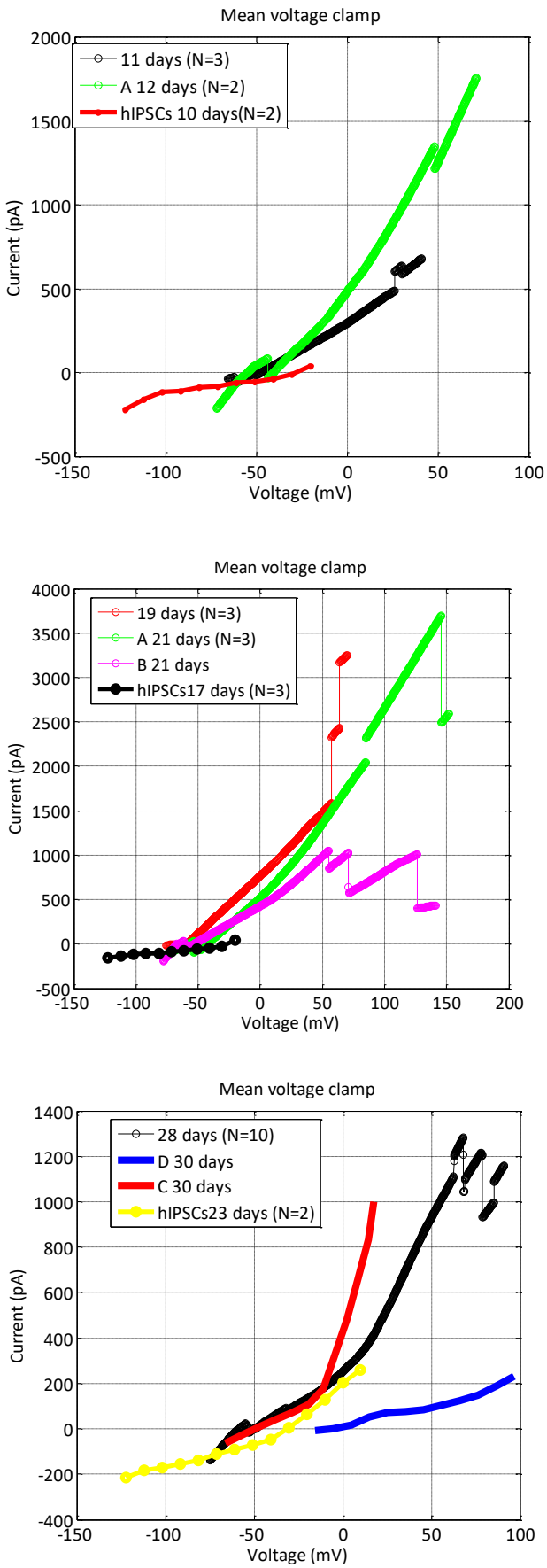

Figure 75. Comparison of the V-I curves for all protocols at different stages.

SUMMARY.

Summarizing: protocol C gave the best results in terms of resting potential, while the other protocols produced cells with resting potential between -40 and -50 mV. The highest number of positive cells was detected for the protocol D (35%) followed by C, B, A, and F.

Considering the patch clamp data, we can conclude that the cells are not completely functional neurons. No genuine action potentials were detected, but we observed two different behaviours in the current clamp recordings. The first was the appearing of action-potential like-peaks at very high current stimulations between 16 and 23 days. The second was detected during the lasts experiments (between day 25 and 34 of differentiation), and is very similar to that observed in Schwann cells current clamp recordings. This observation could support the hypothesis that the cells correctly developed the potassium, but not the sodium channels. To clarify this issue, in absence of enough experimental data, we performed simulations of the current clamp experiments based on the Hodgkin Huxley model (see 3.3).

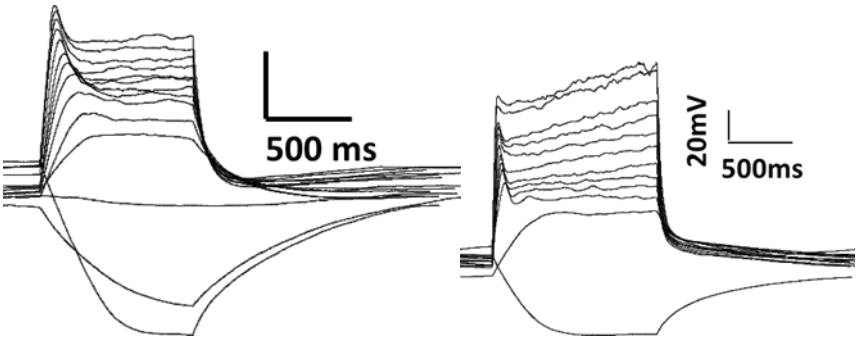

Schwann cell at 46 days **MSCs derived neuron-like cell.**

Figure 76. Comparison between Schwann cell (left) and MSCSs derived neuron-like cell (right) current clamp.

Blocker were applied during experiments for protocols B, C, and D. The AP-like peaks were not suppressed neither by TTX nor by $NiCl_2$, but more experiments are needed, since it is possible that the blockers were not working properly due to incorrect concentration or problems in the perfusion system. TEA and 4-AP applied during the voltage clamp for protocol C and D leaded to a suppression of the currents, indicating that the cells are correctly expressing potassium channels.

3.3 ACTION POTENTIALS SIMULATION.

Since the patch clamp experiments carried out in MSCs have shown an unusual current-voltage behaviour, we tried to interpret the current clamp data by numerical simulations in Matlab using the Hodgkin-Huxley model of the squid giant axon [16].

The differential equations were solved using the Euler first order approximation. The membrane capacitance was assumed as 1 µF/cm², and the other parameters were set according to the following table:

	K^+	Na^+	*Leakage*
E (mV)	+12	-115	10.6
$\bar{g}$ (mS/ cm²)	36	120	0.3

Table 11. Experimental cells parameters.

The equations to be solved were:

$$C_m \frac{dV_m}{dt} + I_{ion} = I_{ext},$$

$$I_{ion} = \bar{g}_{Na} m^3 h (V - E_{Na}) - \bar{g}_K n^4 (V - E_K) - \bar{g}_l (V - E_l),$$

$$\begin{cases} \dfrac{dn}{dt} = \alpha_n(V)(1-n) - \beta_n(V)n, \\ \dfrac{dm}{dt} = \alpha_m(V)(1-m) - \beta_m(V)m, \\ \dfrac{dh}{dt} = \alpha_h(V)(1-h) - \beta_h(V)h. \end{cases}$$

$$\alpha_m(V) = \frac{0.1(25-V)}{e^{\frac{(25-V)}{10}} - 1}, \qquad \alpha_n(V) = \frac{0.01(10-V)}{e^{\frac{(10-V)}{10}} - 1}, \qquad \alpha_h(V) = 0.07 e^{\frac{-V}{20}},$$

$$\beta_m(V) = 4.0 e^{-\frac{V}{18}}, \qquad \beta_n(V) = 0.125 e^{\frac{V}{80}}, \qquad \beta_h(V) = \frac{1}{e^{\frac{(30-V)}{10}} - 1}$$

We tried to reproduce the current clamp traces observed during the experiments with MSCs by varying the conductance of sodium and potassium channels.

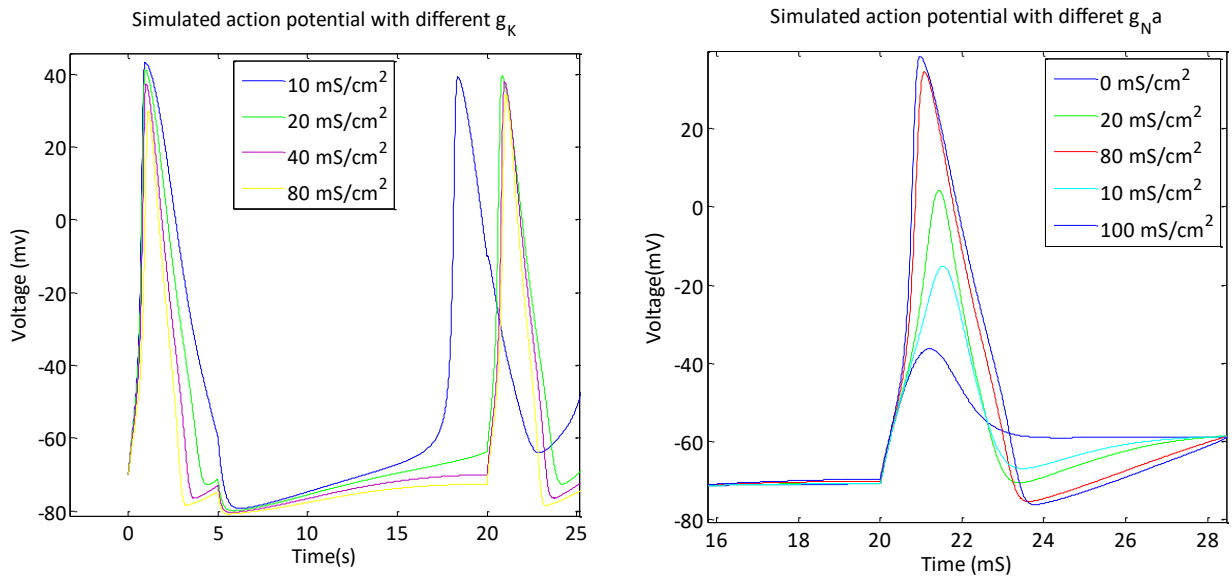

Figure 77. Simulated action potentials with variable $\bar{g}_K$ (left) and $\bar{g}_{Na}$ (right). *As the potassium conductance was increasing the refractory period becomes longer and the second action potential is shifted. Changes in sodium channels conductance affected both the duration of the action potential and the height of the peak.*

The next step is to use these simulations to reproduce our patch clamp data. Form the voltage clamp data we knew that the cells were expressing voltage-activated potassium currents; and, in the current clamp we distinguished two different behaviours, as discussed before. We started form the simulation of the current clamp traces observed between 16 and 23 days, performing a simulation in which the sodium channels contribution was almost absent by setting $\bar{g}_{Na}$ = 2 mS/ cm²; while the potassium conductance was maintained constant at 36 mS/ cm². Varying the current stimulus, we obtained the following results:

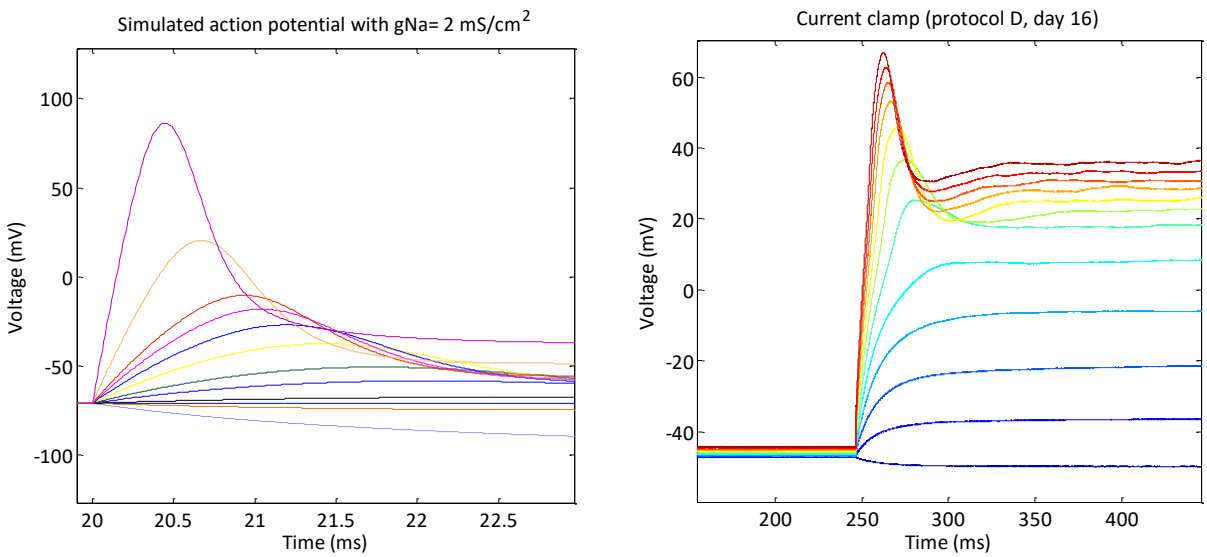

Figure 78. Simulated action potential without sodium channel for different injected currents (left) and current clap at day 16 for protocol D (right).

As can be seen in Figure 78 the simulated traces are very similar to the recorded ones between 16 and 23 days. Thus, these simulations confirmed our hypothesis that the cells were not expressing the correct quantity of sodium channels. The differences in the duration of the initial transient and in the voltage in the steady state can be attributed to the fact that in the simulation we are considering only one type of potassium channels and sodium channels with a small leakage current. In addition, to that in immature neurons also calcium channels contribute to the generation of premature action-potentials [29] [28]. And, also we have to take in account that we were comparing our data with a simulation in which is performed for the squid giant axon.

After that, we performed a simulation in which the potassium channel conductance was again 36 mS/ cm², while the sodium channels conductance was set to $\bar{g}_{Na}$ = 10 mS/ cm², to see if we could reproduce the current clam data observed during the last experiments (Figure 79). The simulations suggested that the observed behaviour could be related to a small contribution of sodium channels. The same considerations about the differences made before can be applied also to this case.

In conclusion, we these simulations helped us to have a more clear idea of the role of each type of ionic channel in the generation of the action potential. The next step could be the extension of this model to our experimental data, but for this purpose more voltage clamp experiments with channels inhibitors are needed.

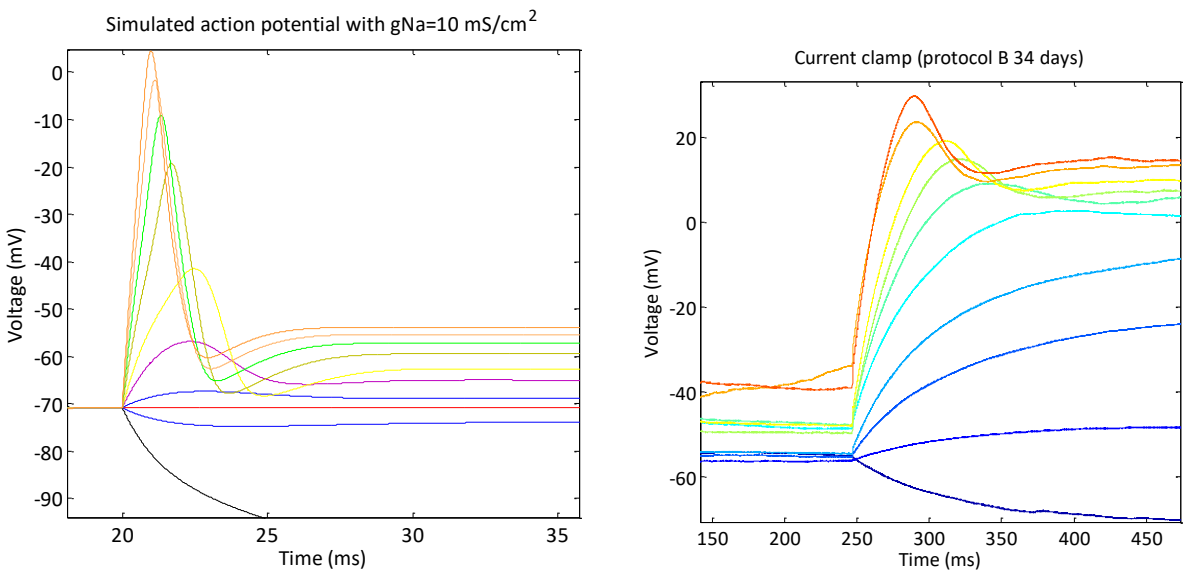

Figure 79. Simulated action potential with $\bar{g}_{Na}$ = 10 mS/ cm² (left) compared with the experimental recordings of

4.DISCUSSION

In this work, we have applied standard biophysical techniques to perform biomolecular and functional characterization of motor neurons and Schwann cells derived from two different sources of stem cells: iPSCs and MSCs both derived from human skin.

IPSC differentiated into motor neuros and Schwann cells with modified protocols, previously described in [26] and [27], were tested with patch clamp experiments and immunofluorescence analysis (performed by other colleagues in the lab) at different stages. During the pluripotency stage and the neuronal differentiation steps, our cells were found to correctly express the expected markers, as in [26]. In particular, mature motor neurons expressed HB9, NF, GAP43, NF, NeuN, and TUJ1 at day 20 of maturation. Patch clamp experiments, performed at day 10, 17 and 23 during maturation, demonstrated that these cells have reached a complete neuronal maturation. We recorded trains of action potentials by current clamp stimulation, and detected voltage-activated sodium and potassium currents by delivering TTX and TEA-Cs in the extracellular solution, respectively. Altogether, our experiments further characterized the iPSC-derived neurons in respect to [26].

Schwann cells derived from human iPSCs were here first characterized electrophysiologically. Their properties were very similar to those known from cultured Schwann cells [30]. The resting potential we measured was around -36 mV, while the membrane conductance was sensitive to voltage stimulations that we explained by the presence of a high density of voltage-activated potassium channels, as expected for Schwann cells [22], [30]. Immunofluorescence performed (by other members of the lab) on mature Schwann cells demonstrated that the cells are expressing typical marker for myelinating Schwann cells, MBP, S100β. However, we found a subpopulation of cells positive for the neuronal marker TUJ1. This result could be explained by the fact that the iPSCs were first differentiated into neural crest stem cells which are precursors also for some types of neurons. It is possible that the cells sorted for P75 marker included marginally this population. Thus, we cannot exclude that our patch clamp data refer also to these cells.

In MSCs, we detected incomplete neuronal maturation, despite the results are original and encouraging as they overcome previous limitations found in the literature [31]. The differentiation protocol that we used was based on the same small molecule composition of the iPSC differentiation protocol (mainly Chir, DMH1, TGFβ inhibitor, retinoic acid, and puromorphamine), which permitted us to obtain high efficiency in terms of number of differentiated cells. As small voltage-activated currents similar to sodium ones observed with differentiated iPSCs were detected in MSC experiments protocols C and F, we suspect that the timing/concentration of the small molecules we used should be changed. Typical neuronal markers NF, NueN, GAP43, and MAP2 were found to be expressed but the incomplete maturation resulted from the cell morphology which didn’t show the typical neuronal network and axonal elongation to form synapses.

5.ONGOING WORK AND FUTURE PERSPECTIVES.

At present, we are focusing on co-culturing human iPSCs-derived motor neurons and Schwann cells. To induce axonal myelination in this model we are intended to test potential pro-myelinating drugs. A commercial microfluidic chamber available from Millipore (Figure 80) will be exploited as a system to study this mechanism. The advantage of this device is the possibility to separate motor neurons and Schwann cells in two different compartments, which allows a controlled interaction of the two cells populations in a strictly regulated enviroment.

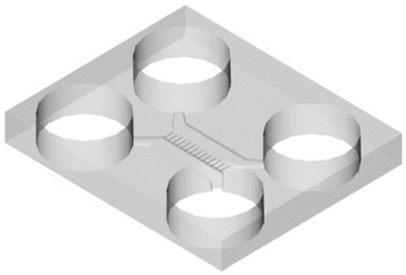

Figure 80, Microfluidic chamber for axonal elongation.

If this model of myelination will be successful, the next step would be to generate motor neurons and Schwann cells derived from patients carrying the mutations of the Cx32 related to the Charcot-Marie-Tooth disease.

CONCLUSIONS.

Stem cell technology has the enormous potential to advance medical therapy by personalizing regenerative medicine and creating novel human disease models for research and therapeutic testing. iPSC-derived neurons have opened new opportunities to understand the development of several neurologic diseases, such as CMT1X. Thus, cell models based on iPSC-derived neuron-Schwann cell co-culture appear to be a promising *in vitro* tool, alternative to animal models, for a biophysical analysis of the molecular mechanisms and to elucidate the disease development, paving the way for a cure. This thesis work represents a preliminary effort towards the generation of a myelinating co-culture system using neurons and Schwann cells derived from the same individual. This cellular model could be used to study the expression and function of Cx32 carrying CMT1X mutations and as a powerful drug screening platform for personalized therapy.

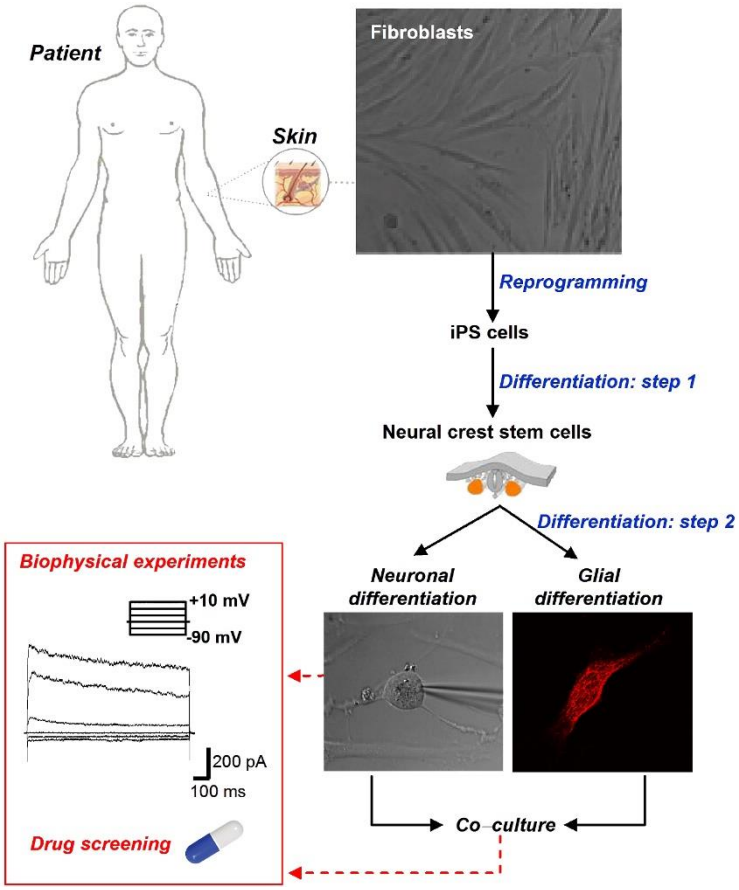

Figure 81.Generation of a functional stem cell-derived myelinating co-culture is a major challenge for the study of peripheral neuropathies and for therapeutic drug screening

APPENDIX A: PROTOCOLS FOR IPSCS.

NEURAL CREST DIFFERENTIATION PROTOCOL

IPS cells are detached with TrypLE, counted and seeded 100.000 cells/cm²in vitronection precoated wells. Neural crest differentiation protocol lasts 7 days, and the medium is changed on day 0, 2, 4, 5, and 6. Around day 5 the cells are confluent. At day 7, cells are dissociated with TrypLE .

1) Day -1.

Coating plates.

Thaw Matrigel, 30' in ice.
Diluite Matrigel in DMEM/F12 (1:50, 500µl/27ml).
Add 1.5 ml of Matrigel on wells and let 2 hours.

Seeding cells in 6 well plates.

Collect old medium (conditioned medium) from cell culture in a 15 ml tube.
Add 700 µl TrypLE (for 6 well plates) to the cells, 5' at 37°C.
Add some medium to the cell suspension and collect cells in 15 ml tube.
Spin 4' at 1039 rpm and resuspend in medium. Count the cells.
Prepare the Matrigel coated plates and add 2 ml of attachment medium (70% fresh hESM and 30 % conditioned medium + Rock Inhibitor, final concentration 10 µM).
Seed 100.000 cells/ well in 6 well plates (10.000 cells/cm²).
For mRNA extraction, resuspend remaining cells in 1 ml Tryzol (d-1) to store at -20°C.

2). Day 0.

Preparation of the medium for the differentiation.
Medium has to be changed on day 0, 2, 5, and 6 (2 ml/well).

3) Day 2, 4, 5, 6.

Change the medium and check the cells under microscope.
The cells will rich confluency around day4-5.

4). Day 7.

Check the cells. They should be very confluent (expected number 5-10 $*10^6$ cells/well) .
Dissociate the cells with TrypLE and count them. A part of the cells can be used to perform analysis, and the other for further differentiation.

MOTOR-NEURON DIFFERENTIATION PROTOCOL

1) hPSCs plating (day -1): hPSCs were dissociated with Dispase II (1mg/ml) or Triple and splitted at 1:6 in Matrigel-coated plates (Matrigel: 10%).

2) MNPs Specification (day 0 to 6): the PSC medium was replaced with ***neural medium***, [DMEM/F12, Neurobasal medium at 1:1, 0.5% N2, 0.5% B27, 0.1mM ascorbic acid, 1% Glutamax and 1% penicillin/streptomycin. CHIR-99021 (3 µM), DMH1 (2 µM) and SB-431542 (2 µM)].
The culture medium was changed every other day.
Human PSCs maintained under this condition for **6 days** were induced into NEP cells.

3) NEP Differentiation (day 7 to 12): cells were then dissociated with Dispase II (1 mg/ml) or Triple and splitted at 1:6 with the same medium described above. RA (0.1 µM) and Pur (0.5 µM) were added in combination with CHIR-99021 (1 µM), DMH1 (2 µM) and SB-431542 (2 µM).
The medium was changed every other day.

NEP cells maintained under this condition for **6 days** differentiated into OLIG2+ MNPs.

4) MNs Differentiation phase I (day 13 to 18): The OLIG2+ MNPs were **expanded** with the same medium containing CHIR-99021 (3 µM) , DMH1 (2 µM), SB-431542 (2 µM), RA (0.1 µM) , Pur (0.5 µM) and VPA (0.5 mM), and split 1:6 once a week with Dispase.
The medium was changed every other day.
OLIG2+ MNPs cells were maintained under this condition for **6 days or more.**

5) MNs Differentiation phase II (day 19 to 24): OLIG2+ MNPs were dissociated with Dispase II and **cultured in suspension** in the above neural medium with RA (0.5 µM) and Pur (0.1 µM).
The medium was changed every other day.
OLIG2+ MNPs under this condition for **6 days** differentiated into MNX1+ MNs.

6) MNs Differentiation phase III (day 25 to 35): The MNX1+ MNs were then dissociated into single cells and plated on Matrigel-coated plates or on astrocytes. Were cultured with RA (0.5 µM), Pur (0.1 µM) and Compound E (0.1 µM). Insulin-like Growth Factor 1, BDNF and Ciliary Neurotrophic Factor (all 10 ng/ml) were added if MNs were plated at low density.
The medium was changed every other day.
MNX1+ MNs were maintained under this condition for **10 days or more to mature into CHAT+ MNs**

APPENDIX B: MESENCHYMAL STEM CELLS

Proliferation medium

DMEM/F12 (1:1) with 10% **FBS**

B27 (without vitamin A, 2% in volume)

EGF (20 ng/ml)

FGF2 (40 ng/ml)

P/s 1X

Heparing (5 μg/ml)

Plating medium

DMEM/F12 (1:1) with 10% **FBS**

B27 (without vitamin A, 2% in volume)

EGF (20 ng/ml)

FGF2 (40 ng/ml)

P/s 1X
Rock inhibitor (10 μM)

Induction 1

DMEM/F12 50% + Neurobasal 50%
N2 0.5ml
B27 (+Vit A) 1 mL
P/s 1X
Ascorbic acid 0.1 mM
L-Glutamine 1X
DMH1 2μM
TGFβ inhibitor (SB431542) 2μM

Induction 2

DMEM/F12 50% + Neurobasal 50%
N2 0.5ml
B27 (+Vit A) 1 mL
P/s 1X
Ascorbic acid 0.1 mM
L-Glutamine 1X
DMH1 2μM
TGFβ inhibitor(SB431542) 2μM

Differentiation

DMEM/F12 50% + Neurobasal 50%
N2 0.5ml
B27 (+Vit A) 1 mL
P/s 1X
Ascorbic acid 0.1 mM
L-Glutamine 1X
DMH1 2μM
TGFβ inhibitor (SB431542) 2μM
Chir 1μM
Retinoic acid 0.1 μM
Puromorphamine 0.1 μM
IGF 10 ng/ml
CNTF 10 ng/ml
BDNF 10 ng/ml

Differentiation_NGF

DMEM/F12 50% + Neurobasal 50%
N2 0.5ml
B27 (+Vit A) 1 mL
P/s 1X
Ascorbic acid 0.1 mM
L-Glutamine 1X
DMH1 2μM
TGFβ inhibitor (SB431542) 2μM
Chir 1μM
Retinoic acid 0.1 μM
Puromorphamine 0.1 μM
IGF 10 ng/ml
CNTF 10 ng/ml
BDNF 20 ng/ml
NGF 20 ng/ml

Spheroids (MSC)

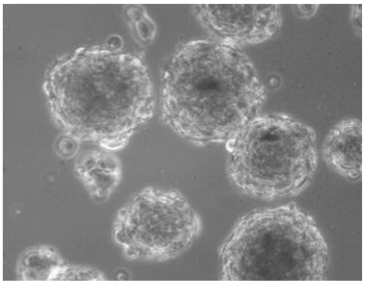

Control D0 (MSC)

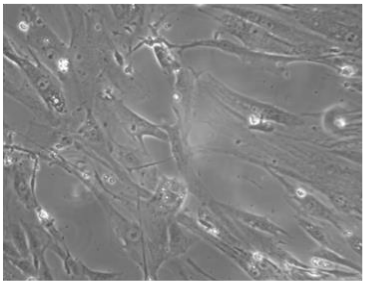

Day 03

A

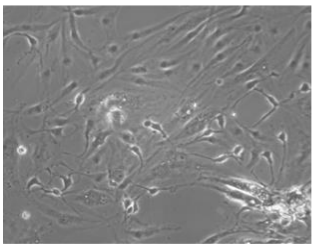

B

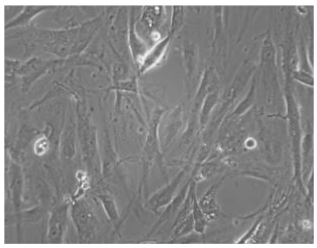

C

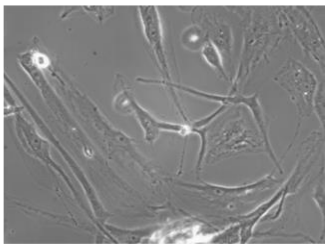

D

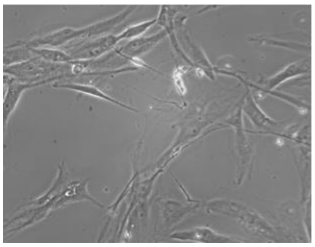

E

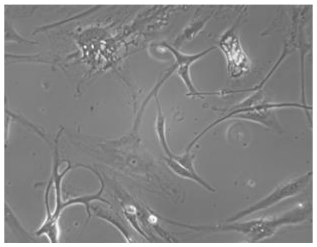

F

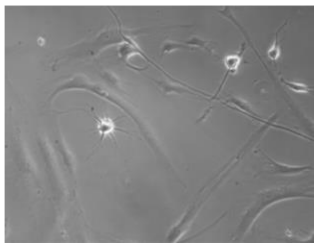

Day 10

A

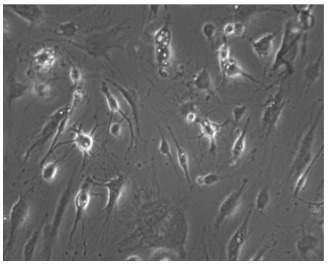

B

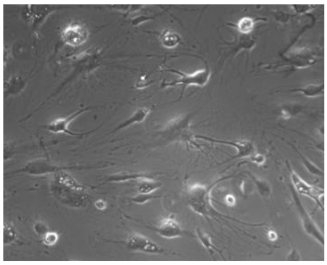

C

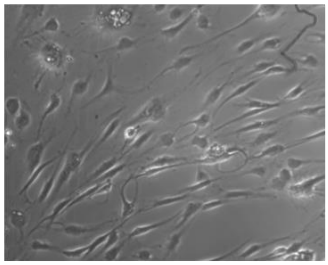

D

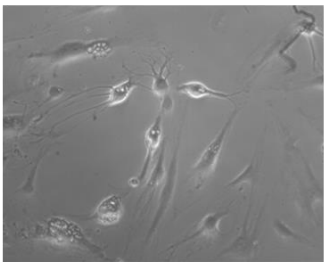

E

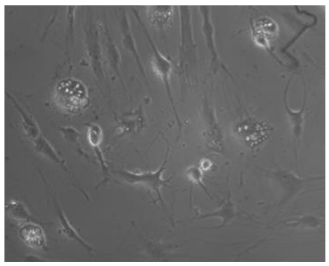

F

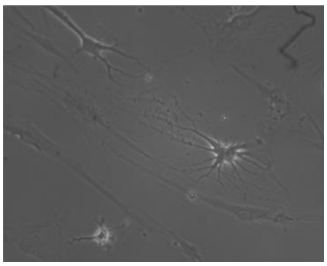

Day 20

A

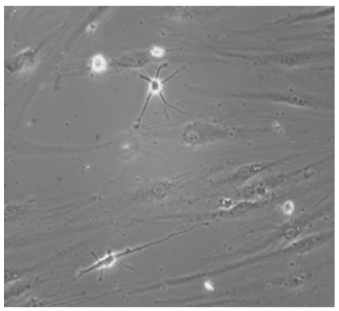

B

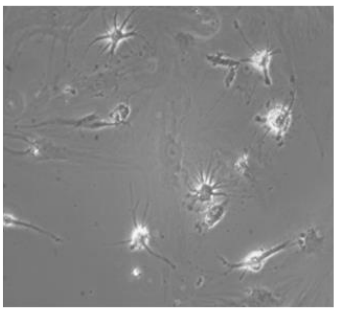

C

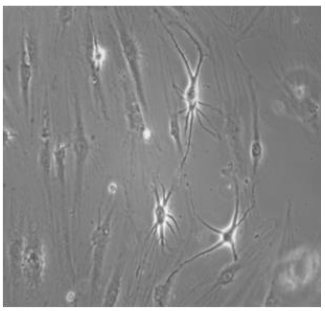

D

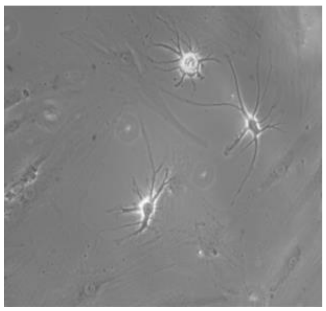

E

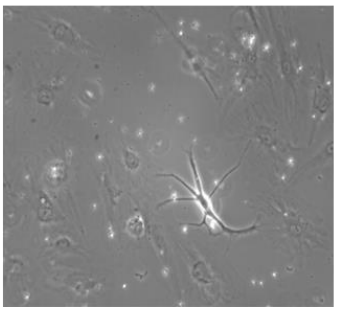

F

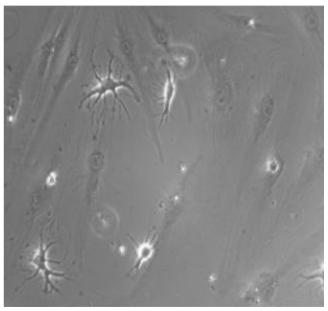

Day 30

A

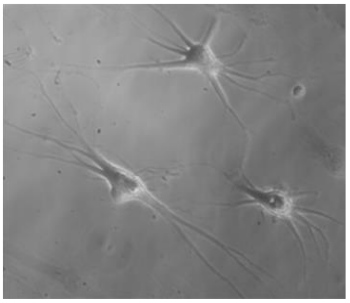

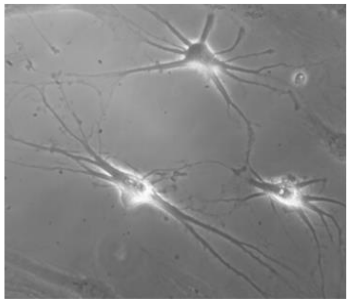

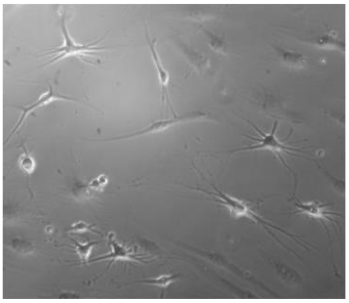

C

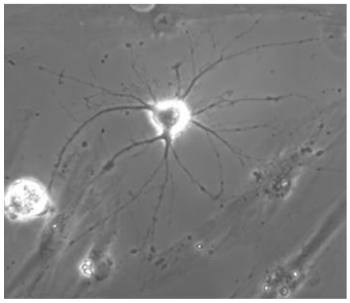

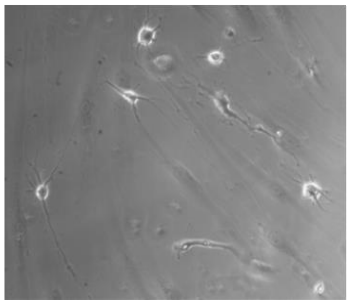

F

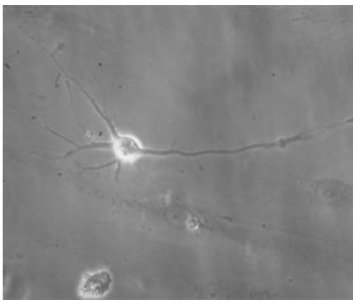

APPENDIX C: MATLAB CODE FOR THE HH MODEL

```
%===simulation time===
simulationTime = 100; %in milliseconds
deltaT=.01;
t=0:deltaT:simulationTime;


%===specify the external current I===
changeTimes = [0]; %in milliseconds
currentLevels = [50]; %Change this to see effect of different currents on
voltage (Suggested values: 3, 20, 50, 1000)

%Set externally applied current across time

I(1:500) = currentLevels; I(501:2000) = 0; I(2001:numel(t)) = currentLevels;
%Comment out the above line and uncomment the line below for constant current,
and observe effects on voltage timecourse
%I(1:numel(t)) = currentLevels;


%===constant parameters for the squid giant axon===%

gbar_K=36; gbar_Na=20; g_L=.3;
E_K = -12; E_Na=115; E_L=10.6;
C=1;


%===set the initial states===%
V=0; %Baseline voltage
alpha_n = .01 * ( (10-V) / (exp((10-V)/10)-1) );
beta_n = .125*exp(-V/80);
alpha_m = .1*( (25-V) / (exp((25-V)/10)-1) );
beta_m = 4*exp(-V/18);
alpha_h = .07*exp(-V/20);
beta_h = 1/(exp((30-V)/10)+1);

n(1) = alpha_n/(alpha_n+beta_n);
m(1) = alpha_m/(alpha_m+beta_m);
h(1) = alpha_h/(alpha_h+beta_h);

%Compute coefficients, currents, and derivates at each time step
for i=1:numel(t)-1

    %---calculate the coefficients---%

    alpha_n(i) = .01 * ( (10-V(i)) / (exp((10-V(i))/10)-1) );
    beta_n(i) = .125*exp(-V(i)/80);
    alpha_m(i) = .1*( (25-V(i)) / (exp((25-V(i))/10)-1) );
    beta_m(i) = 4*exp(-V(i)/18);
    alpha_h(i) = .07*exp(-V(i)/20);
    beta_h(i) = 1/(exp((30-V(i))/10)+1);


    %---calculate the currents---%
```

```
    I_Na = (m(i)^3) * gbar_Na * h(i) * (V(i)-E_Na);
    I_K = (n(i)^4) * gbar_K * (V(i)-E_K);
    I_L = g_L *(V(i)-E_L);
    I_ion = I(i) - I_K - I_Na - I_L;


    %---calculate the derivatives using Euler first order approximation---%
    V(i+1) = V(i) + deltaT*I_ion/C;
    n(i+1) = n(i) + deltaT*(alpha_n(i) *(1-n(i)) - beta_n(i) * n(i));
    m(i+1) = m(i) + deltaT*(alpha_m(i) *(1-m(i)) - beta_m(i) * m(i));
    h(i+1) = h(i) + deltaT*(alpha_h(i) *(1-h(i)) - beta_h(i) * h(i

end


V = V-70; %Set resting potential to -70mv

%===plot Voltage===%

subplot(2,1,1);plot(t,V,'LineWidth',1);legend({'voltage'});ylabel('Voltage
(mv)');xlabel('time (ms)');..
title('Voltage over Time in Simulated Neuron');
subplot(2,1,2);p1 = plot(t,gbar_K*n.^4,'LineWidth',1); hold on;..
p2 = plot(t,gbar_Na*(m.^3).*h,'r','LineWidth',1);legend([p1, p2], 'Conductance
for Potassium', 'Conductance for Sodium');..
ylabel('Conductance');xlabel('time (ms)');title('Conductance for Potassium and
Sodium Ions in Simulated Neuron');
```

BIBLIOGRAPHY

[1] A. Molleman, “Patch Clamping: An Introductory Guide to Patch Clamp Electrophysiology.,” *Wiley*, p. 186, 2003.

[2] A. Instruments, “The Axon Guide,” *Br. J. Ophthalmol.*, vol. 94, no. 2500, pp. 1078–82, 2010.

[3] J. A. Jacquez, “A generalization of the Goldman equation, including the effect of electrogenic pumps,” *Math. Biosci.*, vol. 12, no. 1–2, pp. 185–196, 1971.

[4] E. R. Kandel, J. H. Schwartz, and T. M. Jessell, *Principles of Neural Science*, vol. 3. 2000.

[5] B. Hille, “Ion Channel Excitable Membranes,” *Sunderland Massachusetts USA*. pp. 1–37, 2001.

[6] R. Kar, N. Batra, M. A. Riquelme, and J. X. Jiang, “Biological role of connexin intercellular channels and hemichannels,” *Arch. Biochem. Biophys.*, no. March, 2012.

[7] a L. Harris, *Emerging issues of connexin channels: biophysics fills the gap.*, vol. 34, no. 3. 2001.

[8] J. C. Sáez, J. E. Contreras, F. F. Bukauskas, M. A. Retamal, and M. V. L. Bennett, “Gap junction hemichannels in astrocytes of the CNS,” *Acta Physiol. Scand.*, vol. 179, no. 1, pp. 9–22, 2003.

[9] I. Fasciani *et al.*, “Regulation of connexin hemichannel activity by membrane potential and the extracellular calcium in health and disease,” *Neuropharmacology*, vol. 75, pp. 479–490, 2013.

[10] D. A. Goodenough and D. L. Paul, “Gap Junctions,” pp. 1–19, 2009.

[11] A. Pfenniger, A. Wohlwend, and B. R. Kwak, “Mutations in connexin genes and disease,” *Eur. J. Clin. Invest.*, vol. 41, no. 1, pp. 103–116, 2011.

[12] C. K. Abrams, S. Oh, Y. Ri, and T. A. Bargiello, “Mutations in connexin 32: The molecular and biophysical bases for the X- linked form of Charcot-Marie-Tooth disease,” *Brain Res. Rev.*, vol. 32, no. 1, pp. 203–214, 2000.

[13] G. J. Donahue, “Facts About Charcot-Marie- Tooth Disease & Related Disease,” *Muscular Dystrophy Assoc.*, no. December, pp. 1–13, 2009.

[14] G. Karadima, G. Koutsis, M. Raftopoulou, P. Floroskufi, K. M. Karletidi, and M. Panas, “Four novel connexin 32 mutations in X-linked Charcot-Marie-Tooth disease. Phenotypic variability and central nervous system involvement,” *J. Neurol. Sci.*, vol. 341, no. 1–2, pp. 158–161, 2014.

[15] M. De Miguel, B. Larrosa, D. Gonza, L. C. Barrio, and J. M. Go, “Molecular basis of calcium regulation in connexin-32 hemichannels,” 2003.

[16] a L. Hodgkin and a F. Huxley, “A quantitative description of membrane current and its applicaiton to conduction and excitation in nerve,” *J Physiol*, vol. 117, no. 4. pp. 500–544, 1952.

[17] M. Jackson, “Molecular and Cellular Biophysics,” *Uma ética para quantos?*, vol. XXXIII, no. 2, pp. 81–87, 2014.

[18] A. Verkhratsky and A. Butt, *Glial Physiology and Pathophysiology*. 2013.

[19] R. J. Balice-Gordon, L. J. Bone, and S. S. Scherer, “Functional gap junctions in the Schwann cell myelin sheath,” *J. Cell Biol.*, vol. 142, no. 4, pp. 1095–1104, 1998.

[20] R. H. Quarles, W. B. Macklin, and P. Morell, “Biochemistry,” pp. 51–72, 2006.

[21] M. D. Baker, “Electrophysiology of mammalian Schwann cells,” *Prog. Biophys. Mol. Biol.*, vol. 78, no. 2–3, pp. 83–103, 2002.

[22] a Verkhratsky and C. Steinhäuser, “Ion channels in glial cells.,” *Brain Res. Brain Res. Rev.*, vol. 32, no. 2–3, pp. 380–412, 2000.

[23] A. Atala, *Essentials of Stem Cell Biology*. 2009.

[24] M. Berdasco and M. Esteller, “DNA methylation in stem cell renewal and multipotency,” *Stem Cell Res Ther*, vol. 2, no. 5, p. 42, 2011.

[25] E. Sakmann, B., & Neher, *Single-channel recording.*, vol. Chapter 6. 2001.

[26] Z.-W. Du *et al.*, “Generation and expansion of highly pure motor neuron progenitors from human pluripotent stem cells.,” *Nat. Commun.*, vol. 6, p. 6626, 2015.

[27] Q. Liu *et al.*, “Human Neural Crest Stem Cells Derived from Human ESCs and Induced Pluripotent Stem Cells: Induction, Maintenance, and Differentiation into Functional Schwann Cells,” *Stem Cells Transl. Med.*, vol. 1, no. 4, pp. 266–278, 2012.

[28] S. R. Lockery and N. C. Spitzer, “Reconstruction of action potential development from whole-cell currents of differentiating spinal neurons.,” *J. Neurosci.*, vol. 12, no. 6, pp. 2268–87, 1992.

[29] M. C. Moe *et al.*, “Multipotent progenitor cells from the adult human brain: Neurophysiological differentiation to mature neurons,” *Brain*, vol. 128, no. 9, pp. 2189–2199, 2005.

[30] M. D. Baker, “Electrophysiology of mammalian Schwann cells,” *Progress in Biophysics and Molecular Biology*, vol. 78, no. 2–3. pp. 83–103, 2002.

[31] G. F. Barnab?? *et al.*, “Chemically-induced RAT mesenchymal stem cells adopt molecular properties of neuronal-like cells but do not have basic neuronal functional properties,” *PLoS One*, vol. 4, no. 4, 2009.